UNCLASSIFIED

CENTRAL RESEARCH LIBRARY
DOCUMENT COLLECTION

ORNL-2323
Chemistry-General
TID-4500 (13th ed.)

Cy. 4

MARTIN MARIETTA ENERGY SYSTEMS LIBRARIES
3 4456 0350490 0

ACTIVITIES IN THE $KCl-FeCl_2$ AND $LiCl-FeCl_2$ SYSTEMS

C. Beusman

CENTRAL RESEARCH LIBRARY
DOCUMENT COLLECTION
LIBRARY LOAN COPY
DO NOT TRANSFER TO ANOTHER PERSON
If you wish someone else to see this document, send in name with document and the library will arrange a loan.

OAK RIDGE NATIONAL LABORATORY
OPERATED BY
UNION CARBIDE NUCLEAR COMPANY
A Division of Union Carbide and Carbon Corporation
UCC
POST OFFICE BOX X · OAK RIDGE, TENNESSEE

UNCLASSIFIED

Printed in USA. Price 55 cents. Available from the

Office of Technical Services
U. S. Department of Commerce
Washington 25, D. C.

LEGAL NOTICE

This report was prepared as an account of Government sponsored work. Neither the United States, nor the Commission, nor any person acting on behalf of the Commission:

A. Makes any warranty or representation, express or implied, with respect to the accuracy, completeness, or usefulness of the information contained in this report, or that the use of any information, apparatus, method, or process disclosed in this report may not infringe privately owned rights; or

B. Assumes any liabilities with respect to the use of, or for damages resulting from the use of any information, apparatus, method, or process disclosed in this report.

As used in the above, "person acting on behalf of the Commission" includes any employee or contractor of the Commission to the extent that such employee or contractor prepares, handles or distributes, or provides access to, any information pursuant to his employment or contract with the Commission.

UNCLASSIFIED

ORNL-2323
Chemistry-General
TID-4500 (13th ed.)

Contract No. W-7405-eng-26

CHEMISTRY DIVISION

ACTIVITIES IN THE KCl-$FeCl_2$ AND LiCl-$FeCl_2$ SYSTEMS

C. Beusman

DATE ISSUED

MAY 15 1957

OAK RIDGE NATIONAL LABORATORY
Operated by
UNION CARBIDE NUCLEAR COMPANY
A Division of Union Carbide and Carbon Corporation
Post Office Box X
Oak Ridge, Tennessee

UNCLASSIFIED

MARTIN MARIETTA ENERGY SYSTEMS LIBRARIES
3 4456 0350490 0

ORNL-2323
Chemistry-General
TID-4500 (13th ed.)

INTERNAL DISTRIBUTION

1. C. E. Center
2. Biology Library
3. Health Physics Library
4-5. Central Research Library
6. Reactor Experimental Engineering Library
7-26. Laboratory Records Department
27. Laboratory Records, ORNL R.C.
28. A. M. Weinberg
29. L. B. Emlet (K-25)
30. J. P. Murray (Y-12)
31. J. A. Swartout
32. E. H. Taylor
33. E. D. Shipley
34. S. C. Lind
35. M. L. Nelson
36. C. P. Keim
37. J. H. Frye, Jr.
38. R. S. Livingston
39. S. J. Cromer
40. F. L. Culler
41. A. H. Snell
42. A. Hollaender
43. M. T. Kelley
44. K. Z. Morgan
45. T. A. Lincoln
46. A. S. Householder
47. C. S. Harrill
48. C. E. Winters
49. D. W. Cardwell
50. E. M. King
51. D. D. Cowen
52. D. S. Billington
53. J. A. Lane
54. M. J. Skinner
55. W. H. Jordan
56. G. E. Boyd
57. C. J. Barton
58. J. P. Blakely
59. M. Blander
60. F. F. Blankenship
61. C. M. Blood
62. S. Cantor
63. R. B. Evans
64. H. A. Friedman
65. R. A. Gilbert
66. W. R. Grimes
67. H. Insley
68. F. Kertesz
69. E. E. Ketchen
70. F. A. Knox
71. S. Langer
72. R. E. Meadows
73. R. E. Moore
74. G. J. Nessle
75. R. F. Newton
76. L. G. Overholser
77. J. D. Redman
78. J. H. Shaffer
79. R. J. Sheil
80. N. V. Smith
81. R. A. Strehlow
82. B. J. Sturm
83. R. E. Thoma
84. L. E. Topol
85. W. T. Ward
86. G. M. Watson
87. M. A. Bredig
88. S. Datz
89. R. E. Minturn
90. A. S. Dworkin
91. G. P. Smith
92. M. T. Robinson
93. A. J. Miller
94. P. M. Reyling
95. C. E. Larson (consultant)
96. P. H. Emmett (consultant)
97. H. Eyring (consultant)
98. G. T. Seaborg (consultant)
99. R. R. Dickison

EXTERNAL DISTRIBUTION

100. R. F. Bacher, California Institute of Technology
101. Division of Research and development, AEC, ORO
102-104. University of Cincinnati (1 copy ea. to H. S. Green, J. W. Sausville, and T. B. Cameron)
105. W. W. Grigorieff, Oak Ridge Institute of Nuclear Studies
106-644. Given distribution as shown in TID-4500 (13th ed.) under Chemistry-General category (100 copies – OTS)

CONTENTS

ABSTRACT 1

1. INTRODUCTION 3
   - Objects and Definitions 3
   - Thermodynamics Background and Activity Concept Applied to Fused Salts 3
   - Methods for Determining Activities in Fused Salts 6

2. MATERIALS 12
   - Potassium Chloride 12
   - Lithium Chloride 12
   - Ferrous Chloride 12
   - Methods of Chemical Analysis 12

3. DETERMINATION OF CONDENSED PHASE DIAGRAMS 14
   - Introduction 14
   - Apparatus 14
   - Materials 14
   - Procedure 14
   - Experimental Results 16
   - Thermodynamic Evaluation of the Phase Diagrams 18

4. TOTAL VAPOR PRESSURE MEASUREMENTS: RODEBUSH METHOD 22
   - Theory of the Rodebush Method 22
   - Description of Apparatus 29
   - Procedure 32

5. TRANSPORTATION METHOD 34
   - Therory of Transportation Method 34
   - Description of Apparatus 35
   - Procedures 37

6. RESULTS OF VAPOR PRESSURE MEASUREMENTS: PURE COMPOUNDS 40
   - Total Pressures by Rodebush Method 40
   - Discussion 40
   - Determination of Molecular Weight of Individual Pure Salt Vapors 45
   - Discussion 48

7. RESULTS OF VAPOR PRESSURE MEASUREMENTS: MIXTURES 57
   - Total Pressures by Rodebush Method 57
   - Experimental Transportation Data for Mixtures 64
   - Partial Pressure Calculation from Transport and Total Pressure Data 70

8. THERMODYNAMIC CALCULATIONS 84
   - Relating Activity to Partial Pressure of Monomer Species 84
   - Calculation of Activities 85
   - Calculation of Partial Molar Entropies and Enthalpies of Solution 87

9. SUMMARY 93

10. BIBLIOGRAPHY 94

APPENDIX A: CHEMICAL MICROSCOPY AND X-RAY DIFFRACTION SUMMARY 97

APPENDIX B: MASS SPECTROMETERIC STUDY OF SALT VAPORS IN THE $FeCl_2$-KCl SYSTEM 99

ACKNOWLEDGMENTS 100

ACTIVITIES IN THE $KCl\text{-}FeCl_2$ AND $LiCl\text{-}FeCl_2$ SYSTEMS

C. Beusman

ABSTRACT

Phase equilibria in the $KCl\text{-}FeCl_2$ and $LiCl\text{-}FeCl_2$ systems were studied by means of thermal analysis and vapor pressure measurements. From a combination of two vapor pressure measurements, thermodynamic activities were determined in the $KCl\text{-}FeCl_2$ system, based on partial pressures of monomer species in the vapor. A vapor compound, $KFeCl_3$, was shown to exist. Partial pressures and activities could not be calculated for the $LiCl\text{-}FeCl_2$ system because of the variety of associated molecules in the vapor. Partial molar thermodynamic functions were calculated from the activity data for the $KCl\text{-}FeCl_2$ system.

The solid-liquid equilibria were studied by conventional cooling curves and differential cooling curves taken simultaneously on well-stirred samples. Petrographic and X-ray diffraction analysis helped identify the phases present in the solid state. The two systems differed markedly in the degree of complexity of the phase diagrams. The $KCl\text{-}FeCl_2$ system contained two well-defined compounds in the solid state, K_2FeCl_4 and $KFeCl_3$, as shown by both thermal results and diffraction results. Both compounds undergo solid transitions and are somewhat hygroscopic. The $LiCl\text{-}FeCl_2$ system showed continuous solid solution formation across the entire composition range of the diagram.

Total vapor pressure measurements in these systems were made by a "quasi-static" method which gave reliable and rapid data. In this method, the melt half-filled a small metal cell placed in a furnace. The cell included two vertical metal tubes, one leading to an intermittent pump and the other leading to a mercury manometer and inert gas reservoir. A sensitive differential manometer indicated the pressure difference between the two tubes. The apparatus was filled with an inert gas to a pressure greater than the expected vapor pressure and the furnace was brought to constant temperature. Successive portions of the inert gas were pumped out of the cell, sufficient time being allowed between withdrawals for the differential manometer to adjust itself. As long as the inert gas pressure was greater than the vapor pressure, no permanent difference in levels could be established in the differential manometer; when the inert gas pressure equaled the vapor pressure, a permanent difference was observed, and the inert gas pressure was read on the absolute manometer.

Total pressures for pure KCl, LiCl and $FeCl_2$ obtained with this method showed satisfactory agreement with literature values. In addition, total pressures over the entire composition ranges were determined in the two systems: $KCl\text{-}FeCl_2$ and $LiCl\text{-}FeCl_2$. In both cases, negative deviations from ideal behavior were observed; the deviations were greater in the $KCl\text{-}FeCl_2$ system than in the $LiCl\text{-}FeCl_2$ system. This difference was attributed to a difference in cation size.

Because of recent evidence for polymerization in alkali halide vapors, the total pressure measurements were combined with transportation measurements to give an average molecular weight for each of the pure salt vapors studied. The transportation apparatus was of quartz and consisted of an inert gas delivery tube connected to a cylindrical sample chamber. A concentric quartz tube inside the gas delivery tube served as a condenser for the salt vapor being removed from the sample holder. After temperature equilibration of the entire quartz assembly in a furnace, purified argon was passed through the delivery tube and over the sample melt contained in the holder. During this process the argon became saturated with salt vapor, and the gas-vapor mixture passed into the condenser where the vapor solidified. Thus stripped of vapor, the argon was collected in a Mariotte flask. The number of moles of argon was calculated from the observed temperature, pressure and volume of the entrapped gas. The average molecular weight of the vapor sample was then calculated using Dalton's Law in the form:

$$p_s = \left[\frac{\frac{w}{M}}{n_A + \frac{w}{M}} \right] P_T \quad ,$$

where

p_s = static pressure measured by "quasi-static" method,

w = weight of condensate collected,

M = average molecular weight of vapor,

n_A = moles of argon used during determination,

P_T = total pressure of argon-vapor mixture.

If only monomer and dimer species are known to be present in the vapor, partial pressures can be obtained directly from the average molecular weight; where higher polymers are known to exist, no information is obtained concerning specific partial pressures. Both KCl and $FeCl_2$ were shown to contain solely monomers and dimers; consequently partial pressures were calculated.

Mixtures in the two binary systems were studied using the combined total pressure and transportation data. The data in both systems could only be explained with the assumption of a vapor compound of the type $MFeCl_3$ (M = alkali cation). Direct mass spectrographic evidence was also obtained for a $KFeCl_2^+$ species in the vapor above an equimolar KCl-$FeCl_2$ sample, proving the existence of the $KFeCl_3$ compound in the vapor phase. From a combination of transportation data and total pressure data for the mixtures, along with equilibrium constants determined for the dimerization reactions of the pure salt vapors, values for the partial pressures of the KCl, K_2Cl_2, $KFeCl_3$, $FeCl_2$ and Fe_2Cl_4 species were obtained. Because of the existence of trimer molecules in LiCl vapor, no unique solution for the partial pressures could be obtained from similar LiCl-$FeCl_2$ data.

Thermodynamic activities were calculated from the monomer pressures obtained for the KCl-$FeCl_2$ system. The activity values corroborated the negative deviations observed previously in the total pressure measurements. Partial molar enthalpies and partial molar entropies were calculated from the activity data; these functions indicate that the negative deviations were both enthalpic and entropic in origin. In addition, activities obtained from vapor pressure measurements were shown to be consistent with activities calculated from the liquidus curves for the KCl-$FeCl_2$ system.

1. INTRODUCTION

OBJECTS AND DEFINITIONS

Thermodynamic investigations of fused salts have received attention in recent years, since the data obtained can be applied to a wide range of metallurgical equilibria. Of primary interest from a thermodynamic standpoint are the partial molar free energies of the various components in fused salt solutions. Since the absolute value of the free energy cannot be determined directly, the partial molar free energies are referred to an arbitrarily chosen standard state. Throughout this work the standard states are arbitrarily chosen to be the pure liquid salts comprising the binary solutions.

Partial molar free energies in solutions are most conveniently determined from experimental measurements of the activity, first defined by Lewis[1] as:

$$\bar{F}_i - F_i^0 = -RT \ln a_i \quad , \tag{1}$$

where

$\bar{F}_i$ = partial molar free energy of component i in the solution, kcal/mole,

F_i^0 = partial molar free energy of component i in the standard state, viz., pure liquid i at temperature T, kcal/mole,

T = absolute temperature, °K,

R = gas constant, cal/mole deg,

a_i = thermodynamic activity of component i in solution.

Thus, a determination of the activity of component i as a function of temperature and composition gives directly the partial molar free energy of component i, relative to the chosen standard state. From thermodynamics, it is also possible to obtain the partial molar entropies and partial molar enthalpies for the various components from the activity data thus obtained. As with the partial molar free energy, these partial quantities depend on the standard state chosen for the calculation.

The object of the present study was threefold:

1. determination of the activities of a divalent metal chloride, i.e., $FeCl_2$, in binary solutions with two alkali chlorides, i.e., KCl and LiCl, and to observe the effect of the change in alkali cation size on the activity of $FeCl_2$;
2. determination of the binary phase diagrams of the two systems and investigation of possible relationships between the observed solid crystal structure and the liquid structure;
3. determination of the existence and effect of vapor phase association on activities, based on partial pressure studies.

As discussed in the following sections, the desired activities were obtained from vapor pressure measurements on binary solutions prepared from pure salts.

THERMODYNAMICS BACKGROUND AND ACTIVITY CONCEPT APPLIED TO FUSED SALTS

Before a discussion of the experimental techniques available for activity determinations, it is advisable to complete the thermodynamic introduction and to show the method used for calculating partial molar enthalpies and entropies from activity data. In addition, the activity concept, as applied to the highly ionic fused salts under consideration, will be discussed further.

Consider the thermodynamic system formed by a solution of components designated by the subscript i. For convenience, the partial molar free energy of the ith component can be written as

$$\bar{F}_i - F_i^0 = F_i^m \quad .$$

Similarly, the partial molar entropy and partial molar enthalpy can be written as

$$\bar{S}_i - S_i^0 = S_i^m$$

$$\bar{H}_i - H_i^0 = H_i^m \quad .$$

Since

$$F_i^m = H_i^m - TS_i^m \quad , \tag{2}$$

for systems at constant pressure, and where the work done on mixing is only work of expansion,

$$\left(\frac{\partial F_i^m}{\partial T}\right)_P = -S_i^m \quad . \tag{3}$$

[1] G. N. Lewis, "Outline of a New System of Thermodynamics," *Z. physik. Chem.* 61, 129 (1908).

Substituting Eq. 3 into Eq. 2 yields

$$F_i^m = H_i^m + T\left(\frac{\partial F_i^m}{\partial T}\right)_P \quad . \tag{4}$$

Rearrangment gives

$$H_i^m = F_i^m - T\left(\frac{\partial F_i^m}{\partial T}\right)_P \quad . \tag{5}$$

Differentiation of Eq. 1 with respect to temperature yields

$$\left(\frac{\partial F_i^m}{\partial T}\right)_P = R \ln a_i + RT \frac{d \ln a_i}{dT} \quad . \tag{6}$$

Substitution of Eq. 6 into Eqs. 3 and 5 relates the partial molar enthalpies and entropies to the temperature dependence of the activities:

$$S_i^m = -R \ln a_i - RT \frac{d \ln a_i}{dT} \quad , \tag{7}$$

$$H_i^m = -RT^2 \frac{d \ln a_i}{dT} \quad . \tag{8}$$

It is often convenient to introduce the concept of an activity coefficient, defined by the equation

$$\gamma_i = \frac{a_i}{x_i} \quad , \tag{9}$$

where

γ_i = activity coefficient of component i in melt,

x_i = mole fraction of component i in melt.

While the activity coefficient may be difficult to interpret, as discussed by Wagner:[2] "The reason for the introduction of . . . activity coefficients is that in ideal mixtures, the activities equal the mole fractions. Numerous real systems . . . do not deviate from ideal behavior to a large extent and hence activity coefficients often represent relatively small correction factors." In addition, activity coefficients represent the most convenient method of comparing large deviations from ideal behavior, and serve to compact thermodynamic relations.

The concept of activity, defined by Eq. 1, was first introduced as an "effective concentration" for components in solution, and correlates the effect of the forces acting between component molecules. Consider two liquids, composed of molecules A and B. Attractive forces are present which bind the liquid molecules together, retarding evaporation. If the two liquids are mixed, three cases are possible,[3] depending on the magnitude of the forces between unlike species (A–B) compared to the forces between the pure liquids which are assumed equal (A–A and B–B):

1. A–B = A–A (or B–B)
2. A–B > A–A (or B–B)
3. A–B < A–A (or B–B)

The first case represents the ideal solution, where the relative binding forces between unlike species equal those between the pure components. Here, the effective concentration or activity equals the actual concentration of each component, and the activity coefficient is therefore unity for the whole range of composition. The second case represents negative deviations from ideal behavior. Since the forces between unlike species are greater than those between the pure molecules, each component is more tightly bound in solution than in the pure state. As an extreme case, compound formation may occur between A and B. Thus, the effective concentration or activity is smaller than the actual concentration, and consequently the activity coefficients are smaller than unity. In the third case, repulsions exist between unlike species, and the activities in solution are greater than the actual concentrations. In the extreme, an immiscibility gap may exist, whereby the solution actually breaks up into two liquid phases.

The foregoing discussion of the concept of activities applies only to solutions where the components exist as molecules. This is a serious simplification when applied to fused salt systems, where solutions are mainly ionic in nature, as evidenced from electroconductivity studies. Since a solution formed between two fused salts is ionic, the determination of activity can be interpreted as the determination of an effective concentration of the various ion species.

The first attempt to relate the activity of one component to the effective concentration of the

[2] C. Wagner, *Thermodynamics of Alloys*, Addison–Wesley, Cambridge, 1952.

[3] O. Kubachewski and E. L. Evans, *Metallurgical Thermochemistry*, 2d ed., Wiley, New York, 1956.

ions of that component is due to Herasymenko,[4] who defined the activity of one component as an ideal ionic mixture as follows:

$$(10)\quad a_{A_1^+B_1^-} = \left[\frac{n_{A_1^+}}{\sum_i n_{A_i^+} + \sum_i n_{B_i^-}}\right] \times \left[\frac{n_{B_1^-}}{\sum_i n_{A_i^+} + \sum_i n_{B_i^-}}\right] \gamma_{A_1^+B_1^-} ,$$

where

$a_{A_1^+B_1^-}$ = activity of component comprised of cation A_1 and anion B_1,

$n_{A_1^+}$ = number of cations A_1 in the solution,

$n_{B_1^-}$ = number of anions of B_1 in the solution,

$\sum_i n_{A_i^+}, \sum_i n_{B_i^-}$ = total number of cations and anions in the solution, respectively,

$\gamma_{A_1^+B_1^-}$ = activity coefficient of component $A_1^+B_1^-$.

This expression assumes that the ions are distributed at random in the melt, independent of charge. Clearly, this definition of activity can only be true at extremely high temperatures, where the random thermal motions of the ions can overcome the electrostatic repulsions between like ions.

A definite improvement in this definition was introduced by Temkin,[5] who defined activity as

$$(11)\quad a_{A_1^+B_1^-} = \left[\frac{n_{A_1^+}}{\sum_i n_{A_i^+}}\right]\left[\frac{n_{B_1^-}}{\sum_i n_{B_i^-}}\right]\gamma_{A_1^+B_1^-}$$

This model has a much more reasonable statistical basis. Because of attractive forces between anions and cations, each cation should have a cage of anions surrounding it, and vice versa. This signifies that the cations are arranged in a cation lattice, interpenetrated by a similar anion lattice. On the basis of the definition proposed by Temkin, each cation is considered to be randomly distributed throughout the cation lattice, with a similar random distribution of anions throughout the anion lattice. In this model, no provision is made for ions of different charges, cations being considered equivalent regardless of their valency state.

Temkin's model is sometimes interpreted in terms of the product of a cation fraction and an anion fraction, as:

$$(12)\quad a_{A_1^+B_1^-} = n_{A_1^+} \cdot n_{B_1^-} \cdot \gamma_{A_1^+B_1^-} .$$

From Eq. 11, the cation and anion fractions are then equal to

$$(13)\quad n_{A_1^+} = \frac{n_{A_1^+}}{\sum_i n_{A_i^+}} , \qquad n_{B_1^-} = \frac{n_{B_1^-}}{\sum_i n_{B_i^-}} .$$

A further refinement of this model was proposed by Flood *et al.*,[6] which provides for differences in cation and anion charge. They define an equivalent fraction equal to the ion fraction obtained when the number of moles of each species of ion is multiplied by the charge of the ion. As an example, the equivalent ionic fractions for solutions in the $KCl\text{-}FeCl_2$ system would be written as

$$(14)\quad n_{Fe^{++}} = \frac{2n_{Fe^{++}}}{n_{K^+} + 2n_{Fe^{++}}} , \qquad n_{K^+} = \frac{n_{K^+}}{n_{K^+} + 2n_{Fe^{++}}} , \qquad n_{Cl^-} = 1 .$$

[4] P. Herasymenko, "Electrochemical Theory of Slag-Metal Equilibria," *Trans. Faraday Soc.* 34, 1295 (1938).

[5] M. Temkin, "Mixtures of Fused Salts as Ionic Solutions," *Acta. Physicochim. (U.R.S.S.)* 20, 411 (1945).

[6] H. Flood, T. Forland, and K. G. Rjotheim, "Über den Zusammenhang Zwischen Konzentrationen und Aktivitäten in Geschmolzenen Salzmischungen," *Z. anorg. u. allgem. Chem.* 276, 289 (1954).

This assumes that the solution consists simply of K^+, Fe^{++}, and Cl^- ions. These concepts of cation fraction, anion fraction and equivalent ionic fraction will be used in later discussions.

METHODS FOR DETERMINING ACTIVITIES IN FUSED SALTS

In principle, activities can be derived experimentally from measurements of any equilibrium involving the solution and a gaseous or solid phase. The methods for determining activities in salt melts are similar to those used in aqueous and nonaqueous systems. These methods have been reviewed by various authors,[2,3] and a wide discussion of applicability will not be undertaken here. However, a brief outline of the general applicability of the methods will point out the desirability of using vapor pressure measurements on the systems studied in this work.

The four most widely used methods for the determination of activities are:

1. emf measurements on suitable galvanic cells, or on double concentration cells,
2. determination of liquidus curves of binary phase diagrams,
3. equilibrium studies involving salt-metal or salt-vapor equilibria,
4. determination of partial pressures of components of binary mixtures.

The emf methods generally require that a reversible chemical cell can be made which makes use of the reaction under consideration. Thus, the activity of $MgCl_2$ in mixtures of KCl can be measured from the emf of the following cell, as a function of the mole fraction of $MgCl_2(x_1)$:

$$Mg|MgCl_2(x_1),\ KCl(x_2)|Cl_2(\text{graphite}) \quad .$$

Extensive investigations[7] of such cells have resulted in activity values for the $MgCl_2$; activities of KCl in the melt can be obtained by applying the well-known Gibbs-Duhem rule. These activity values yield partial molar free energy values providing that the usual conditions are met, i.e., electrode reactions are reversible, purely ionic conduction occurs in the melts, and complete knowledge of the cation valence exists. Nearly all of the activities determined in this manner are for cations with a single valence state, e.g., Ag^+, Mg^{++}, Pb^{++}. Activities for compounds having a cation in an intermediate valence state, like $FeCl_2$, are more difficult to obtain from emf measurements since it is virtually impossible to create a single cell which completely avoids oxidation to the higher valence state. Markov[8] and Rempel and Ozeryanaya[9] have recently used cells with an over-all reaction utilizing the unsaturated halide, created by adding two separate cell reactions. The errors in such a procedure are proportionately larger than those occurring in one cell reactions. Consequently, reliable activity values covering a wide range of compositions have not been determined from emf measurements in molten salts containing lower oxidation states of many common cations.

Thermodynamic evaluation of the liquidus curve of binary phase diagrams yields activities of the pure component freezing out upon cooling, providing values for the heat of fusion of the pure salt are known. If the melting point T_m of a mixture of known composition can be determined, then the activity of the component freezing out in a pure form is given by

$$\ln a_i = \frac{\Delta H_f^i}{R}\left[\frac{1}{T_0} - \frac{1}{T_m}\right] \tag{15}$$

where

a_i = thermodynamic activity of i in solution,
ΔH_f^i = heat of fusion of pure component i,
T_0 = melting point of pure component i,
T_m = melting point of mixture,
R = gas constant.

These activity values are only valid at the equilibrium temperature T_m, and the activity at constant temperature can only be obtained if the partial molar heat of mixing is also known. If the mixtures freeze with the formation of solid solutions, the heat of fusion as a function of composition must

[7] B. F. Markov *et al.*, "Thermodynamic Properties of Magnesium Chloride in Alloys of $MgCl_2$-LiCl; $MgCl_2$-NaCl; $MgCl_2$-KCl; $MgCl_2$-RbCl," *J. Phys. Chem. (U.S.S.R.)* 29, 51 (1955).

[8] B. F. Markov, "Calculation of Thermodynamic Constants of Unsaturated Halides from EMF's and $\Delta T/\Delta E$ of Chemical and Daniel-Jacobi Cells," *J. Phys. Chem. (U.S.S.R)* 30, 1537 (1956).

[9] S. I. Rempel and I. N. Ozeryanaya, "The Series of Tensions for Heavy Non-Ferrous Metals and Their Sulfides in Molten Chlorides of Alkaline Metals," *J. Phys. Chem. (U.S.S.R.)* 25, 1181 (1951).

be known before activity values can be obtained, and in general, such heat values are not available. Thus even under favorable conditions, activity values obtained from liquidus curves are too limited in range to afford a complete thermodynamic description of a binary system.

Wagner[2] lists a number of equilibrium studies between fused salts and vapor phases which result in useful values for activities and activity coefficients. For example, Schutza[10] studied the activities of $CdCl_2$-$CdBr_2$ mixtures by means of halogen exchange equilibria:

$$CdCl_2 + Br_2 = CdBr_2 + Cl_2$$

These studies confirm the nonideality of such mixtures in agreement with previous emf measurements on the analogous $PbCl_2$-$PbBr_2$ system.[11] A similar fused salt–vapor equilibrium

$$KCl + Na = NaCl + K$$

was studied by Rinck[12] who was able to show approximately ideal behavior for KCl-NaCl mixtures, in agreement with many other investigators. Such equilibrium studies are most valuable for specific cases in which a conveniently studied reaction can be found, and have little general application.

The method promising to have most general applicability for the measurement of activities in fused salts is the measurement of partial pressures of the components over melts of known compositions. Experimental methods for studying vapor pressures are usually divided into either static or dynamic methods. The method best suited for a specific system depends on the range of pressure measurements and the number of volatile components. Static methods measure pressure directly, and can be used to determine activities directly only for systems where one species is present in the vapor. Thus, using a static method, Johnstone and coworkers[13] determined the vapor pressure of Fe_2Cl_6 from mixtures of $FeCl_3$-NaCl; since the ferric chloride dimer was the only volatile species, activities of $FeCl_3$ could be calculated based solely on these static pressure values. However, when more than one component is volatile, or when the vapors exist as mixtures of polymers, some provision must be made for sampling the vapor and determining its composition. Since static methods generally required a gas-tight cell, sampling of the vapor is often difficult to accomplish, and a dynamic method is chosen if vapor phase analysis must be made. The dynamic methods serve to sample the vapor under equilibrium conditions and hence provide values for the vapor composition. Jellinek and co-workers[14–16] have applied dynamic methods to many pure salts, and to some fused salt mixtures. If there is evidence of polymerized species in the vapor, it is necessary to combine the static data and dynamic data to obtain reliable values for partial pressures (see later discussion).

The significant feature of vapor pressure measurements in general is their wide applicability to fused salt systems. There are no restrictions on the valence state of the cations in the melt, and measurements can be taken over any temperature range of interest. In addition, many systems have inherently high vapor pressures, which hinders the use of other methods. In addition to the purely thermodynamic value of vapor pressure measurements, the data obtained provide information about the vapor phase above salt mixtures.

Early workers in the field, such as Jellinek, generally assumed that the salts were strictly monomeric in the vapor phase, and calculated vapor pressures from transportation data on this basis. In a few cases, agreement between static pressures and transportation pressures (using the monomer assumption) was so poor that the vapors could only be purely dimeric in nature. For example,

[10] H. Schutza, "Halogen Exchange Equilibrium in the $CdBr_2$-$CdCl_2$ System," *Z. anorg. u. allgem. Chem.* 239, 245 (1938).

[11] E. J. Salstrom and J. H. Hildebrand, "The Thermodynamic Properties of Molten Solutions of Lead Chloride in Lead Bromide," *J. Am. Chem. Soc.* 52, 4641 (1930).

[12] E. Rinck, "Equilibria Between Na-K Alloys and Molten Salts," *Ann. Chim. Justus Liebigs* 18, 395 (1932).

[13] H. F. Johnstone *et al.*, "The System Ferric Chloride–Sodium Chloride," *J. Am. Chem. Soc.* 64, 241 (1942).

[14] K. Jellinek and A. Golubowski, "Über die Dampfspannungen Geschmolzener Mischungen von $PbBr_2$ und $PbCl_2$ bei Höheren Temperaturen," *Z. physik. Chem.* A47, 464 (1930).

[15] K. Jellinek and B. Greiner, "Über die Dämpfe des Reziproken Salzpaares NaCl, KI, und der Binären Gemische $PbCl_2$, $PbBr_2$, $PbCl_2$, PbI_2," *Z. physik. Chem.* A165, 97 (1933).

[16] K. Jellinek and H. Hintz, "Über die Verdampfungsgleichgewichte der Binären Salzmischung $HgCl_2$-$HgBr_2$, sowie des Reziproken Salzpaares (Na, K) (Cl, Br)," *Z. Elektrochem.* 42, 187 (1936).

in vapors like Al_2Cl_6, Cu_2Br_2, agreement between static pressures and dynamic pressures could only be obtained if the species were assumed to be all dimer. Recent mass spectrometer information[17,18] and velocity distribution experiments[19] have conclusively exhibited appreciable amounts of dimer species in salt vapors heretofore thought to be strictly monomeric, e.g., KCl, NaCl, LiCl. In some cases, notably LiCl and NaF, appreciable amounts of trimerized species have been observed. In view of the possible complexity of the vapor phase under consideration, it is necessary to determine the equilibrium content of the various polymerized species for each *pure* component before the transportation data can be analyzed to yield partial pressures.

An additional complicating factor arises when the vapor phase is studied in order to obtain activities in the liquid mixtures. Recent vapor pressure measurements have required the existence of vapor phase compounds in order to obtain reasonable explanations of the observed transportation data. For example, Dewing[20] concluded that a vapor compound $NaAlCl_4$ exists above solutions containing 50 mole % $AlCl_3$. When the vapor phase above any salt solution is studied, the possibility of such vapor compounds between the pure components cannot be ignored. Provision for such a compound must be included in any calculation of partial pressures, if there is evidence for its existence.

A brief example using data obtained for pure $FeCl_2$ will show how the equilibrium polymer content is calculated from a combination of static total pressure and dynamic transportation measurements. In the transportation method, a known volume of a carrier gas such as argon is slowly passed over the salt held at temperature T; the saturated gas-vapor mixture is then passed into a condenser where the vapor is deposited. The vapor pressure of the ferrous chloride can be calculated by Dalton's Law of Partial Pressures:

$$p = \left[\frac{\frac{w}{M}}{n_A + \frac{w}{M}} \right] P_T \ , \tag{16}$$

where

p = vapor pressure of $FeCl_2$ at temperature T,

w = weight of $FeCl_2$ deposited in condenser,

M = molecular weight of $FeCl_2$ in vapor phase,

n_A = total moles of argon passed into condenser,

P_T = total pressure of argon-vapor mixture.

From experimental data, 389 mg of ferrous chloride was transported by 18.77 mmoles of argon at a total pressure of 736.1 mm. The liquid ferrous chloride under study was held at 829°C. If the vapor is assumed to be all monomer, the vapor pressure at this temperature would be, by Eq. 16,

$$p = \left[\frac{389}{126} \right] [736.1] \left[\frac{1}{18.77 + 389/126} \right]$$

$$= 105.8 \text{ mm} \ .$$

However, at 829°C the vapor pressure of ferrous chloride measured *directly* by total pressure methods was only 91.5 mm. If this total pressure is substituted in Eq. 16, an average molecular weight of ferrous chloride vapor can be calculated:

$$91.5 = \left[\frac{389}{\overline{M}} \right] [736.1] \left[\frac{1}{18.77 + 389/\overline{M}} \right] ,$$

whence

$$\overline{M} = 150 \text{ g} \ .$$

Using this average molecular weight, the equilibrium amounts of monomer and dimer can be obtained from the following relationship:

$$\overline{M} = 126x_1 + 252x_2 \ , \tag{17}$$

where

x_1 = mole fraction of monomer in vapor,

x_2 = mole fraction of dimer in vapor.

Substitution of the observed average molecular

[17] H. Rosenstock *et al.*, *Mass Spectra Studies of Silver Halides and Alkali Halides*, Paper No. 34, ASTM Committee E-14 on Mass Spectrometry, 4th Ann. Meeting, Pittsburgh, 1956.

[18] L. Friedman, "Mass Spectrum of LiI Vapor," *J. Chem. Phys.* 23, 477 (1955).

[19] R. Miller and P. Kusch, "Molecular Composition of Alkali Halide Vapors," *J. Chem. Phys.* 25, 860 (1956).

[20] E. Dewing, "Vapor Pressures of the System Sodium Chloride-Aluminum Chloride," *J. Am. Chem. Soc.* 77, 2639 (1955).

weight indicates the following values for the monomer and dimer mole fractions:

$$x_1 = 0.82$$
$$x_2 = 0.18 \ .$$

This method of calculation assumes that only monomer and dimer are present in the vapor. If the vapor contains appreciable amounts of more highly polymerized species, the above calculation of vapor mole fractions is incorrect, since it essentially considers trimers as one and one-half dimer molecules, etc. It is impossible to compute the equilibrium concentrations of more highly associated species from vapor pressure data alone. However, the value obtained for the average molecular weight is still correct even where higher polymer molecules are present.

As discussed earlier, vapor pressure methods in general are divided into two classes: static methods and dynamic methods. In the following paragraphs, the number of types of each method will be discussed, and their relative merits discussed. Three static pressure methods were considered for this work. The static apparatus chosen for the experimental work had to satisfactorily

1. measure pressures from 5–300 mm over a temperature range of 700–1100°C,
2. provide for rapid and convenient sample interchange, since a large number of samples required study,
3. function reliably and be readily fabricated.

Among the static methods which met the above requirements was a diaphragm method, devised by Osugi,[21] utilizing a unique null point detector. In this method, samples of mixtures were introduced into a chamber which was subsequently outgassed thoroughly and sealed closed. As the mixture was heated, the vapor pressure exerted extended a quartz diaphragm which could be brought back to the balance or null point by an applied external pressure. The quartz diaphragm formed one plate of a condenser, and any deflection of the diaphragm was measured very accurately in a bridge circuit. At a given temperature, the applied external pressure was slowly increased until the null point was reached, indicating that the external pressure equaled the vapor pressure. While the method was attractive because of the ease and speed of readings, difficulties in outgassing and instrumentation seemed certain.

Another static technique considered was the boiling point method first applied to salt vapor pressure determination by von Wartenburg.[22] In this method, the salt mixture was loaded into a cell which was first flushed and then filled with nitrogen or argon. The gas pressure was maintained at some desired pressure by a manostat, and the cell and melt were heated slowly. The temperature of the charge was followed by a thermocouple placed a short distance above the liquid surface. When the temperature curve indicated a halt, the mixture vapor pressure equaled the inert gas pressure, and the mixture began to boil. The temperature at the halt corresponds to the boiling temperature for the mixture under the applied external pressure. Outgassing problems are not present with this method, but the tendency for the liquid to superheat can lead to erroneous temperature values. For this reason, the boiling point method was not chosen. Bloom and Barton[23] have very recently developed a boiling point method in which the liquid is stirred by a slow gas stream introduced from the bottom of the cell. This method offers a simple way to avoid superheating, and should prove useful for salt mixture determinations.

A total pressure method developed by Rodebush and Dixon[24] for use on fused salt and liquid metal vapor pressures appeared to offer the best combination of advantages. In this technique (see Fig. 1), a metal cell contained the mixture under study, the cell being half filled by the liquid. Two tubes, B and C, connected to a sensitive differential manometer D outside the furnace (indicated by the dotted lines). Tube B was attached to an intermittent pump, while tube C was connected to a mercury manometer E and argon reservoir F. The cell was flushed and then filled with argon to a pressure greater than the expected vapor pressure, and the sample was brought to constant temperature. Successive portions of the gas were pumped off from tube B, sufficient time being allowed

[21] J. Osugi, "A Sensitive Diaphragm Method for Static Pressures," *Rev. Phys. Chem. Japan* 21, 86 (1951).

[22] H. von Wartenburg and P. Albrecht, "Die Dampfdrucke Einiger Salze," *Z. anorg. u. allgem. Chem.* 27, 162 (1921).

[23] J. L. Barton and H. Bloom, "A Boiling Point Method for Determination of Vapor Pressures of Molten Salts," *J. Phys. Chem.* 60, 1413 (1956).

[24] W. H. Rodebush and A. L. Dixon, "The Vapor Pressures of Metals: A New Experimental Method," *Phys. Rev.* 26, 851 (1925).

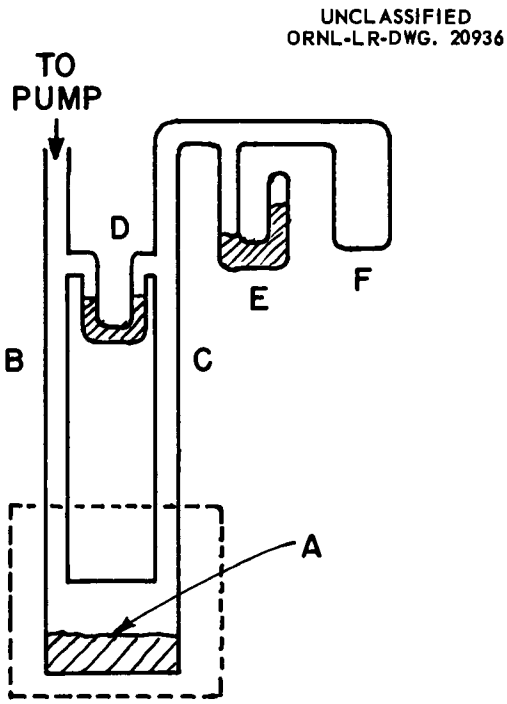

Fig. 1. Rodebush-Dixon Vapor Pressure Cell.

between withdrawals for the differential manometer to return to equilibrium. As long as the pressure of argon in C (measured by manometer E) was greater than the mixture vapor pressure, no permanent difference of the levels in D could be observed. When the pressure in C equaled the vapor pressure, a permanent difference in levels could be maintained in D. The permanent difference persisted since diffusion of the argon from tube C against the vapor streaming up the tube was the only means of relieving the pressure difference created between B and C by the pump. Diffusion under these conditions was slow. The total amount of vapor streaming up the tubes and condensing in the cooler portions was small, providing the argon pressure was not reduced appreciably below the vapor pressure.

This method is capable of good accuracy as shown by Rodebush and Dixon, who carefully checked its performance with mercury and obtained results in excellent agreement with previously accepted figures. In order to fix the pressure accurately at a given temperature, the pressure reading must be obtained when the difference of levels in D is as small as can be observed. Results obtained by this method[25] for the vapor pressures of many alkali halides have been accepted by Kelley[26] as the best data for these compounds. While the method had not been used for a number of years, recent work[27] on the vapor pressure of ThF_4 indicates renewed interest in this rapid and reliable experimental technique.

The Rodebush-Dixon method seemed eminently suited for the work reported here, since loading is simple, samples can be interchanged readily, and the experimental cell is easily fabricated. There are no outgassing problems, since the system can be flushed between single determinations if needed. Full details of the apparatus and experimental procedure are given in Chap. 4 of this report.

Since effusion techniques are applicable to the measurement of only very low pressures, it was necessary to use the carrier gas or transportation method to determine the vapor composition in the temperature and pressure range of interest. Three alternative transportation methods were potentially suitable. The first method, developed by Jellinek, has recently been applied by Sense[28] to the NaF-ZrF_4 system. Here a steady stream of argon entered a long tube placed in a tube furnace. The argon was slowly passed over the melt of interest, placed in the center of the tube and furnace, and held there at constant temperature. The gas swept out the equilibrium vapor and deposited it in a condenser extending from the end opposite the gas inlet. Chemical analysis of the condensate gave the amount of each component carried by the argon; from the total amount of argon passed and a knowledge of the vapor molecular weight, the partial pressures of each component can be determined. As in all transportation methods to be discussed, saturation was experimentally shown to exist at low but finite streaming rates.

The apparatus used by Sense had certain disadvantages, namely, the existence of cold zones at

[25] W. H. Rodebush and E. Fiock, "The Vapor Pressures and Thermal Properties of Potassium and Some Alkali Halides," *J. Am. Chem. Soc.* **48**, 2522 (1926).

[26] K. K. Kelley, "Free Energy of Vaporization and Vapor Pressures of Inorganic Substances," *Bull. 383, U. S. Bureau of Mines*, 1935.

[27] S. S. Yosim and T. A. Milne, *Vapor Pressure of ThF_4 and Some Other Properties*, NAA-SR-1603.

[28] K. A. Sense *et al.*, *Vapor Pressures and Derived Information of the Sodium Fluoride–Zirconium Fluoride System*, BMI-1064.

each end of the tube where vapor could continually condense, thereby depleting the liquid sample of the most volatile component. Also, no provision was made for the exchange of condensers during one heating cycle of the melt. A more efficient apparatus would allow exchange of condenser while the sample was maintained at experimental temperatures, thus allowing a number of condensate samples to be taken from a single melt. A useful modification of the Jellinek apparatus was developed by Fischer and Gewehr,[29] and provided for the desired condenser exchange. Further, a supplementary source of inert gas was also used to convey the saturated gas-vapor mixture from the cell into the condenser. During exchange of the condenser, this supplementary gas stream served to sweep out any atmospheric contamination from the cell, and also served to flush the condenser after insertion. Initially, this method was used in the present study, but it was discarded in favor of a simpler, more direct experimental arrangement which permitted condenser exchange without the complications of two inert gas supplies.

[29]W. Fischer and R. Gewehr, "Eine Neve Anordung zur Dampfdruckmessung bei der Mitführungsmethode," *Z. anorg. u. allgem. Chem.* **209**, 17 (1932).

The more convenient design (Fig. 2) closely resembled that developed by Wagner and Stein[30] and was used for the transportation data in this work. Argon was introduced into a quartz cell A through a long delivery tube B. After saturation with the salt vapor in bulb C, the gas-vapor mixture flowed into the condenser D placed inside the delivery tube of the cell proper. After depositing the vapor in the condenser, the argon flowed out of the condenser to a Mariotte flask where the total amount of argon passed during the determination was measured. During condenser interchange, argon streamed directly from the side delivery tube out through the end of the cell; this argon blanket served to sweep out any air which enters the cell during removal of the condenser. After insertion of a fresh condenser, another sample of the vapor was taken after temperature equilibrium had been reestablished. Full details of the apparatus and experimental procedures used are given in Chap. 5.

[30]C. Wagner and V. Stein, "Die Flüchtigkeit von Chromhalogeniden und über Gleichgewichte bei der Chromierung von Eisen," *Z. physik. Chem.* **192A**, 324 (1943).

UNCLASSIFIED
ORNL-LR-DWG. 20937

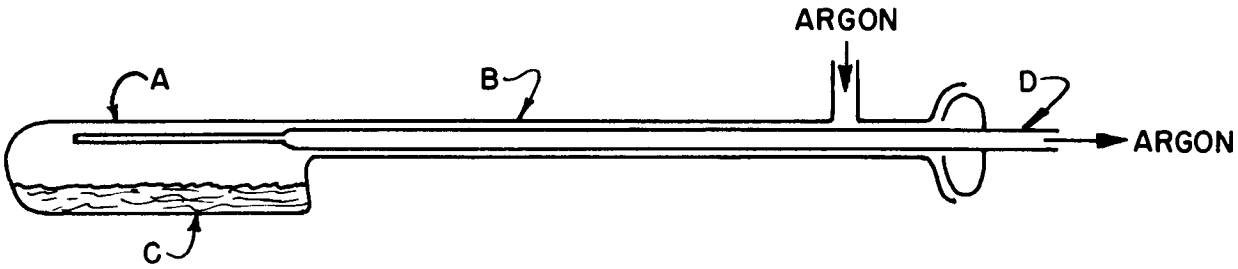

Fig. 2. Transportation Apparatus.

2. MATERIALS

POTASSIUM CHLORIDE

The potassium chloride used in this work was selected from crystals produced by slowly cooling after fusion under helium. J. T. Baker and Co. "Baker Analyzed" KCl was used as the starting material. The salt (mp = 772°C) was placed in a graphite crucible held in a nickel pot and heated slowly to 800°C under a steady flow of dry helium. After cooling, which caused segregation of impurities, the container was placed in a dry box, and the melt was cracked. The purest crystals were chosen on the basis of clarity and crystal appearance. A typical analysis of the KCl used was 51.8% K^+, 46.8% Cl^- (theo.: 52.5% K^+, 47.5% Cl^-). Spectrographic analysis showed less than 0.1% contamination from other alkali cations, and the aqueous solution was neutral, indicating no oxide contamination.

LITHIUM CHLORIDE

Initial attempts to purify LiCl by fusion under dry helium gave poor results. Analyses after purification by fusion showed Li_2O present, as evidenced by a high lithium content and by the alkalinity of aqueous solutions. The second purification procedure involved drying and fusing the LiCl under a steady stream of HCl. The LiCl used was J. T. Baker and Co. "Baker Analyzed" LiCl. The salt (mp = 613°C) was placed in a quartz flask which was heated slowly to 700°C, while a steady stream of HCl, dried with H_2SO_4, flowed through the LiCl. After temperature was reached, the reaction flask was purged with dry helium to remove the HCl and the remainder of the process described for KCl was followed. A typical analysis of the material thus obtained was 16.3% Li^+, 85.1% Cl^-, 0.5% H_2O (theo.: 16.3% Li^+, 83.7% Cl^-). Again, spectrographic analysis showed less than 0.2% contamination from other alkali cations, and the aqueous solution showed no alkalinity.

FERROUS CHLORIDE

Anhydrous ferrous chloride was prepared in a manner similar to that used for LiCl. Anhydrous $FeCl_2$ is very hygroscopic, forming a series of stable hydrates whose transition points are as follows:[31]

$$0 \xrightarrow[155^\circ C]{} 1 \xrightarrow[120^\circ C]{} 2 \xrightarrow[76^\circ C]{} 4 \xrightarrow[12^\circ C]{} 6$$

To prevent hydrolysis of the salt, an HCl atmosphere was maintained at all times during the actual drying process. Baker and Adamson "Baker Analyzed" $FeCl_2 \cdot 4H_2O$ was used as the starting material. Anhydrous HCl, dried with H_2SO_4, was passed through the tetrahydrate crystals which were slowly heated to 500°C. After thorough flushing at this temperature, the anhydrous $FeCl_2$ obtained was flushed with dry helium to purge the HCl from the reaction flask during the cooling period. The container was sealed and transferred to the dry box, where the anhydrous salt was recovered. A typical analysis of the $FeCl_2$ prepared in this manner was 44.7% Fe^{++}, 55.8% Cl^-, 0.5% H_2O (theo.: 44.1% Fe^{++}, 55.9% Cl^-). Spectrographic analysis showed 0.2% Mn, 0.02% Cu, with no other significant cation contaminants.

METHODS OF CHEMICAL ANALYSIS

Careful and accurate analysis of the salt condensates obtained from the transportation experiments was a prime requirement. The Analytical Chemistry Division of the Oak Ridge National Laboratory successfully completed all of the analyses required. The analytical techniques used for these salts are summarized below for reference.

Ferrous Iron and Total Iron

Ferrous iron and total iron was determined by standard redox titrations. Samples were dissolved in 5% H_2SO_4 to prevent any change in oxidation state of the iron. To determine ferrous iron, aliquot samples were titrated with potassium dichromate to a diphenylaminesulfonate end point. To determine total iron in the solution, an aliquot sample was withdrawn, and an excess of stannous chloride was added, reducing all the ferric iron to the ferrous state. The excess stannous chloride was oxidized by the addition of mercuric chloride. Sulfuric acid and phosphoric acid were added, and the total ferrous ion was titrated as before, using potassium dichromate with diphenylaminesulfonate as an indicator. Ferric iron present in the initial sample was calculated from the difference of the total iron titration and the ferrous iron titration.

[31] J. W. Mellor, *Inorganic and Theoretical Chemistry*, Vol. XIV, Sect. 36, p 9–40, Longmans, New York, 1935.

Potassium Ion

Potassium ion was determined gravimetrically as potassium tetraphenylboron, using a technique developed by Gloss.[32] An aliquot sample containing 8–15 mg of potassium ion was generally used. Sodium hydroxide was added until the solution was just alkaline; then 5–10 ml of a citric acid–sodium carbonate buffer (pH = 2.8 to 3.0) was added. The solution was warmed to 75–80°C, and about 30 ml of sodium tetraphenylboron solution (1.5 g/250 ml) was slowly added. The solution was cooled, filtered, and the filtrate was dried and weighed. Potassium ion content was then calculated from the weight of precipitate. This technique is specific for potassium, rubidium and cesium. Since spectrographic analysis of the potassium chloride used in this work indicated no contamination from rubidium or cesium, the tetraphenylboron precipitate was considered to contain only the potassium salt.

Lithium Ion

Lithium chloride can be determined in the presence of potassium and sodium ion by virtue of its specific solubility in anhydrous 2-ethylhexanol.[33] The procedure followed has been reported by Goldberg and White.[34] Samples are dissolved in 2.5% sulfuric acid, and a 5-ml aliquot was generally taken. To the aliquot is added Dowex-2 resin, converted to the hydroxide form by previous equilibration with sodium hydroxide. The resin is added to the solution and the resulting slurry is stirred until slightly alkaline. This converts the lithium chloride to lithium hydroxide. The solution is passed through a column containing the Dowex-2 hydroxide resin, and the column is washed until neutral, the washings being added to the solution. This ensures complete conversion of the chloride to the hydroxide. The total hydroxide of the solution is now titrated with HCl to a methyl red end point. Any sodium or potassium ion present in the sample will contribute to the hydroxide total at this point.

After titration with HCl, the solution is reduced in volume by boiling and 25 ml of 2-ethylhexanol is added. The solution is then heated to 135°C to drive off the water. Under these conditions, KCl and NaCl salt out of the solution; these salts were removed by filtration through a dry frit. Lithium chloride is then titrated in the 2-ethylhexanol solution with silver nitrate to the (usual) silver thiocyanate end point. Since the samples used in this work contained only lithium chloride, the hydroxide step generally served as a check on the final titration. Occasional trace contaminations of sodium and potassium were noted.

Chloride Ion

Chloride analyses were accomplished by well-known methods. For chloride analyses of the transportation samples, titration to a turbidimetric end point with mercuric nitrate to a nitroprusside end point was used. For chloride analyses of pure salt samples, the standard gravimetric method using silver nitrate was used.

---

[32] G. H. Gloss, "A Gravimetric Determination of Potassium Ion," *Chemist Analyst* 42, 50 (1953).

[33] E. R. Caley and H. D. Axelrod, "Anhydrous 2-Ethyl Hexanol as a Specific Extractant for Alkali Chlorides," *Ind. Eng. Chem., Anal. Ed.* 14, 242 (1942).

[34] G. Goldberg and J. C. White, "Application of the Volhord Method Titration to the Determination of LiCl Using 2-Ethyl Hexanol," *Anal. Chem.* 27, 1188 (1955).

3. DETERMINATION OF CONDENSED PHASE DIAGRAMS

INTRODUCTION

As discussed earlier, thermodynamic evaluation of the liquidus curves of binary phase diagrams yields values for the activity of the pure component freezing out upon cooling. The deviation of liquid activities from ideality can sometimes be correlated with the stoichiometry and crystal structures of the solid phases appearing in the binary system. In any case, it is of interest to compare the possible structural units and coordination numbers in the liquid and solid at the same composition.

No published information was available concerning the phase diagram for the condensed binary systems: $KCl\text{-}FeCl_2$ and $LiCl\text{-}FeCl_2$. Therefore, the investigation of these systems was undertaken. The phase diagrams were determined by conventional cooling and differential cooling curves, taken simultaneously from well-stirred mixtures. The somewhat novel use of differential cooling techniques coupled with simultaneous conventional cooling curves helped greatly in the determination of the liquidus temperature for small sample loads. Solid transformations occurring upon cooling were also easily identified by this method (see below).

APPARATUS

The apparatus had to be easy to load under dry-box conditions and had to provide for agitation or stirring of the liquid to prevent supercooling. To allow X-ray and petrographic examination of the condensed phases, the slowly cooled samples had to be easily recovered, and an inert gas blanket was needed to prevent oxidation of ferrous chloride. Since molten chlorides can be contained in glass, the apparatus was designed to employ commercially available test tubes. The use of glass test tubes also permitted visual observation of the melts during cooling. The final design of the apparatus is shown in Fig. 3.

The melts were contained in a Vycor test tube A, 25 mm ID and 200 mm long. The tube was capped by a graphite plug B which contained a nickel paddle C mounted on a 0.125-in. nickel rod, and a nickel thermocouple well D, 0.12 in. OD and 0.10 in. ID. In order to obtain both differential and direct cooling curves, the thermocouple well contained two 28 gage Chromel-Alumel thermocouples insulated with pyrex fabric. The graphite plug also held gas inlet and exit tubes E through which an argon purge stream was passed. The graphite plug was sealed to the Vycor tube by pressure sensitive polyethylene tape. The entire Vycor tube assembly rested in a nickel block, or heat sink, containing a thermocouple hole G into which a 24 gage Chromel-Alumel thermocouple was placed. The stirring paddle was driven by a low speed stirring motor H.

MATERIALS

The materials used for the phase diagram investigations were purified by the methods discussed in Chap. 2. After purification, the salts were stored in an argon dry box for later use. Because of the hygroscopic nature of the salts used, all loading and sampling procedures were performed in the dry box. Samples were loaded by the procedure discussed below. At the completion of a series of cooling and heating cycles, the sample tube was returned to the dry box, where the tube was broken and the entire melt sample was recovered. Each melt was ground and homogeneized, with a small sample for X-ray analysis being mounted in a Plexiglas holder, covered by a ½ mil polystyrene window. The remainder of the sample was stored for future use. Both X-ray and petrographic analysis was done on the sample melts to differentiate clearly the phases present.

PROCEDURE

The mixture to be used for a cooling curve was weighed into the Vycor tube inside the argon dry box. Generally a 40-g sample was ground and used. The nickel stirrer and thermocouple well were inserted into the powdered sample; then the graphite plug was attached to the tube with the plastic tape. The entire assembly was placed in the nickel block inside a Hoskins pot furnace. Argon, dried over $MgClO_4$ and purified over Cu^0 at 500°C, flowed through the sample tube for thirty minutes before heating was started. Samples were heated until visual observation indicated complete melting had occurred; then the stirring motor was attached and the cooling curve was begun. Generally, two heating and cooling cycles were followed by this technique to eliminate supurious effects.

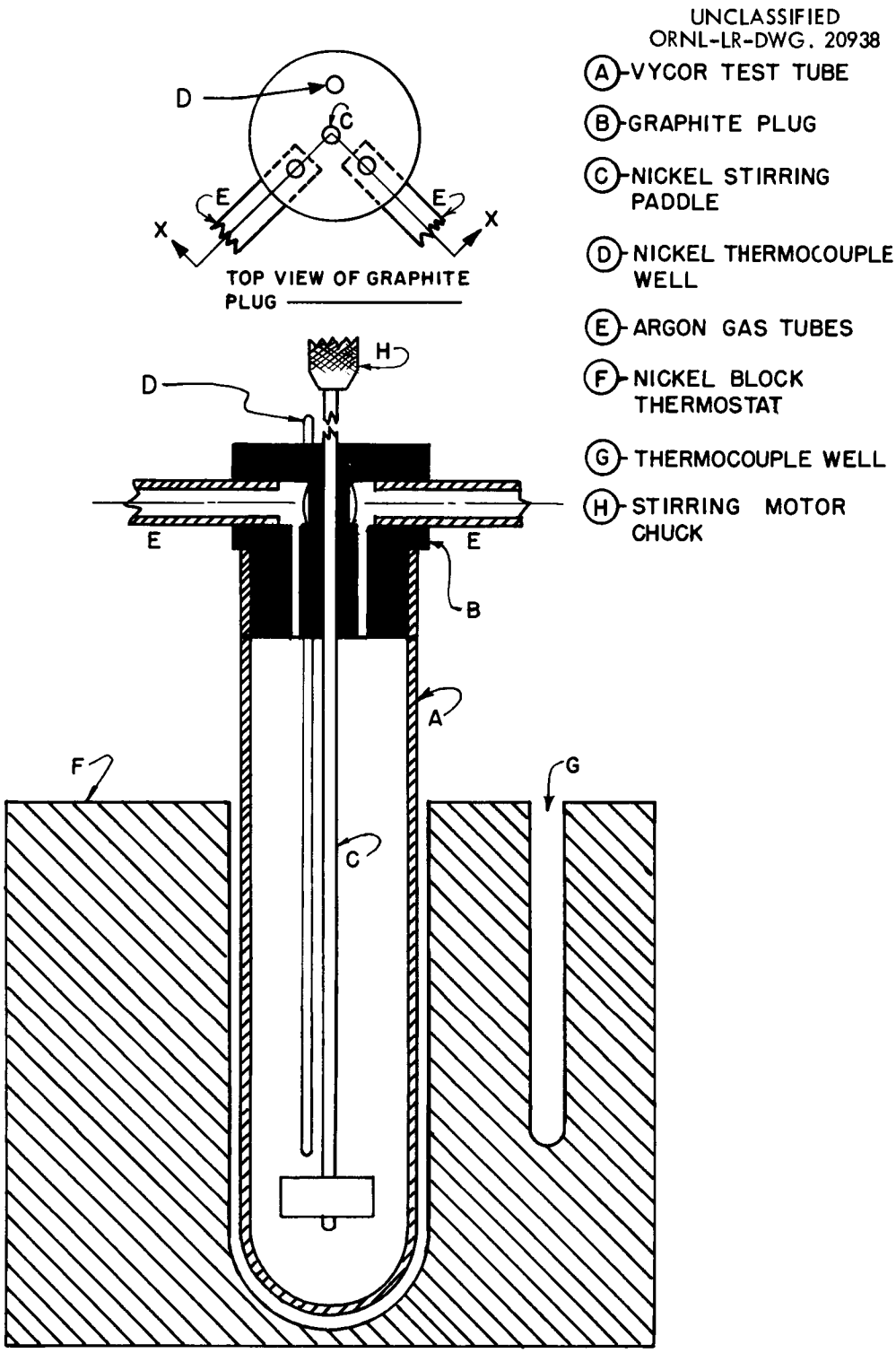

Fig. 3. Cooling Curve Apparatus.

The cooling behavior of the stirred melt was followed on a Brown Electronik recorder. One of the thermocouples inside the nickel thermocouple well (see Fig. 3) was used to follow the simple cooling behavior, while the other thermocouple in the same well was connected to a Brown Electronik differential recorder. This differential recorder measured the difference in temperature between the melt thermocouple and the thermocouple placed in the well in the nickel heat sink. This differential temperature method was very sensitive to small heat effects occurring in the melts; by synchronizing the time scales of the two Brown recorders, a sharp indication of the temperature of these effects was obtained.

An actual pair of simultaneous differential cooling and conventional cooling curves is reproduced in Fig. 4, showing the experimental cooling behavior of a 41% $FeCl_2$–59% KCl mixture. The superposition of the differential curve on the conventional curve aided in the determination of the liquidus temperature as well as the solid transformation temperatures. In a number of mixtures, solid transformations could not have been observed from the simple cooling curve alone.

EXPERIMENTAL RESULTS

The binary phase diagram for the KCl-$FeCl_2$ system is shown in Fig. 5. The diagram is complicated by the presence of two well-defined compounds: K_2FeCl_4 and $KFeCl_3$. The 2:1 compound melts incongruently, and undergoes a solid transformation at 255°C. The 1:1 compound melts congruently, at 400°C, and undergoes a solid transition at 300°C. Optical and X-ray properties of these two compounds are summarized in Appendix A. While there is evidence[31] that both these compounds have been prepared as the dihydrates, only K_2FeCl_4 has been reported previously as the anhydrous salt. The X-ray diffraction patterns and optical properties for these two compounds are given in Appendix A.

The coordination number of the ferrous ion in these compounds can be tentatively assigned. Solid $FeCl_2$ is isomorphous with $CdCl_2$ and $MgCl_2$, as indicated by the formation of continuous solid solutions[31] between these salts and the similarity between the X-ray diffraction patterns of the salts. Thus, solid ferrous chloride has a layered structure, as shown in Fig. 6. The Fe^{++} ion is surrounded by six Cl^- ions, and each Cl^- ion is in contact with three Fe^{++} ions on one side and three Cl^- ions on the other. The empirical crystal radii, as given by Goldschmidt, are: 1.81 for Cl^- and 0.75 for Fe^{++}, giving a radius ratio of 0.41. For a radius ratio above 0.414, simple geometric calculations (taken from Wells, *Structural Inorganic Chemistry*, 2d ed., Oxford Press, London, 1952) assuming the ions to be hard spheres indicate that a coordination number of 6 is most stable, while lower values of the radius ratio favor the coordination number 4. This explains the sixfold coordination of ferrous chloride in the solid state. However, the borderline value of the radius ratio relative to that for stable sixfold coordination makes reasonable the assumption that the coordination will be fourfold in the less dense liquid state.

It is not possible to definitely assign the crystal structure of the two compounds observed in the KCl-$FeCl_2$ system. It is likely that $KFeCl_3$ forms a distorted perovskite structure. The relative size difference between the K^+ ion (r = 1.33Å) and the Cl^- ion (r = 1.8Å) does not permit a close-packed cubic lattice of the AB type (as in $KMgF_3$). The X-ray pattern observed for this compound does not correspond to a cubic lattice. There is undoubtedly distortion of the close-packed lattice, resulting in a lower symmetry for the crystal form, perhaps of the orthorhombic or tetragonal type.

The binary phase diagram for the LiCl-$FeCl_2$ system is shown in Fig. 7. Compared to the previous diagram it is strikingly simple. A continuous series of solid solutions are formed between these two salts which is surprising in view of the dissimilarities usually considered to exist between the crystal structures of the two salts; LiCl crystallizes in a cubic or rock-salt lattice, while $FeCl_2$ has a hexagonal layered lattice. However, as discussed by Hückel,[35] there actually exists a great deal of similarity between these two salts. In the ferrous chloride lattice, the large Cl^- ions are in a close-packed cubic array, with the small Fe^{++} ions placed in one-half of the available octahedral sites. This results in a layered structure, with the layers being held together rather loosely by Van der Waal's forces. Similarly, the lithium chloride lattice may be considered a close-packed cubic array of the large Cl^- ions, with the much smaller Li^+ ions

[35] W. Hückel, "Structural Chemistry of Inorganic Compounds," p 731, Elsevier, New York, 1951.

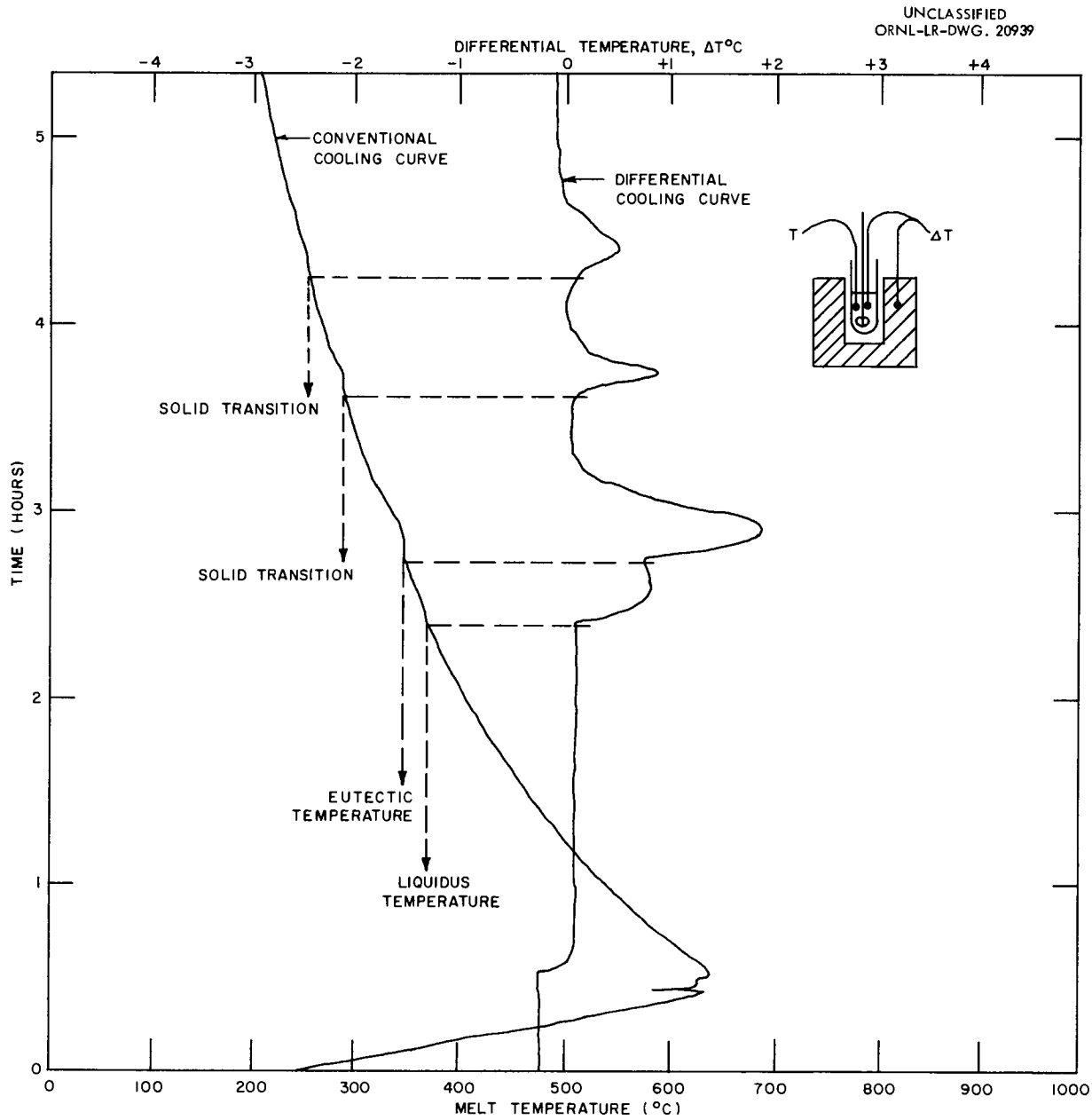

Fig. 4. Cooling Curves Obtained for 41% $FeCl_2$–59% KCl Mixture.

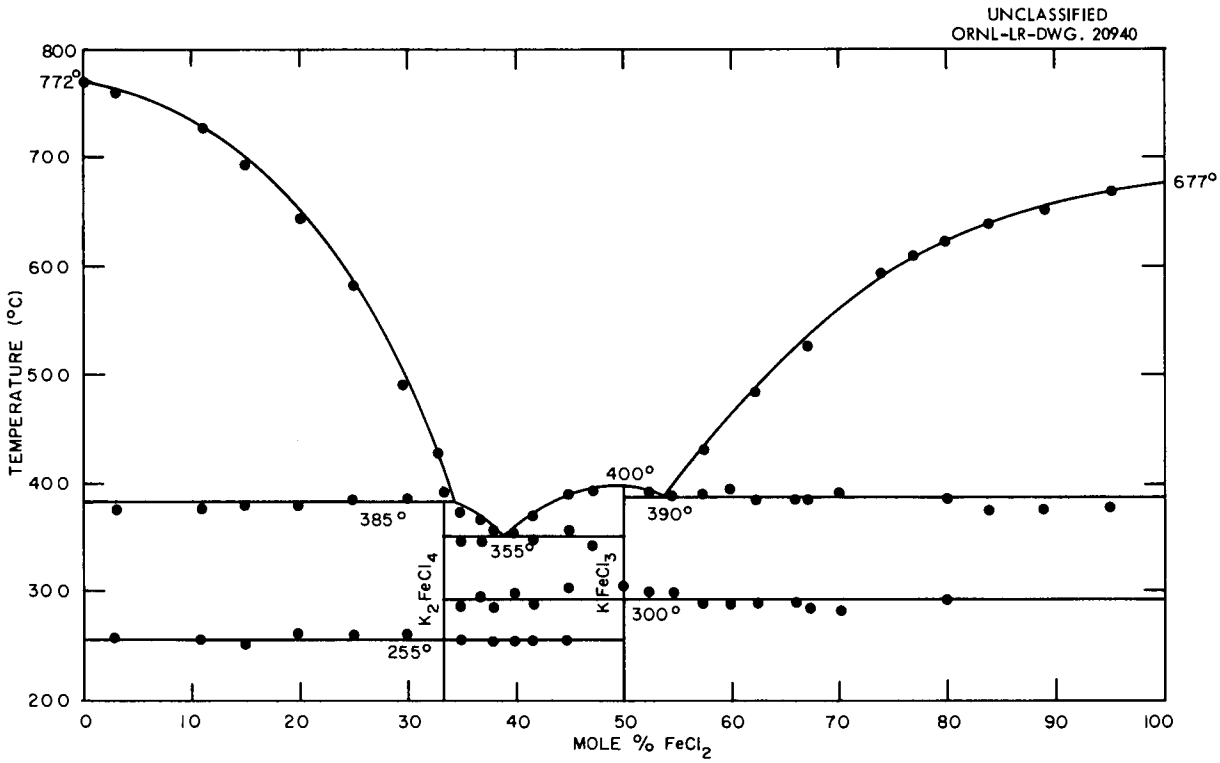

Fig. 5. The $FeCl_2$-KCl System.

filling all the available octahedral holes. Thus, the Cl^- ions in both crystals form a close-packed cubic lattice. The formation of a continuous solid solution between these two salts can occur simply by filling the interstitial holes in the chloride lattice at random, in one case, by two Li^+ ions, and in the other, by an Fe^{++} ion (leaving the second available hole unoccupied).

The thermal data obtained on this system could only be explained by the formation of a continuous series of solid solutions. In addition, X-ray analysis yielded results that were in agreement with the observed solid solution formation. Petrographic examination indicated that a homogeneous crystal form existed throughout the system, again indicating that no two-phase regions were present.

THERMODYNAMIC EVALUATION OF THE PHASE DIAGRAMS

As discussed in Chap. 1, activities may be calculated from the liquidus curves obtained for the two systems under study. Providing there is no solid solution formation, the activity of a component first freezing out upon cooling can be obtained from the liquidus temperature and the heat of fusion for the component:

$$\ln a_i = \frac{\Delta H_f^i}{R}\left[\frac{1}{T_0} - \frac{1}{T_m}\right] . \qquad (1)$$

The following heat of fusion values were obtained from a critical compilation by Kelley:[36] 6.1 kcal/mole for KCl, and 10.3 kcal/mole for $FeCl_2$. Using these heat of fusion values and the experimentally determined liquidus curves for the KCl-$FeCl_2$ system (Fig. 5), it is possible to estimate activities up to the respective eutectic and peritectic composition. A plot of the activity of KCl and $FeCl_2$ is given in Fig. 8. The standard state on which the activity values are based is chosen as the pure liquid salt at temperature T.

[36] K. K. Kelley, "Evaluation of the Heats of Fusion of Metals and Metal Compounds from Data on Freezing Point Lowering," *Bull. No. 393, U. S. Bureau of Mines* (1936).

UNCLASSIFIED
ORNL-LR-DWG. 20941

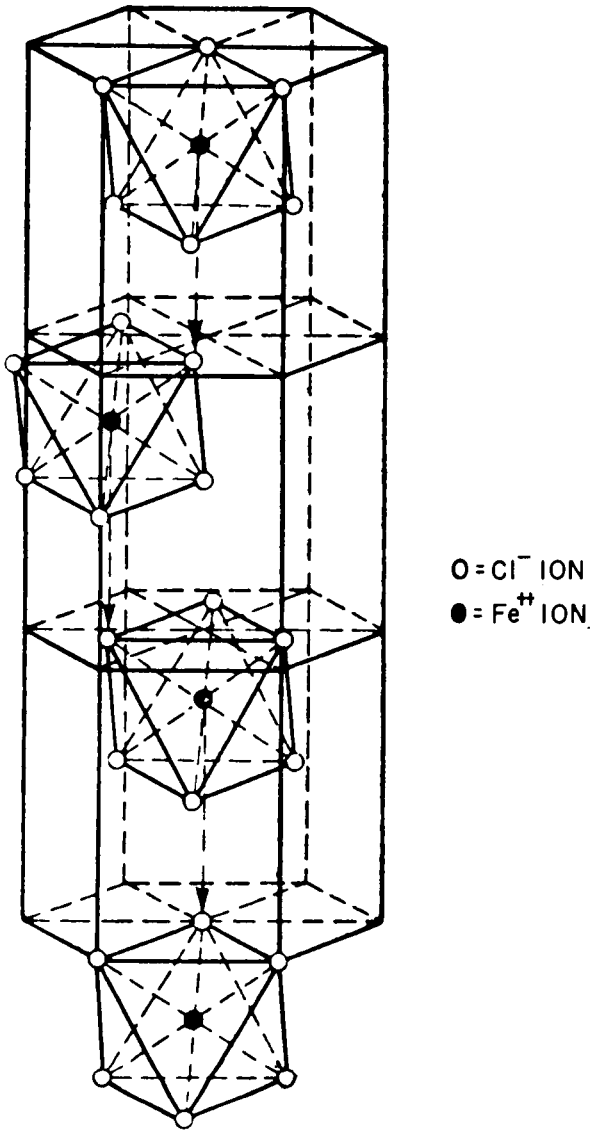

Fig. 6. Crystal Structure of Ferrous Chloride.

A recent model, proposed by Flood and Ürnes,[37] gives an insight into the structure of the liquid in this system and to the entropy changes occurring on mixing. Referring to Chap. 1, it was seen that the activity of a component in a fused salt melt could be written as a product of an anion and cation fraction:

$$a_{A_1^+B_1^-} = n_{A_1^+} \cdot n_{B_1^-} \cdot \gamma_{A_1^+B_1^-} \quad . \tag{2}$$

For structural reasons discussed earlier, it seems reasonable that the Fe^{++} ion exists in the liquid in a fourfold coordination state. This fourfold coordination is assumed to occur in the following manner:

$$2K^+ + 2Cl^- + FeCl_2 = 2K^+ + FeCl_4^{--}$$

Thus, if $FeCl_2$ is added to a lattice arrangement of K^+ ions and Cl^- ions, this model proposes that dissolution occurs with the formation of the complex ion $FeCl_4^{--}$. The ionic fractions for the K^+ and Cl^- ions can then be written as follows:

$$n_{K^+} = \frac{n_{K^+}}{n_{K^+}} = 1$$

(3)

$$n_{Cl^-} = \frac{n_{Cl^-}}{n_{Cl^-} + n_{FeCl_4^{--}}} = \frac{n_{KCl} - 2n_{FeCl_2}}{[n_{KCl} - 2n_{FeCl_2}] + n_{FeCl_2}}$$

and substitution of these values into Eq. 2 above yields:

$$a_{KCl} = n_{K^+} \cdot n_{Cl^-} \cdot \gamma_{KCl} = \left[\frac{n_{KCl} - 2n_{FeCl_2}}{n_{KCl} - n_{FeCl_2}}\right] \gamma_{KCl} \quad . \tag{4}$$

As a first approximation, the activity coefficient is set equal to unity. A plot of the KCl activity calculated according to Eq. 4 is shown in Fig. 8, along with the activity determined directly from the liquidus curve of the binary phase diagram. It is seen that the activity based on the assumed complex formation agrees very well with the experimentally determined curve. Other complexes with less probable structures yield activity curves showing large deviations from the experimental curve.

A similar expression can be developed for the activity of $FeCl_2$, based on the assumption of complex formation. Assuming that the addition of

[37] H. Flood and E. Ürnes, "Calculation of the Activities in Magnesium Chloride–Alkali Chloride Melts from Structure Models," *Z. Elektrochem.* 59(a), 834 (1955).

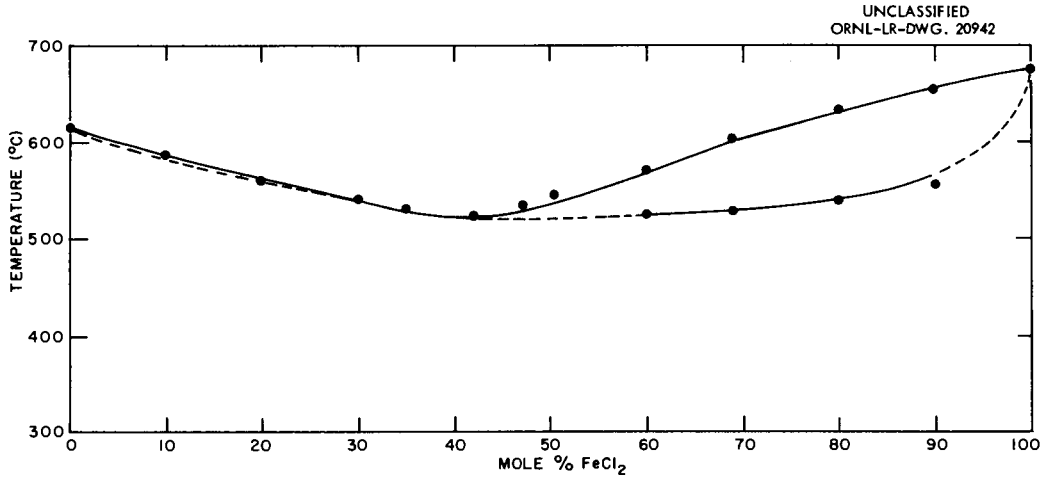

Fig. 7. The $FeCl_2$-LiCl System.

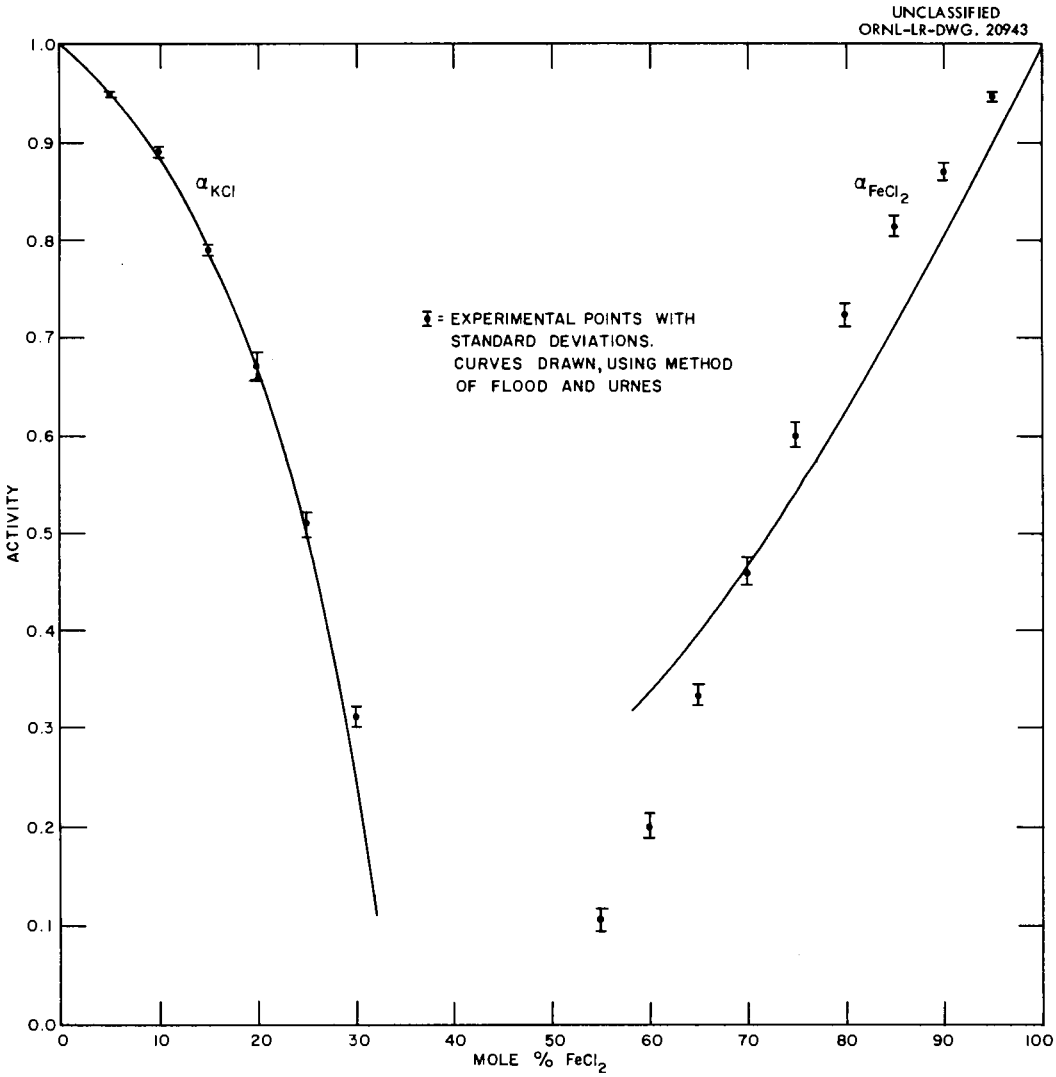

Fig. 8. Activities of KCl and $FeCl_2$ from Liquidus Curves.

KCl transfers the ferrous ions into four-coordinated complex ions, the following equilibrium exists:

$$2KCl + Fe^{++} + 2Cl^{-} = 2K^{+} + FeCl_4^{--}$$

Thus, the melt on the $FeCl_2$-rich side consists of four ion species: Fe^{++}, Cl^{-}, K^{+}, and $FeCl_4^{--}$. The ionic fractions are given by the following expressions:

$$n_{Fe^{++}} = \frac{n_{Fe^{++}}}{n_{Fe^{++}} + n_{K^{+}}} = \frac{n_{FeCl_2} - \frac{n_{KCl}}{2}}{n_{FeCl_2} + \frac{n_{KCl}}{2}}$$

$$n_{Cl^{-}} = \frac{n_{Cl^{-}}}{n_{Cl^{-}} + n_{FeCl_4^{--}}} = \frac{2n_{FeCl_2} - n_{KCl}}{2n_{FeCl_2} - \frac{n_{KCl}}{2}}.$$

Substitution of these values into Eq. 12, Chap. 1, written for the activity of ferrous chloride gives:

$$a_{FeCl_2} = n_{Fe^{++}} \cdot (n_{Cl^{-}})^2 \gamma_{FeCl_2}$$

$$a_{FeCl_2} = \left[\frac{n_{FeCl_2} - \frac{n_{KCl}}{2}}{n_{FeCl_2} + \frac{n_{KCl}}{2}}\right] \left[\frac{2n_{FeCl_2} - n_{KCl}}{2n_{FeCl_2} - \frac{n_{KCl}}{2}}\right]^2 \gamma_{FeCl_2}.$$

Again, assuming $\gamma = 1$, the activity curve calculated from this expression is shown in Fig. 8, along with the experimentally determined activity points.

It is seen that this model overestimates the amount of negative deviation for the ferrous chloride activity. Flood and Ürnes have proposed enthalpic correction factors entering into the activity calculation in the γ term which help correct this discrepancy. The assumption of unit activity coefficient assumes that no such enthalpic effects occur upon mixing $FeCl_2$ and KCl.

Since this model only claims a greatly simplified picture of the melt, it seems unnecessary to pursue further the theoretical enthalpy effects proposed by Flood and Ürnes. The activity values based on the liquidus curves can be compared in Chap. 8 with the activities obtained from vapor pressure determinations.

4. TOTAL VAPOR PRESSURE MEASUREMENTS: RODEBUSH METHOD

THEORY OF THE RODEBUSH METHOD

The development of the Rodebush method involves a mathematical treatment similar to that used by W. Gäede[38] in his discussion of the Gäede diffusion pump. The development given by Rodebush and Dixon,[24] while complete, requires amplification of some essential points.

A useful outline of the mathematical treatment of the Rodebush method is:

1. Steady state pressure conditions in the vapor reflux (gas) tubes of the Rodebush cell are established by using Poiseuille's equation for gas flow in combination with a differential equation for flow conditions in the tubes.
2. For a typical case, the steady state pressures in the cell are evaluated and plotted.
3. The rate of inert gas flow through the tubes as the total inert gas pressure is lowered is examined for typical experimental conditions. It is shown that a permanent inert gas pressure difference can be maintained between the two tubes under special conditions.
4. The vapor flow rate up the tubes (as the total inert gas pressure is lowered) is also examined, and is shown to be negligible under normal experimental operating conditions.
5. Important considerations are summarized for the best operating conditions.

Development of Steady State Pressure Conditions

Consider the cell drawn in Fig. 9 containing a salt melt in the bottom as shown. Attached to the cell proper are two vertical gas tubes, 3–4 mm in diameter. The salt melt in the cell exerts a vapor pressure, p_v, corresponding to the temperature T of the cell. The cell proper and gas tubes from B to A are assumed to be at temperature T. At point A, the temperature is assumed to drop very sharply, causing complete condensation of the vapor.

Thus,

$$p_{vB} = p_v \qquad (1)$$
$$p_{vA} = 0 \ ,$$

where

p_{vB} = vapor pressure at B, dyne/cm^2 ,

p_{vA} = vapor pressure at A, dyne/cm^2 .

Clearly, condensation at A creates a pressure gradient in the tube such that vapor flows up the tubes at a constant rate equal to the rate of condensation at A.

Now, consider that the gas tubes are also filled with an inert gas, i.e., argon, diffusing from A to B against the flow of vapor. At point A the total pressure in the tubes equals the pressure of inert gas, since the vapor pressure at A is assumed to be zero. Using symbols, the total pressure at A is:

$$P_{\text{total } A} = P_{iA} + p_{vA} \ , \text{ but } p_{vA} = 0 \ ;$$

whence

$$P_{\text{total } A} = P_{iA} \ , \qquad (2)$$

[38] W. Gäede, "Die Molekularluft Pumpe," *Ann. Physik* 46, 357 (1915).

UNCLASSIFIED
ORNL-LR-DWG 20698

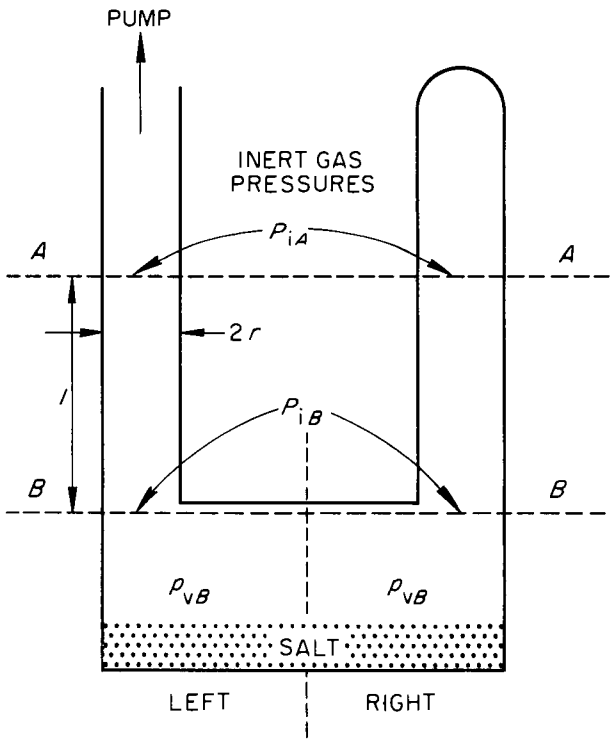

Fig. 9. Schematic Representation of Pressures in the Cell.

where

P_{iA} = inert gas pressure at A, dyne/cm^2 .

Similarly, the total pressure at B will equal the sum of the partial pressures of inert gas and vapor:

(3) $$P_{\text{total } B} = P_{iB} + p_{vB} ,$$

where

P_{iB} = inert gas pressure at B, dyne/cm^2 .

Under normal operating conditions, the total pressure at B is always slightly greater than the total pressure at A, giving rise to a flow of vapor up the tube to A where condensation occurs. This flow of vapor can be expressed by the dynamic equation for gas flow in small bore tubes:

$$\frac{dn}{dt} = \underbrace{\frac{\pi r^4}{8\eta\, lRT} P_{av}(\Delta P)}_{\text{Viscous Flow}} + \underbrace{\frac{\pi r^3}{2lRT} \int_{P_2}^{P_1} \frac{P}{\epsilon}\, dP}_{\text{Molecular Flow}} .$$

It has been shown[39] that for pressures greater than 5 mm, the molecular flow term in the dynamic equation is completely negligible. For all experimental conditions used in this work, the total pressure in the tubes was never less than 5 mm, and thus the flow equation reduces to the simple Poiseuille equation for viscous laminar flow:

(4) $$\frac{dn}{dt} = \dot{n}_v = \frac{\pi r^4}{8\eta\, lRT} P_{av} \Delta P ,$$

where

$\dot{n}_v$ = flow rate of vapor from B to A, mole/sec,

r = radius of tube, cm,

l = length of tube, cm,

η = viscosity of vapor, dyne sec/cm^2,

R = gas constant, dyne cm/mole °K,

T = temperature in tube, °K,

P_{av} = average total pressure in tube from B to A, dyne/cm^2,

ΔP = difference in total pressure from B to A, dyne/cm^2.

From Eqs. 2 and 3, we see:

$$\Delta P = P_{\text{total } B} - P_{\text{total } A} ,$$

or

(5) $$\Delta P = p_{vB} + P_{iB} - P_{iA} .$$

Substituting Eq. 5 into Eq. 4 yields:

(6) $$\dot{n}_v = \frac{\pi r^4}{8\eta lRT} P_{av}(p_{vB} + P_{iB} - P_{iA}) .$$

This is the equation for the net flow of vapor under any pressure conditions that exist in the tube. It is independent of position in the tube, since the rate at which vapor enters and flows up the tube must equal the rate at which it condenses at A. It is also applicable to transient conditions where the pressures change with time, and to steady state conditions where the pressures are time-independent. For transient pressure surges in the tubes, both vapor and inert gas will flow and relieve transient pressure differences. However, at steady state, the inert gas flow is zero; that is, the diffusive flow of inert gas from A to B is just balanced by the mass flow of inert gas from B to A. In order to solve for the pressure relationships that exist at steady state, we must consider the inert gas flow on a differential basis. At steady state:

$$\begin{pmatrix}\text{Diffusive flow of inert} \\ \text{gas from } A \text{ to } B\end{pmatrix} = \begin{pmatrix}\text{Mass flow of inert} \\ \text{gas from } B \text{ to } A\end{pmatrix} .$$

Or:

(7) $$-D \frac{dC(x)}{dx} = W(x)\, C(x) ,$$

where

D = diffusion constant of inert gas in vapor, cm^2/sec,

$C(x)$ = concentration of inert gas at x, mole/cc,

$W(x)$ = flow velocity of inert gas and vapor, cm/sec,

x = any point in tube, where $x = 0$ at B and $x = 1$ at A.

For isothermal conditions in the tube, the ideal gas law gives:

(8) $$C(x) = \frac{P_i(x)}{RT} ,$$

where

$P_i(x)$ = pressure of inert gas at x, dyne/cm^2 .

[39] S. Dushman, "Vacuum Technique," Wiley, New York, 1954.

Substitution of Eq. 8 into Eq. 7 yields:

$$\frac{D\, dP_i(x)}{dx} = W(x)\, P_i(x) \ . \tag{9}$$

The linear velocity of flow $W(x)$ equals the volume flow rate divided by the cross sectional flow area. Using the ideal gas law, the volume flow rate can be expressed as a function of the total flow of vapor and gas, resulting in the following relation for $W(x)$:

$$W(x) = \frac{1}{\pi r^2}\left(\frac{\dot{n}_t RT}{P_t(x)}\right) , \tag{10}$$

where

$\dot{n}_t$ = total flow of vapor and gas at x, mole/sec,

$P_t(x)$ = total pressure at x, dyne/cm^2.

However, at steady state,

$$\dot{n}_t = \dot{n}_v \ , \tag{11}$$

since there is no net flow of inert gas at steady state. Substitution of Eq. 11 into Eq. 10 yields:

$$W(x) = \frac{1}{\pi r^2}\left(\frac{\dot{n}_v RT}{P_t(x)}\right) . \tag{12}$$

Since the total pressure from A to B does not vary greatly, $W(x)$ can also be expressed accurately as:

$$W(x) = \bar{W} = \frac{1}{\pi r^2}\left(\frac{\dot{n}_v RT}{P_{av}}\right) . \tag{13}$$

Substitution of Eq. 13 into Eq. 9 yields an equation that can be integrated directly to give a solution:

$$\frac{D\, dP_i(x)}{dx} = \left(\frac{\dot{n}_v RT}{\pi r^2 P_{av}}\right) P_i(x)$$

$$D\int_{P_{iB}}^{P_{iA}} \frac{dP_i(x)}{P_i(x)} = \frac{\dot{n}_v RT}{\pi r^2 P_{av}}\int_0^l dx$$

$$D \ln \frac{P_{iA}}{P_{iB}} = \frac{\dot{n}_v RTl}{\pi r^2 P_{av}} . \tag{14}$$

Finally, substitution of Eq. 6 expressing $\dot{n}_v$ as a function of the pressures yields:

$$\frac{8\eta D}{r^2} \ln \frac{P_{iA}}{P_{iB}} = p_{vB} + P_{iB} - P_{iA} . \tag{15}$$

Thus we have expressed the pressure of inert gas at Point B as a function of the vapor pressure at B, the inert gas pressure at A, the viscosity of the vapor at temperature T, the radius of the tube, and the diffusion constant of inert gas in vapor. The relationship has been derived under the following assumptions:

1. Isothermal conditions exist between A and B, and a sharp temperature drop at A causes complete condensation of all vapor flowing to A.
2. Total pressure in the tubes is always greater than 5 mm, so that Poiseuille's equation for viscous, laminar fluid flow is strictly applicable.

Calculation of Equilibrium Pressures for Typical Case

Equation 15 can now be used to calculate the equilibrium pressure values, P_{iA} and P_{iB}, that would exist for a typical experimental situation. Assume the following values:

r = 0.25 cm ,

η_v = 1 × 10^{-3} dyne sec/cm^2 ,

p_{vB} = 50.0 mm Hg = 66.6 × 10^3 dyne/cm^2 ,

T = 1000°K .

The diffusion constant for the gas in the vapor (D) is assumed to follow the relationship[39]

$$D_T = D_0 \left(\frac{T}{288}\right)^{3/2} \frac{760}{p_{vB}} ,$$

where

D_0 = diffusion constant evaluated at T = 288°K,
= 0.2 cm^2/sec .

Thus:

$$D_{1000°K} = 26.4 \text{ cm}^2/\text{sec} .$$

Substitution of the above values into Eq. 15 yields:

$$\frac{2.303 \times 8 \times 10^{-3} \times 26.4}{0.25^2} \log_{10} \frac{P_{iA}}{P_{iB}}$$

$$= (50 - P_{iA} + P_{iB})\ 1333 \text{ dyne/cm}^2 \text{ mm Hg} .$$

Or:

$$5.84 \times 10^{-3} \log_{10} \frac{P_{iA}}{P_{iB}} = 50 - P_{iA} + P_{iB} \ .$$

A plot of P_{iB} vs P_{iA} is given in Fig. 10, where P_{iA} decreases from 51 mm to 50 mm; this plot shows that a small but finite inert gas pressure in the cell exists even when the inert gas pressure in the upper tube equals the vapor pressure of the salt.

Evaluation of Inert Gas Flow Rate

From a plot of the steady state pressure conditions existing in the cell for typical experimental conditions, the inert gas flow rate during operation of the cell can be estimated. At the beginning of a determination, the inert gas pressure at A and B are assumed equal to the steady state pressures. If either of these pressure values is changed suddenly, e.g., by pumping, inert gas will flow, relieving the pressure differences set up by the transient condition. Poiseuille's equation will be applicable, giving a quantitative solution for the flow rate in the form:

$$(16) \quad \dot{N}_i = \frac{\pi r^4}{8\eta l R T} P_{av} [(P'_{iA} - P_{iA}) - (P'_{iB} - P_{iB})] \ ,$$

where

$\dot{N}_i$ = moles of inert gas flowing, mole/sec, during pressure transient,

η = viscosity of inert gas, dyne sec/cm^2,

r = radius of tube, cm,

l = length of tube, cm,

T = temperature of tube, °K,

P_{av} = average total pressure in tube, dyne/cm^2,

P_{iB}, P_{iA} = steady state pressures, dyne/cm^2 (see Fig. 10),

P'_{iA}, P'_{iB} = transient pressures of inert gas at A and B, dyne/cm^2.

After steady state pressures are reestablished in the system, Eq. 16 properly indicates that the inert gas flow is zero. That is, when $P'_{iA} = P_{iA}$, and $P'_{iB} = P_{iB}$, $\dot{N}_i = 0$.

Using Eq. 16, in conjunction with Fig. 10 which gives the steady state pressures, the inert gas flow can be evaluated during a typical experimental determination. Consider the cell shown in Fig. 9, where the left tube is attached to a pump system, and the right is sealed. During an individual vapor pressure determination, the inert gas pressure P_{iA} in both the right and left tubes is initially greater than p_{vB}. The pressure P_{iA} is then reduced by successive increments of 0.1 mm by opening the left tube to the pump system via a stopcock. In this manner, P_{iA} in the right and left tubes is gradually reduced, until P_{iA} in the right tube just equals the vapor pressure p_{vB}. When this condition is achieved, the next increment of gas removed from the left tube creates a semipermanent pressure difference between the two tubes. This difference can be relieved only very slowly, since the vapor flowing up the right tube acts as a valve, throttling the inert gas flow from the right tube to the left.

A more comprehensive analysis can be made by considering three cases: first, where the inert gas pressure in the tubes is greater than the vapor pressure; second, where the inert gas pressure equals the vapor pressure; and third, where the inert gas pressure is less than the vapor pressure; i.e.,

I: $P_{iA} > p_{vB}$, II: $P_{iA} = P_{vB}$, and III: $P_{iA} < p_{vB}$.

For these cases, the inert gas flow can be evaluated using Eq. 16, assuming that steady state conditions are disturbed by the removal of inert gas from the left tube, such that $P'_{iA} = P_{iA} - 0.1$ mm. For all of the following cases, assume:

r = 0.25 cm ,

l = 10 cm ,

η = 5×10^{-4} dyne sec/cm^2 (at 1000°K) ,

P_{vB} = 50.0 mm .

Case I: $P_{iA} > p_{vB}$

Transient Pressure Conditions:

P'_{iA} = 50.9 ,

P_{iA} = 51 ,

$P_{iB} = P'_{iB}$ = 1.01 (from Fig. 10) .

(*a*) Left tube: In the left tube, the molar flow rate is given by Eq. 16, so:

$$\dot{N}_i = \frac{\pi r^4}{8\eta l R T} P_{av} [(P'_{iA} - P_{iA}) - (P'_{iB} - P_{iB})] \ .$$

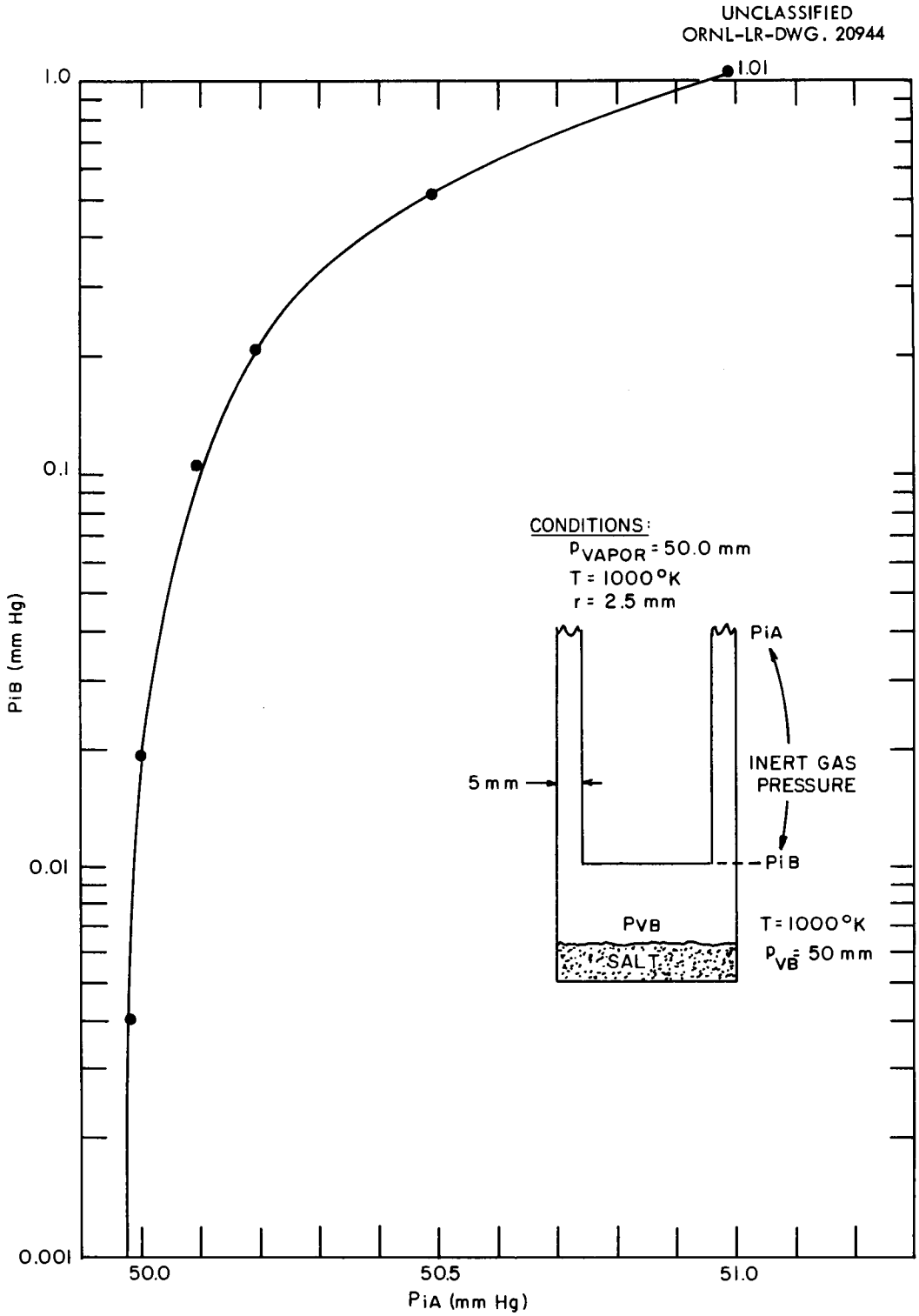

Fig. 10. Steady-State Pressures of Inert Gas in Rodebush Cell.

A more informative value is the linear flow rate:

$$W_i = \frac{\dot{N}_i RT}{\pi r^2 P_{av}} = \frac{r^2}{8\eta l}[(P'_{iA} - P_{iA}) - (P'_{iB} - P_{iB})].$$

Substituting the conditions assumed:

$$W_i = \frac{(0.25)^2}{8 \times 5 \times 10^{-4} \times 10}[50.9 - 51.0] = 2100\,(-0.1)$$

$$W_i = -210 \text{ cm/sec} .$$

The inert gas flows rapidly up the left tube until the new steady state conditions are established, corresponding to P_{iA} = 50.9 mm. From Fig. 10, we see that P_{iB} will be reduced to 0.91 mm when P_{iA} = 50.9, and when the new steady state is established.

(*b*) Right tube: In the right tube, the linear velocity of inert gas down to the cell can be calculated similarly. Here, assume that the rapid flow up the left tube occurs instantly, lowering P_{iB} to 0.91, while P_{iA} (in the sealed end) initially remains at the old steady state value of 51.0 mm. Thus the pressure conditions causing inert gas flow will be:

$$P_{iA} = P'_{iA} = 51.0 ,$$

$$P_{iB} = 1.01 ,$$

$$P'_{iB} = 0.91 .$$

The linear velocity will be:

$$W_i = 2100\,[(P'_{iA} - P_{iA}) - (P'_{iB} - P_{iB})]$$

$$W_i = 2100\,(0.1) = 210 \text{ cm/sec} .$$

Thus, the inert gas flow from the sealed tube at the right is rapid, and steady state pressure conditions will be readily re-established at the lower value of P_{iA}. Consequently, inert gas pressures in the right and left tubes quickly become equalized.

Case II: $P_{iA} = p_{vB}$

Initial Conditions:

$$P_{iA} = p_{vB} = 50.0 \text{ mm} ,$$

$$P_{iB} = 0.049 \text{ mm (Fig. 10)} .$$

(*a*) Left tube: Assume that P_{iA} is reduced instantly by 0.1 mm as before, so that P'_{iA} = 49.9 mm. Then:

$$W_i = 2100\,(49.9 - 50.0)$$

$$W_i = -210 \text{ cm/sec} .$$

Thus, P_{iB} will be reduced to a value lower than the steady state value of 0.049 mm by the rapid flow of inert gas up the left tube.

(*b*) Right tube: Assume that P_{iB} is instantly reduced from its steady state value to 0.001 mm by the rapid flow up the left tube, while the inert gas pressure at the sealed end, P_{iA}, remains at the previous steady state value of 50.0 mm. Thus:

Transient Pressure Conditions:

$$P'_{iA} = P_{iA} = 50.0 \text{ mm} ,$$

$$P_{iB} = 0.019 \text{ mm} ,$$

$$P'_{iB} = 0.001 \text{ mm} .$$

This yields a much lower flow velocity:

$$W_i = 2100\,(0.019 - 0.001)$$

$$W_i = 40 \text{ cm/sec} .$$

The flow velocity down the right tube is now roughly one-fifth of its previous value, indicating that the pressure transient set up in the tube will not be reduced quickly. A comparison between the inert gas pressures at *A* in the right and left tubes shows that $P_{iA(\text{left})}$ = 49.9 mm, while $P_{iA(\text{right})}$ = 50.0 mm. This pressure difference will slowly diminish as inert gas flows down the right tube. However, the pressure difference will be maintained long enough to serve as an experimental indication that $P_{iA} = p_{vB}$ in the right tube.

Case III: $P_{iA} < p_{vB}$

If the inert gas pressure P_{iA} is lower than the vapor pressure p_{vB}, steady state conditions do not exist in the tubes, and vapor will flow rapidly up both tubes (see *Case III* below). This results in an unsaturated condition in the cell proper under which condition boiling starts. If inert gas is removed from the left tube, an even greater pressure difference is maintained between the right and left tubes. This condition of boiling was experimentally detected by a decrease in the cell temperature caused by rapid heat loss.

Evaluation of Vapor Flow Rate

Vapor flow rate up the tubes can be evaluated as outlined in the previous section. The molar flow rate for the vapor is given by Eq. 6:

$$\dot{n}_v = \frac{\pi r^4}{8\eta l RT} P_{av}(p_{vB} + P_{iB} - P_{iA}) \ .$$

The linear vapor velocity is thus:

$$W_v = \frac{\dot{n}_v RT}{\pi r^2 P_{av}} = \frac{r^2}{8\eta l}(p_{vB} + P_{iB} - P_{iA}) \ .$$

The linear velocity of vapor flow up the tubes can now be evaluated for the three cases. Assume:

$$\eta = 5 \times 10^{-4} \text{ dyne sec/cm}^2 \ ,$$
$$l = 10 \text{ cm} \ ,$$
$$r = 0.25 \text{ cm} \ .$$

Case I: $P_{iA} > p_{vB}$

Steady State Pressure Conditions:

$$P_{iA} = 51.0 \text{ mm} \ ,$$
$$P_{iB} = 1.01 \text{ mm} \ ,$$
$$p_{vB} = 50 \text{ mm} \ .$$

The vapor flow velocity under the steady state conditions is:

$$W_v = 2100\ (50.0 + 1.01 - 51.0) = 21.0 \text{ cm/sec} \ .$$

Clearly, the vapor flow up the tubes is small under steady state conditions. The sudden reduction of the inert gas pressure P_{iA} in the left tube to the transient value of 50.9 does not affect the flow rate of vapor greatly, and when the inert gas pressures reach steady state values corresponding to the lower P_{iA}, the flow of vapor is essentially unchanged. In either case, the flow of vapor is negligibly small, since a flow velocity of 20 cm/sec corresponds to a molar flow rate of 4×10^{-6} mole/sec.

Case II: $P_{iA} = p_{vB}$

Steady State Pressure Conditions:

$$P_{iA} = 50.0 \text{ mm} = p_{vB} \ ,$$
$$P_{iB} = 0.019 \text{ mm} \ .$$

(*a*) Left tube: Before any inert gas is removed from the left tube, the vapor velocity is:

$$W_v = 2100\ (50.0 + 0.019 - 50.0) = 50 \text{ cm/sec} \ .$$

When the inert gas pressure, P_{iA}, is reduced by pumping to the lower value of 49.9 mm, the vapor velocity in the left tube increases markedly:

$$W_v = 2100\ (50.0 + 0.019 - 49.4) = 200 \text{ cm/sec} \ .$$

Thus, there is a rapid flow of vapor up the left tube.

(*b*) Right tube: The steady state flow rate in the right tube is the same as that in the left tube. However, after the inert gas transient has lowered P_{iB} in the cell to 0.001 mm, the vapor velocity becomes:

$$W_v = 2100\ (50.0 + 0.001 - 50.0) = 2.1 \text{ cm/sec} \ .$$

Comparing *Case II* with *Case I* shows that the vapor actually flows up the right tube quite slowly. Over-all conditions in the right tube during inert gas transients are identical with the steady state condition where saturation in the cell proper exists.

Case III: $P_{iA} < p_{vB}$

Under the condition where the inert gas pressure at *A* is less than the vapor pressure at *B*, the salt melt in the cell is distilling rapidly. If $P_{iA} = 49.9$ mm in both tubes, $P_{iB} = 0$, and so:

$$W_v = 2100\ (50.0 + 0 - 49.9) = 210 \text{ cm/sec} \ .$$

The vapor is rapidly flowing up both tubes. Depending on the surface area of the salt, this may result in unsaturated conditions in the cell. The rapid flow of vapor under these conditions is accompanied by a rapid loss of heat from the cell, and during actual experimental determinations, this condition was always accompanied by a rapid drop in the cell temperature. In order to avoid plugging of the gas lines with condensate, inert gas was immediately introduced to the cell when this sharp temperature drop was detected.

Summary of Analysis

The steady state conditions existing in the Rodebush cell were examined, and a function relating the pressures of interest was developed:

$$\frac{16\eta_v D}{r^2} \log e \frac{P_{iA}}{P_{iB}} = p_{vB} + P_{iB} - P_{iA} \ .$$

A plot of P_{iA} vs P_{iB} was given for a typical case in Fig. 10.

Expressions for the molar flow rate of vapor and inert gas were developed:

$$\dot{n}_v = \frac{\pi r^4}{8\eta lRT} P_{av}(p_{vB} + P_{iB} - P_{iA})$$

$$\dot{N}_i = \frac{\pi r^4}{8\eta lRT} P_{av}[(P'_{iA} - P_{iA}) - (P'_{iB} - P_{iB})].$$

The flow of inert gas was calculated in both tubes, assuming that a small increment of gas had been removed from the left tube by pumping. If the inert gas pressure P_{iA} exceeded the vapor pressure p_{vB}, rapid flow of inert gas occurred in both tubes, re-establishing equilibrium conditions quickly, and equalizing the pressures of inert gas in the right and left tubes. However, if the inert gas pressure equaled the vapor pressure when the increment was removed, the inert gas flow was still rapid in the left tube, while flow down the right tube was hindered by the counter current flow of vapor molecules. Such conditions led to an observable, semipermanent pressure difference of inert gas between the right and left tubes.

Vapor flow was calculated for similar conditions, and was shown to be small, providing that the inert gas pressure was not reduced below the equilibrium vapor pressure during the pumping process. For the special case where the inert gas pressure in both tubes equaled the vapor pressure, vapor flow up the left tube was rapid after an incremental decrease in P_{iA} on the left; however, vapor flow up the right tube remained low, indicating that the right tube approximated saturation conditions. In experimental practice, reductions in pressure in the left leg must be as small as possible, so that loss of vapor up this tube (when $P_{iA} = p_{vB}$) does not result in an unsaturated condition in the cell. Under these conditions, the inert gas pressure in the right tube will yield an accurate value for the vapor pressure of the salt.

DESCRIPTION OF APPARATUS

The procedure adopted for total vapor pressure measurements was developed by Rodebush and Dixon,[24] and as modified for this study will be called the "Rodebush" apparatus. It consisted of a vacuum manifold, A (see Fig. 11), with attached argon inlet at stopcock 1 and vacuum pump at stopcock 6. Attached to the manifold was a mercury manometer, B, used to measure the argon pressure in the system, and a differential manometer, D, used to measure the pressure difference in the gas leads, H. The differential manometer containing dibutylphthalate was connected to the manifold through stopcocks 4 and 5, while one side of the differential manometer was connected to the mercury manometer through stopcock 3. The differential manometer lines were sealed to two ¼-in. Kovar tubes, which in turn were soldered to a pair of brass Sylphon bellows, G. The bellows formed a flexible connection between the glass system described above and the metal system containing the salt melts. Two copper gas leads soldered to the free end of the bellows completed the stationary fixtures. The copper gas leads were connected to the nickel vapor pressure cell, J.

The materials to be studied were contained in nickel vapor pressure cells designed for ease of attachment to the stationary system and ease of loading. Nickel was chosen as a suitable material because of its inertness to the salts and good high temperature oxidation resistance. The nickel cell used to contain the melts is shown in detail in Fig. 12. Two ⅜-in.-OD nickel tubes, A, were welded to the cell proper, B (fabricated from 2-in. schedule 40 nickel pipe). In the center of the cell was a thermocouple well, C, in which a calibrated thermocouple was placed for measuring the sample temperature. The well extended to within ⅛ in. of the bottom of the cell. The nickel gas leads of the cell were attached to the copper leads (see above) by means of two Swagelok fittings, E. The cell was contained in a heavy nickel liner, D, which served to damp out temperature gradients inside the furnace. Heat loss from the top of the cell was reduced by a divided nickel block placed on top of the cell. This entire assembly was heated in a 5-in. Hoskins pot furnace. To control the temperature, a Chromel-Alumel thermocouple was placed in contact with the resistance heating element of the furnace. This thermocouple was connected to a Brown Pyrovane controller, which held the furnace temperature at this point to ±3°C. The heavy nickel liner damped these temperature fluctuations, resulting in an isothermal condition in the cell proper during a given determination (see later). As an aid in determining the temperature of the cell during heating cycles, an additional Chromel-Alumel thermocouple was placed on top of the cell at the

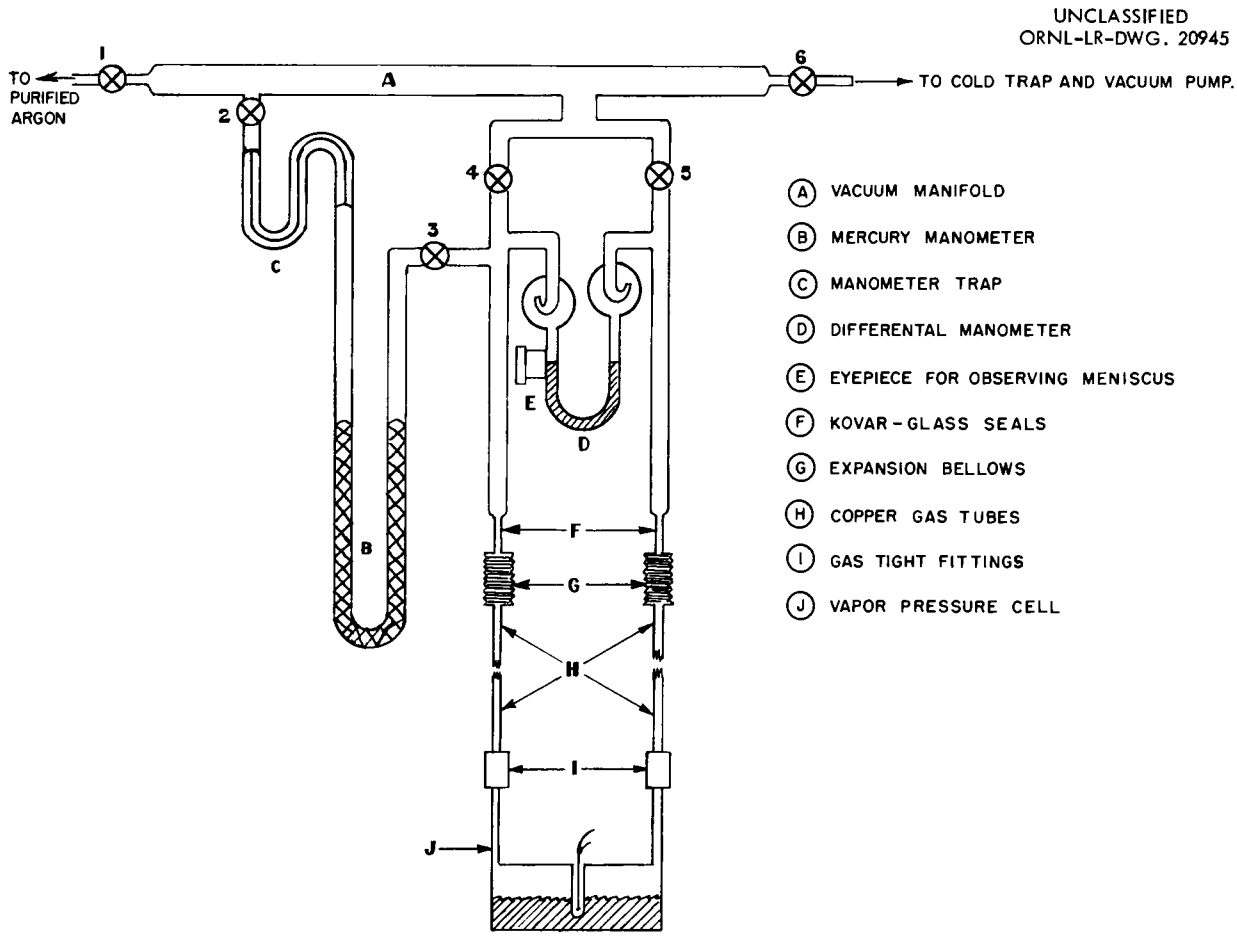

Fig. 11. Total-Pressure Apparatus (Rodebush Type).

thermowell. The temperature at this point was indicated on a Brown Electronik recorder, giving a continuous record of the cell temperature during a determination.

Sample temperature measurements were made with Pt-Pt, 10% Rh thermocouples placed inside the thermocouple well. A Leeds and Northrup precision portable potentiometer was used to measure the thermal emf values; cold junction temperatures were maintained at 0°C in all determinations. The thermocouples were calibrated at frequent intervals against a National Bureau of Standards platinum couple by the following technique:

The unknown couple and the standard couple were wired together with platinum wire to ensure good thermal contact and placed inside a nickel block in a tube furnace. The furnace temperature was controlled by means of a Variac. When isothermal conditions were reached, the emf values for the standard and unknown couples were determined by the apparatus described previously. This procedure was followed for a series of temperatures and a difference curve was constructed for the unknown couple. The largest shifts occurring between calibrations of the thermocouples were 5 μv. Before actual experimentation was begun, the temperature distribution in the furnace and cell was determined at a representative temperature. To show the extent of isothermal conditions in the cell proper, Chromel-Alumel thermocouples were placed around and in the empty cell. After the cell and furnace had reached thermal equilibrium at 950°C, the maximum temperature difference observed in the cell was 5°C, and this existed between the bottom outer edge of the cell (hotter) and the upper plate of the cell near the gas leads (cooler). Similarly, there

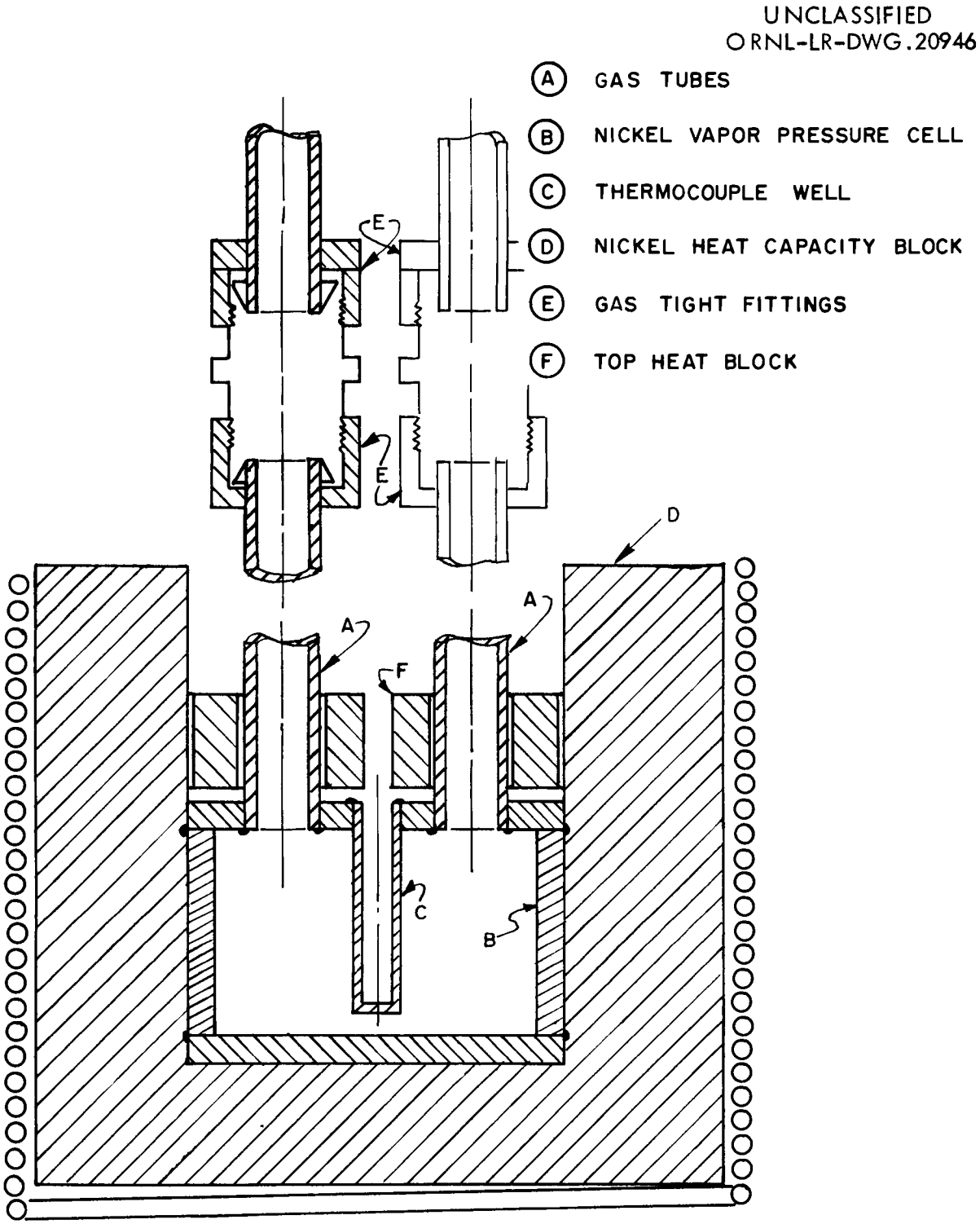

Fig. 12. Vapor Pressure Cell.

existed a 2°C temperature drop from the bottom of the thermowell to the top of the well. At lower temperatures, these gradients were much smaller. The temperature at the bottom of the thermowell was identical with that at the bottom of the cell proper, also, at the center. Since the thermocouple well dipped directly into the upper surface of the melts when liquid, the platinum thermocouple gave an accurate indication of the salt temperature. The temperature gradients were measured with the cell empty, and these should be smaller when a liquid melt was present. The result of this investigation proved that the temperature pattern of the salt melts was isothermal to at least 1–2°C at 950°C, with a smaller difference at lower temperatures. This temperature pattern was considered satisfactory; considering the accuracy of the thermocouple calibration (±0.5°), the temperature of the salt was known to ±1°C.

PROCEDURE

The glass apparatus was readied for use in the following manner: Initially, the mercury manometer was removed from the system, cleaned thoroughly, filled with distilled mercury, and finally resealed to the system. The differential manometer was filled through a sidearm with dibutylphthalate. After the sidearm was sealed, the entire apparatus was evacuated to 20 microns pressure and the mercury and dibutylphthalate were outgassed by careful heating with a hand torch. The manometer assembly used in this apparatus is advantageous, since it can be readily readjusted if any desorption of gas occurs at the glass surfaces. The mercury manometer was readied for use as follows: With the system at 20 microns, stopcock 2 was closed. Stopcock 1 was opened, admitting dry, oxygen-free argon to the system, and forcing the mercury up through the 1 mm capillary trap, C. Stopcock 1 was closed, and stopcock 3 was closed, trapping argon in the right leg of the manometer. After stopcock 6 was opened, the manifold was again pumped down to 20 microns, and stopcock 2 was opened. Thus, the small amount of residual gas trapped in the left leg of the manometer was removed. Stopcocks 2 and 6 were closed, and the argon in the manometer was bled into the vacuum manifold through stopcock 3. A sharp tap of the capillary tubing at point C broke the mercury thread, creating a Torricelli vacuum in the left manometer leg. Between determinations, the Torricelli vacuum could be checked and recreated if needed by following the procedure outlined above. After the manometer had been adjusted, the glass apparatus was ready for a determination.

The nickel vapor pressure cells were cleaned[40] with 20% HCl solution, containing 10 wt % $CuCl_2$. This was followed by a flash pickling solution, consisting of 100 cc H_2O, 150 cc H_2SO_4, 225 cc HNO_3 + 3 g NaCl. The cells were rinsed with distilled water and dried in an oven. The nickel surfaces had a bright, mirror-like appearance after treatment. The mixtures in question were prepared from the pure salts by weighing on a torsion balance (sensitivity ±10 mg). Because of the hygroscopic nature of the salts used, the loading operations were all done in the dry box. Generally, a charge of 50 grams was used. The pure salts were ground and then weighed directly into a small cylindrical funnel (Fig. 13) on the balance pan by a glass tripod. Rubber tubing, 1 in. long, was attached to the end of the funnel and was pinched closed with a spring loaded pinch clamp. After weighing, the salts were thoroughly mixed in the funnel which was then attached to one of the nickel gas leads with the rubber tubing. Removal of the pinch clamp allowed the mixture to flow into the cell. A ⅛ in. nickel rod was needed to ream the powder from the gas line and to show that the line was clear. By this means, total mechanical holdup of the sample was made negligible. In order to protect the sample from moisture upon removal from the dry box, the two gas tubes were then sealed with Sealtite, a putty-like compound. Then the cell was removed from the dry box and placed in the nickel liner in the pot furnace. The Sealtite was removed from the tubes and the Swagelok fittings on the tubes were quickly attached to the copper tubing leading to the glass apparatus. Now connected to the glass apparatus, the cell was evacuated and flushed by suitable manipulation of stopcocks 1 and 6. After a leak test, the furnace was heated to 400°C and the cell was outgassed overnight by pumping.

After pumping overnight, a pressure of about 30 cm of argon was introduced into the system and the control point of the furnace was set at the desired experimental temperature. When temperature equilibrium was reached, as indicated by the Chromel-Alumel couple placed on the top of the cell near

[40] American Society for Metals: *Metals Handbook*, 1948 ed., p 1045.

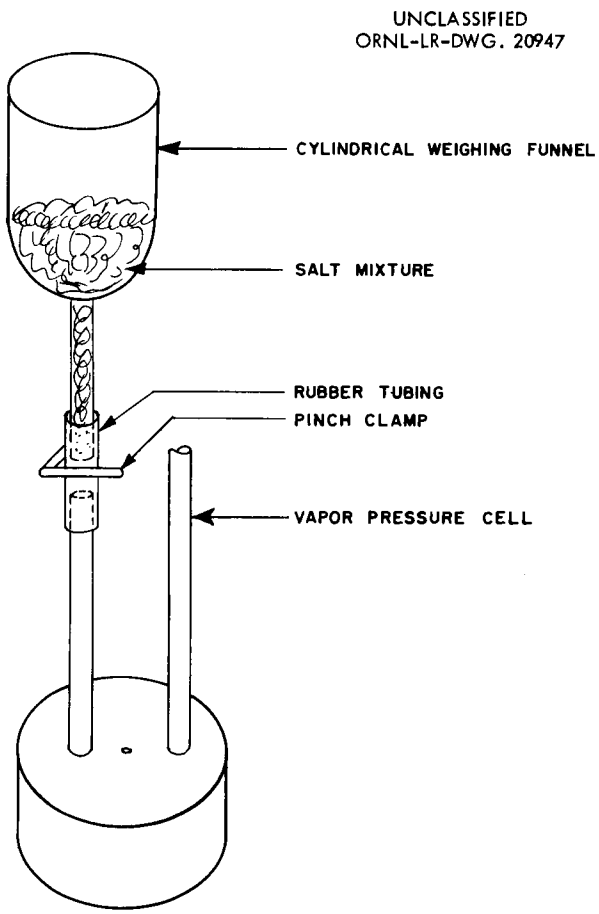

Fig. 13. Loading Assembly (Schematic).

the thermowell, a pressure measurement was made. The argon pressure was reduced by pumping to a value about 1 cm greater than the vapor pressure. At this point, the incremental pressure reductions were begun. Small volumes of argon were removed from the cell by quickly opening and closing stopcock 6, creating a pressure difference observed by the differential manometer. (Stopcocks 3 and 4 were open, while stopcock 5 was closed.) Thus, as argon was removed from the manifold, the meniscus in the differential manometer at point E rose, as observed with the eyepiece E. Gas flow from both the right leg of the cell and the cell itself into the manifold equalized the pressure difference between the two legs, and the meniscus observed at E returned to its equilibrium position, indicated by a hairline in the eyepiece. In this manner, argon was removed incrementally from the cell and the total cell pressure was slowly reduced. Between each increment, the differential manometer was allowed to return to its equilibrium value. When the argon pressure equaled the vapor pressure of the material in the cell, the free flow of argon from the right leg through the cell was restricted by the counter current of condensing salt vapors from the sample, and a permanent difference in pressure was observed with the differential manometer. At this indication, the total argon pressure in the system was measured with the mercury manometer and a Gaentner cathetometer. The temperature of the melt was recorded with the platinum thermocouple and then argon was readmitted to the system. Two such determinations were made at each temperature; the reproducibility of measurements averaged about 2%. Following the second determination the furnace control was raised about 25°C and two more pressure measurements were made after thermal equilibrium had been established. With the completion of the series of measurements on a sample, the cells were cooled and disconnected at the Swagelok fittings, and the salt was dissolved. The cell was then ready for cleaning by etching as before and stored for later re-use.

During early experiments, some difficulty was noted with plugging of the cells with sublimed vapor. When the argon swept through the cell, it carried out vapor which deposited in the colder zones of the gas leads. This sublimation problem was circumvented by heating the tubes after each individual pressure determination, using an oxygen-propane torch. Since the sublimed material is mostly $FeCl_2$, with a melting point of 677°C, the tubes can be heated until the deposit melts and runs down into the cell, thereby reducing changes in composition due to volatilization. The differential manometer was attached to the manifold so as to reduce pressure differentials in the gas leads of the cell. Thus, when argon is admitted to the system, it flows simultaneously into both sides of the differential manometer legs and hence into the vapor cell, reducing these "sweeping" effects.

5. TRANSPORTATION METHOD

THEORY OF TRANSPORTATION METHOD

In the transportation apparatus, a steady stream of inert gas passes over the salt under study, which is held under isothermal conditions in a tube furnace. The inert gas removes the vapor above the salt at a rate dependent on the relative pressures and on the flow rate of gas. The vapor condenses out of the inert gas stream and is collected for subsequent chemical analysis.

Two main sources of error, as outlined by Jellinek, are:

1. diffusion of the vapor into the condenser,
2. incomplete equilibration of the vapor and transporting gas stream.

The effect of diffusion on the amount of condensate collected can be shown to be insignificant, providing certain design requirements are met. By experimentally varying flow rate during the determinations and observing the effect on total condensate load, saturation conditions can be shown to exist.

A mathematical treatment by Wagner and Stein[30] indicates the restrictions on condenser dimensions which will reduce the diffusion error. Consider two gases, 1 and 2, in a mixture flowing in direction x through a tube. The rate of transfer of material 2 is given by

$$(1) \qquad \dot{n}_2(x) = -Dq \frac{dC_2(x)}{dx} + WqC_2(x) ,$$

where

$\dot{n}_2(x)$ = moles of substance 2 passed per second,

D = diffusion coefficient of 2 in gas 1, cm^2/sec,

q = uniform cross sectional flow area, cm^2,

$C_2(x)$ = concentration of 2 at point x, moles/cc,

W = constant flow velocity of mixture, cm/sec.

Under steady state conditions, $\dot{n}_2(x)$ is independent of position, whence differentiation of Eq. 1 with respect to x gives

$$(2) \qquad 0 = \frac{d\dot{n}_2}{dx} = -Dq \frac{d^2C_2}{dx^2} + Wq \frac{dC_2}{dx} .$$

This differential equation can be solved directly, with the following boundary conditions:

$$C_2 (x = 0) = C_2^0 ,$$

where

$x = 0$ is at the center of the furnace;

$$C_2 = 0 ,$$

where

$x = L$, L being the length of the condenser tube.

These boundary conditions essentially state that saturation conditions exist above the sample, and that complete condensation of the vapor takes place in the condenser of length L. Application of the conditions to the solution of Eq. 2 gives

$$(3) \qquad C_2 = C_2^0 \left[\frac{e^{-(W/D)(L-x)} - 1}{e^{-WL/D} - 1} \right] .$$

With the solution for C_2 as a function of x, Eq. 1 can be rewritten as a linear equation. Thus, substitution of Eq. 3 into Eq. 1 gives

$$(4) \qquad \dot{n}_2 = \frac{qC_2W}{1 - e^{-WL/D}} .$$

If the gases behave ideally, and with the assumption that saturation exists at the center of the furnace, it follows that

$$(5) \qquad C_2^0 = \frac{p_2^0}{RT} ,$$

where

p_2^0 = equilibrium pressure of substance 2 in center of furnace,

T = temperature of sample at center of furnace.

Furthermore the stream velocity equals the total volume flow rate divided by the cross-sectional area:

$$(6) \qquad W = \frac{V_t}{q} .$$

The total volume flow rate can be obtained from the ideal gas law:

$$(7) \qquad V_t = (\dot{n}_1 + \dot{n}_2) \frac{RT}{P_t} ,$$

where

$\dot{n}_1, \dot{n}_2$ = moles of substance 1 and 2 flowing into condenser per second,

T = temperature inside furnace,

P_t = total pressure of 1 and 2 above sample.

Substitution of Eq. 7 into Eq. 6 yields

$$W = (\dot{n}_1 + \dot{n}_2) \frac{RT}{P_t} . \tag{8}$$

Substituting Eqs. 8 and 5 into Eq. 4 yields

$$\frac{\dot{n}_2}{\dot{n}_1 + \dot{n}_2} = \frac{p_2^0}{P_t} \left(\frac{1}{1 - e^{-V_t L/qD}} \right) . \tag{9}$$

The exponential term in Eq. 9 represents the diffusion error. Since V_t should be kept small to ensure equilibrium with the liquid, the diffusion error can be reduced by using a small cross section q in the condenser and a large length of condenser, L. The effect of inert gas is reflected in the diffusion coefficient D. Thus, hydrogen as a carrier gas will have a large diffusion correction because of its high diffusion coefficient in comparison to heavier gases like nitrogen or argon.

The magnitude of the diffusion correction can be estimated for the apparatus used (see "Description of Apparatus"). In the actual experimental apparatus, the following values were chosen:

r = radius of condenser inlet = 0.05 cm,

l = length of condenser inlet = 10.0 cm,

V_t = normal experimental gas velocity = 20 cc/min.

For argon, the diffusion coefficient is given by:

$$D_T = 0.2 \left(\frac{T}{288} \right)^{3/2} .$$

Since the operating temperatures were in the range of 1000°K, the diffusion coefficient becomes:

$$D_T = 1.3 \text{ cm}^2/\text{sec} .$$

Substitution of these values into the exponential term of Eq. 9 yields the following value:

$$e^{-V_t L/qD} = e^{-(20\times10)/(\pi)(0.05)^2(1.3)} = e^{-20,000} .$$

Thus, the diffusion correction is entirely negligible for the conditions of the experiments, a fact which was checked experimentally.

The amount of vapor diffusing against the argon stream into the gas delivery tube can be calculated with Eq. 9. If a negative value of the volume flow rate is introduced into Eq. 9 ($V_t = -|V_t|$) the magnitude of this back-diffusion can be estimated. The conditions will be comparable to those assumed in the previous case; however, the flow area is now calculated for the annular space between the condenser and delivery tube:

$$q = \pi(0.8^2 - 0.7^2) ,$$

$$q = 0.47 \text{ cm}^2 ,$$

$$L = 15 \text{ cm} .$$

Thus, the amount of gas vapor diffusing back against the incoming inert gas (n_2') is given by:

$$\frac{\dot{n}_2'}{\dot{n}_1 + \dot{n}_2'} = \frac{p_2^0}{P_t} \left[\frac{1}{e^{V_t L/qD} - 1} \right] . \tag{10}$$

Substitution of the numerical values in the exponential yields

$$\frac{\dot{n}_2'}{\dot{n}_1 + \dot{n}_2'} = \frac{p_2^0}{P_t} \left[\frac{1}{e^{20\times15/0.47\times1.3} - 1} \right]$$

$$= \frac{p_2^0}{P_t} \left(\frac{1}{e^{500}} \right) .$$

Thus, even if the partial pressure of salt in the cell equals the total pressure, ($p_2^0/P_t = 1$), the amount of vapor diffusing back against the incoming inert gas is small. For the partial pressures studied in this work, this effect was negligible.

DESCRIPTION OF APPARATUS

The transportation apparatus designed by Wagner and Stein[30] was used with only a few modifications (Fig. 14). Tank argon for use as the carrier gas was dried over Dehydrite [$Mg(ClO_4)_2$] in tower A, and deoxygenated over copper turnings held at 650°C in quartz tube B. The argon flowed through needle valve 1, used to regulate the flow rate, past a calibrated dibutylphthalate flowmeter C, a dibutylphthalate manometer D and over pressure vent E.

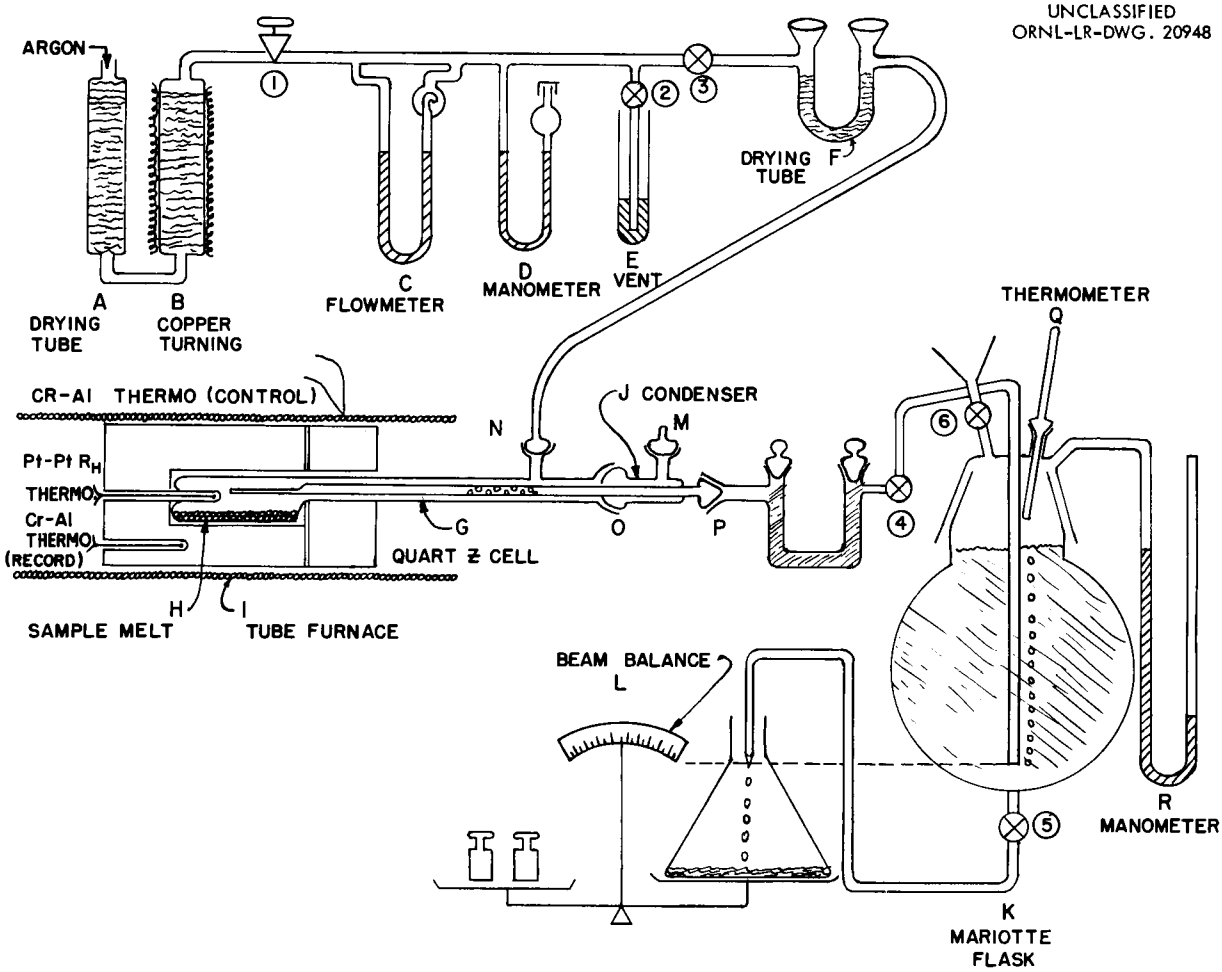

Fig. 14. Transportation Apparatus.

Schwartz trap F, filled with Dehydrite, removed final traces of water from the argon entering the vapor pressure cell G. After becoming saturated with vapor from the melt H, held isothermally in a Hoskins 3-in. tube furnace I, the gas passed through condenser J. The salt vapor was completely condensed in J and then the argon passed into the Mariotte flask K, where the argon displaced water weighed on a balance L. The number of moles of argon collected was calculated by noting the temperature and pressure of the gas in K.

A more detailed drawing of the cell and condenser is given in Fig. 15. The cell was constructed entirely of quartz, while the condensers were quartz and pyrex as indicated. The argon entered at joint 1 and flowed down to the saturation chamber. The tubing used for the gas inlet to the cell was 8 mm ID quartz tubing, while the tubing for the condenser was 7 mm OD tubing. The argon flowed through the 1 mm gap between the two tubes and achieved temperature equilibrium before reaching the melt.

The argon-vapor mixture entered the condenser through a 1 mm quartz capillary tube 10 cm long; the salt vapor was deposited in the condenser. A steep temperature gradient existed along the condenser causing some salt vapor to condense in the center of the gas stream rather than on the condenser walls. This effect was noted only at flow rates above 30 ml/min. Indentations placed in the condenser tube effectively stripped out the entrained salt particles. After the salt vapor was deposited in the condenser, the argon left the condenser from joint 5 leading to the Mariotte flask.

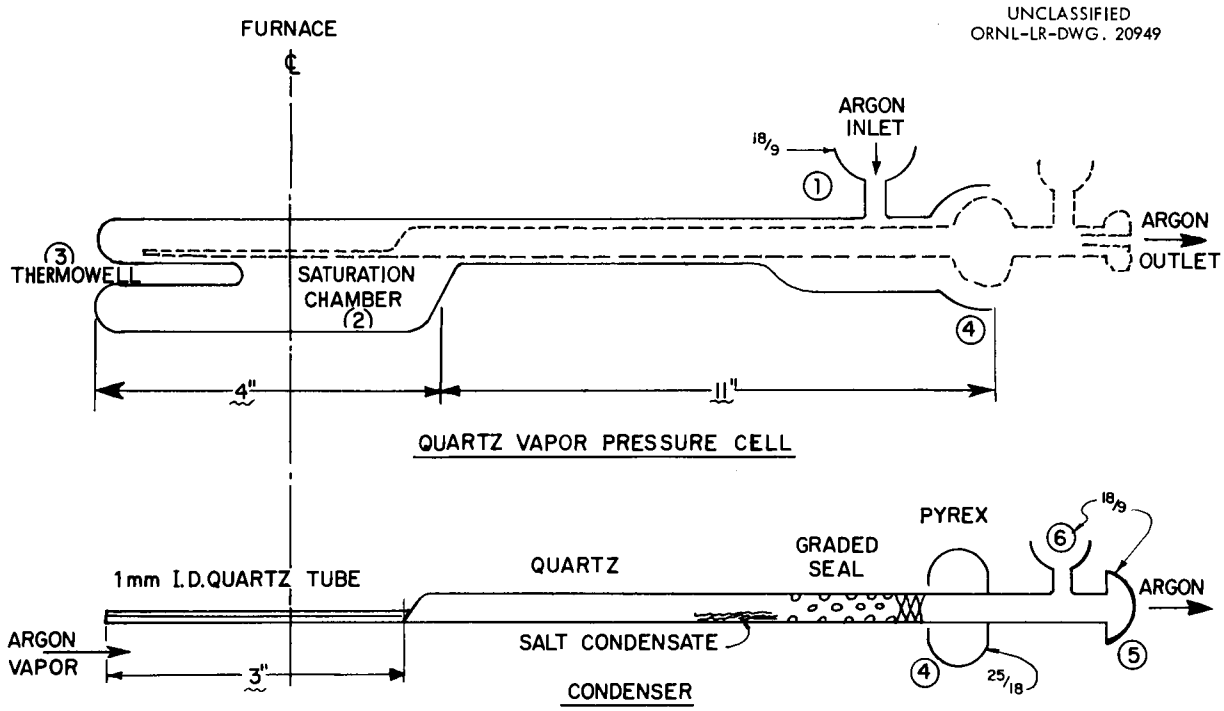

Fig. 15. Transportation Cell and Condenser.

The large ball joint 4 on the condenser was sawed off, leaving a flat shoulder as shown. This eliminated the problem of grease pickup by the condenser tube during insertion. The small ball joint 6 on the end of the condenser served as a purge outlet during the exchange of condensers outlined below.

Isothermal conditions in the quartz cell were achieved by surrounding the quartz cell with a nickel heat block. The heat block is shown in Fig. 16. It consisted of a 3 in. nickel cylinder bored to accommodate the quartz cell. A $^3/_{16}$-in. hole allowed insertion of a Pt-Pt, 10% Rh thermocouple into the thermowell of the cell. An additional hole was drilled which held a Chromel-Alumel thermocouple used to record the temperature of the block on a Leeds and Northrup Micromax recorder. Temperature control was obtained with a Brown Pyrovane controller, actuated by a Chromel-Alumel thermocouple placed next to the resistance element of the tube furnace. In addition to the main nickel heat block, a split nickel block, also shown in Fig. 16, was placed around the quartz cell inlet tube.

Experimental temperatures were measured with calibrated Pt-Pt, 10% Rh thermocouples using a Leeds and Northrup portable precision potentiometer; cold junction temperatures were maintained at 0°C. The thermocouples were calibrated as indicated earlier (see "Description of Apparatus," chap. 4), and showed a maximum of 5 μv drift between calibrations. Measurements were taken with Chromel-Alumel thermocouples to establish the extent of the "isothermal zone" in the tube furnace. At thermal equilibrium near 900°C, the temperature profile shown in Fig. 16 was obtained, indicating that the salt temperature was known to ±2°C. Also, gas flow rates up to 70 ml/min had no observable effect on the temperature pattern, indicating that the argon was heated sufficiently during its entrance to the saturation chamber. Beyond the split heat block the temperature dropped very steeply such that the temperature of the exterior ball joint assembly of the cell was never greater than 50°C during any experiment.

PROCEDURES

The quartz vapor pressure cells were loaded in the argon dry box in the same manner as the

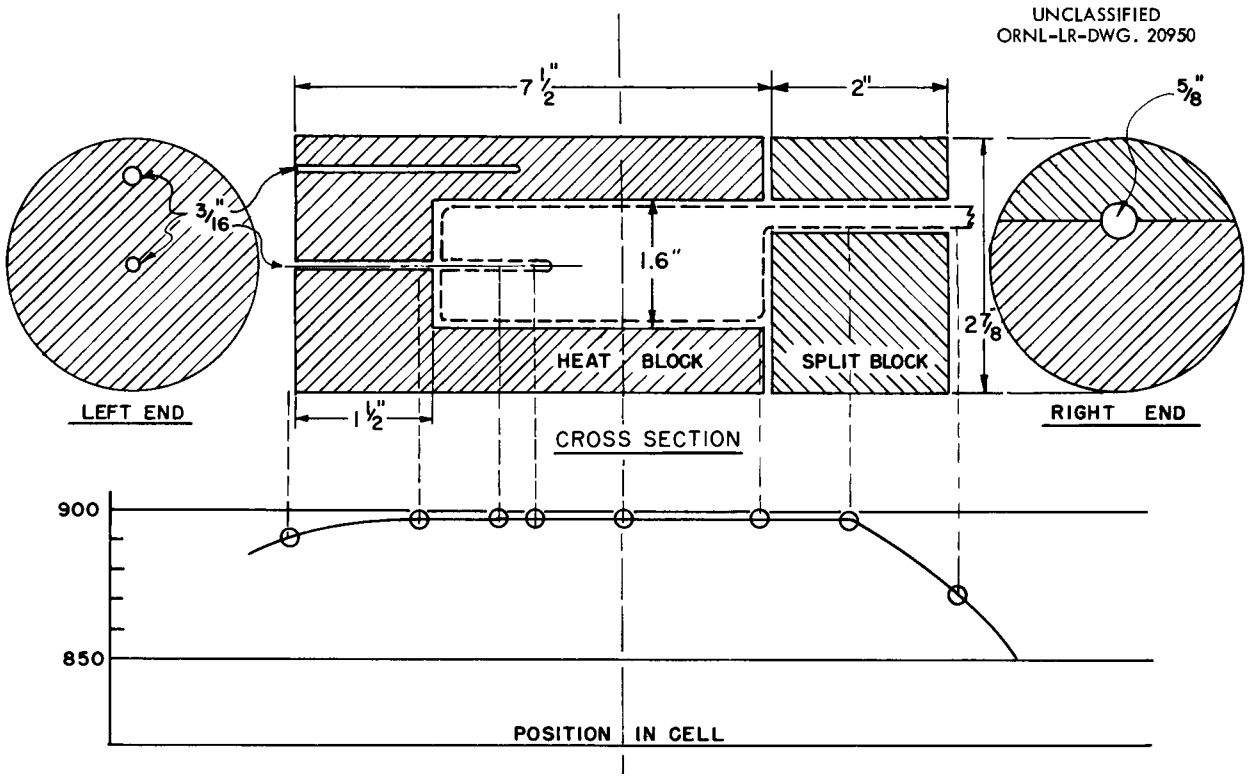

Fig. 16. Temperature Distribution in Nickel Heat Block and Nickel Split Block.

Rodebush cells. After a cleaning and rinsing with distilled water, the cell was dried in an oven, then flushed with dry argon following removal from the oven. The cell was then placed in the dry box and a mixture of the desired composition was weighed into the cylindrical funnel (see "Description of Apparatus," chap. 4). The funnel was attached to a ¼-in. nickel tube placed in the vapor pressure cell, and the dry powder mixtures were admitted to the cell. A charge of 50 g of mixture was used in all determinations. After all the salt mixture was introduced into the quartz cell, the nickel tube was removed and the ball joints of the cell were sealed with sealing compound. The cell was evacuated and flushed with purified argon. This procedure was repeated three times to ensure complete removal of oxygen. The cell was then installed in the nickel heat blocks and attached to the apparatus at joint N (see Fig. 14). Argon gas flow was maintained at a rate of 60–80 ml/min while the cell was baked out at 400°C overnight to remove any residual adsorbed water in the system. To start a determination, the gas flow was shut off and the furnace was heated rapidly to the desired experimental temperature. To start a determination, the following procedure was used (see Fig. 14):

1. Valve 3 was closed and 2 was opened.
2. With the argon flowing through the vent E, the flow rate was adjusted to the desired value with needle valve 1.
3. The water container on the balance was weighed and the temperature of the cell was measured with the platinum thermocouple. Valve 4 was opened, connecting the cell to the Mariotte flask.
4. When the flow rate had been set, valve 2 was closed and valve 3 was immediately opened. Argon flow through the cell had begun, and the flow rate and cell pressure were noted at C and D.
5. After the desired amount of argon had passed over the melt, valve 3 was closed and 2 was immediately opened, allowing the argon flow to vent through E.
6. The displaced water was weighed and the temperature and pressure of the argon trapped in K were noted. Barometric pressure was recorded,

completing the information required for the determination.

At the completion of the run, the condenser was removed and a fresh condenser was inserted by the following procedure:

1. The argon gas flow was raised to a high value (~80 ml/min), with the gas being vented at E.
2. The small ball socket M was removed and valve 3 was opened. Argon flowed into the cell at joint M and swept out at N.
3. The large ball joint O was opened and the condenser was slowly removed. The high flow rate of argon in N and out O served to keep the cell oxygen-free.
4. The filled condenser was separated from the Mariotte flask system at joint P. A new condenser, previously flushed with purified argon, was attached at P.
5. The new condenser was slowly inserted into the cell until a seal at the large socket O was secured. The argon flow was maintained for three to four minutes to sweep out air trapped in the ring seal of the condenser.
6. Valve 3 was closed, and ball socket M was replaced. Argon over-pressure was vented at E.
7. The temperature control point was raised, and after equilibrium was reached the argon flow rate was adjusted with valve 1 to the desired value.
8. A second determination was started as described above.

When the new condenser had been secured in the cell, and temperature equilibration was being reached, the Mariotte flask was refilled with distilled water. This procedure follows:

1. Valves 4 and 5 were closed. Valve 6 was opened and the thermometer was removed from the flask.
2. The Ehrlenmeyer container was removed from under the drip tip and the water was poured into the flask through the funnel at valve 6. The argon in the flask was displaced through the thermometer socket.
3. After the flask was full, valve 6 was closed, and the thermometer was replaced in its socket. The container was returned to its position under the drip tip and valve 5 was opened.
4. Water flowed from the drip tip until the pressure in the long delivery tube returned to atmospheric pressure. Valve 4 was opened to the condenser and the Mariotte flask was ready for a second determination.

The use of a Mariotte flask of this design allowed the argon to flow through the entire system against a constant back pressure, namely, atmospheric pressure. It also gave a simple and rapid method of determining the amount of argon passed during the run. The moles of argon passed can be calculated from the temperature and pressure observed in the flask and from the weight of the displaced water, with density corrections and a correction for the partial pressure of the water vapor in the gas space. Expansion or contraction of the residual gas left in the flask after the filling operation had a negligible effect on the amount of water displaced, since room temperature changes during a determination were small and the amount of gas remaining was small (<25 cc).

After removal, the condensers were placed in a cooling tube consisting of a sealed pyrex tube, ending in a $^{25}/_{18}$ ball socket. After cooling, all grease was carefully removed from the condensers and the outer surfaces were wiped clean of any salt. The condensers were then weighed on a Voland balance to 0.1 mg. After weighing, the condensate was dissolved in 5% H_2SO_4 and diluted to 100 ml. Following removal of the condensate, the condensers were rinsed with distilled water and acetone, dried with an argon stream, and reweighed. The weight of condensate was obtained by difference, and served as a check on the analytical results obtained later.

Generally, enough argon was passed so that 100–150 mg of salt condensate were obtained. For vapor pressures near 10 mm, each determination took about 1½ hr, while at higher pressures, the determinations took less time. Temperatures were noted repeatedly during each determination and when drift was observed, an average value for the temperature was used. Temperature drifts during a determination were small, amounting generally to less than 0.5°C.

6. RESULTS OF VAPOR PRESSURE MEASUREMENTS: PURE COMPOUNDS

TOTAL PRESSURES BY RODEBUSH METHOD

For a definitive treatment of partial pressures from salt mixtures, the vapor pressure and equilibrium vapor composition for the pure compounds must be known. The Rodebush method was used to determine the static vapor pressures of the three pure compounds used in this work. The data obtained from the Rodebush apparatus are given in Tables 1, 2, and 3 and were fitted by the method outlined by Kelley[26] in which the vapor pressure p is related to the absolute temperature T, by a function of the form

$$(1)\ \log_{10} p = \frac{-\Delta H_0}{4.576} T^{-1} + \frac{\Delta C_p}{4.576} \log_{10} T + I \ ,$$

where

p = vapor pressure, mm Hg,

T = absolute temperature, °K,

ΔH_0 = heat of vaporization per mole at 0°K, kcal/mole,

ΔC_p = difference in heat capacity between liquid and vapor, cal/mole °K,

I = integration constant, related to the entropy of vaporization.

The values used for ΔC_p were −8 cal/mole deg for LiCl and −7 cal/mole deg for KCl (similar values were used by Kelley[26]). For $FeCl_2$, ΔC_p was −10.4 cal/mole deg based on the following values: $C_p(FeCl_2, gas) = 14.0 \pm 0.5$ cal/mole deg (estimated for 900–1500°K), and $C_p(FeCl_2, liq) = 24.4$ cal/mole deg (950–1100°K[41]). The results of the calculation are summarized in Table 4. In each case, the derived equations express the relationship between experimental values of log p and T to within 2%. The experimental results and results obtained by other investigators are shown in Figs. 17, 18, and 19; the equation fitting the experimental data in each case is shown by the solid line.

The heat of vaporization can be obtained from the constants in Eq. 1. Values for the heat of vaporization for the salts studied are given in Table 5, in comparison with the results obtained by Kelley.[26]

[41] G. E. Moore, "Heat Contents at High Temperatures of the Anhydrous Chlorides of Ca, Fe, Mg, Ni, and K," *J. Am. Chem. Soc.* 65, 1700 (1943).

DISCUSSION

KCl. – Recent vapor pressure measurements by Barton and Bloom[23] for KCl by the boiling point method appear to be the most reliable values, agreeing very well with the older data obtained by Rodebush and Fiock.[25] The values obtained here are in general about 1.5°K lower at a given pressure than the values of Rodebush and Fiock, agreeing with the data of Barton and Bloom to within experimental reproducibility. Extrapolation of Eq. 1 for KCl yields a value of 1688°K for the boiling point (cf. Barton and Bloom, 1686°K; Rodebush and Fiock, 1680°K; von Wartenburg and

Table 1. Total Pressure of Pure KCl

$$\log_{10} p_{mm} = -10{,}950\ (T^\circ K)^{-1} - 3.526 \log_{10} T^\circ K + 20.747$$

T (°C)	p_{mm} Observed	p_{mm} Calculated
987	13.6	13.4
987	13.4	13.4
988	13.5	13.5
1005	16.7	16.8
1013.5	19.2	18.7
1013.5	18.9	18.7
1027	21.0	22.0
1026.5	21.3	21.8
1037	24.9	24.6
1037	25.2	24.6
1039	25.8	25.6
1038	25.2	25.2
1050	27.7	28.8
1050	28.7	28.8
1073	38.2	38.0
1073	37.4	38.0
1074	37.9	38.0
1074	37.0	38.0
1115	60.7	59.3
1115	59.9	59.3
1137	73.2	74.6
1137	74.0	74.6
1150	85.9	85.3
1164	98.7	98.0
1164	97.7	98.0
1186	122.5	122.2
1186	117.8	122.2

Table 2. Total Pressure of Pure LiCl

$$\log_{10} p_{mm} = -10{,}599\ (T^{\circ}K)^{-1} - 4.026 \log_{10} T + 22.249$$

T (°C)	p_{mm} Observed	p_{mm} Calculated
921.5	9.8	9.7
922.5	9.9	9.9
982	21.3	21.4
981.5	21.5	21.2
981	21.0	21.0
1002	27.0	27.2
1003	27.6	27.5
1029.5	38.2	37.3
1029.5	37.4	37.3
1046.5	45.2	45.2
1046.0	44.7	44.9
1064	54.9	54.5
1064	54.9	54.5
1083.5	67.5	66.8
1083.5	67.9	66.8
1105	84.2	83.0
1104.5	83.9	82.6

Albrecht,[22] 1690°K; Ruff and Mugdan,[42] 1688°K). The heat of vaporization for KCl shows satisfactory agreement with the value quoted by Kelley (based on the data of Rodebush and Fiock).

LiCl. – Vapor pressure data on LiCl are somewhat meager. The data obtained in this work show satisfactory agreement with the results of Maier[43] (who claims only "technical accuracy" for his values) and those of von Wartenburg and Schultze.[44] The vapor pressures given by Ruff and Mugdan[42] appear to be too high. Extrapolation of Eq. 1 for LiCl yields a value of 1653°K for the boiling point (cf., von Wartenburg and Schultze, 1655°K; Maier, 1656°K; Ruff and Mugdan, 1610°K). The heat of vaporization for LiCl again shows satisfactory agreement with the value quoted by Kelley (based on the data of von Wartenburg and Schultze).

[42] O. Ruff and S. Mugdan, "Messung die Dampfdruck bei Hohen Temperaturen der Alkalihalogenide," *Z. anorg. u. allgem. Chem.* 117, 147 (1921).

[43] C. G. Maier, "Vapor Pressures of the Common Metallic Chlorides and a Static Method for High Temperatures," *Tech. Paper 360, Bureau of Mines*, 1929.

[44] H. von Wartenburg and H. Schulze, "Der Dampfdruck Einiger Salze," *Z. Elektrochem.* 27, 568 (1921).

Table 3. Total Pressure of Pure $FeCl_2$

$$\log_{10} p_{mm} = -9{,}856\ (T^{\circ}K)^{-1} - 5.234 \log_{10} T^{\circ}K + 26.829$$

T (°C)	$(T^{\circ}K)^{-1} \times 10^4$	p_{mm} Observed	p_{mm} Calculated
740	9.870	23.3	24.1
739	9.879	23.2	23.7
748	9.787	29.6	27.7
748	9.787	27.5	27.7
764	9.641	34.8	35.3
764	9.641	36.0	35.3
772	9.567	40.6	40.0
773	9.558	40.5	40.0
789	9.414	51.6	51.7
789	9.414	51.7	51.7
796	9.353	57.5	57.3
796	9.353	56.1	57.3
812	9.215	73.3	72.1
812	9.215	72.7	72.1
820	9.147	79.3	80.9
820	9.147	77.6	80.9
833	9.040	99.7	96.7
833	9.040	97.7	96.7
845	8.943	114.8	113.8
845	8.943	111.5	113.8
858	8.840	137.5	135.2
857	8.848	135.1	133.5
869	8.755	156.6	156.0
870	8.747	155.5	158.0
886	8.627	195.1	193.2
887	8.619	200.5	195.9
892	8.582	203.0	208.3
892	8.582	208.3	208.3
906	8.480	250.1	247.2

Table 4. Vapor Pressure Equations for Pure Salts

(P_{mm}, $T^{\circ}K$)

KCl	$\log_{10} P = -10{,}950\ T^{-1} - 3.526 \log_{10} T + 20.747$
LiCl	$\log_{10} P = -10{,}599\ T^{-1} - 4.026 \log_{10} T + 22.249$
$FeCl_2$	$\log_{10} P = -9{,}856\ T^{-1} - 5.234 \log_{10} T + 26.829$

$FeCl_2$. – The data of Maier[43] are the only published values for the vapor pressure of ferrous chloride by a static pressure method. The data ob-

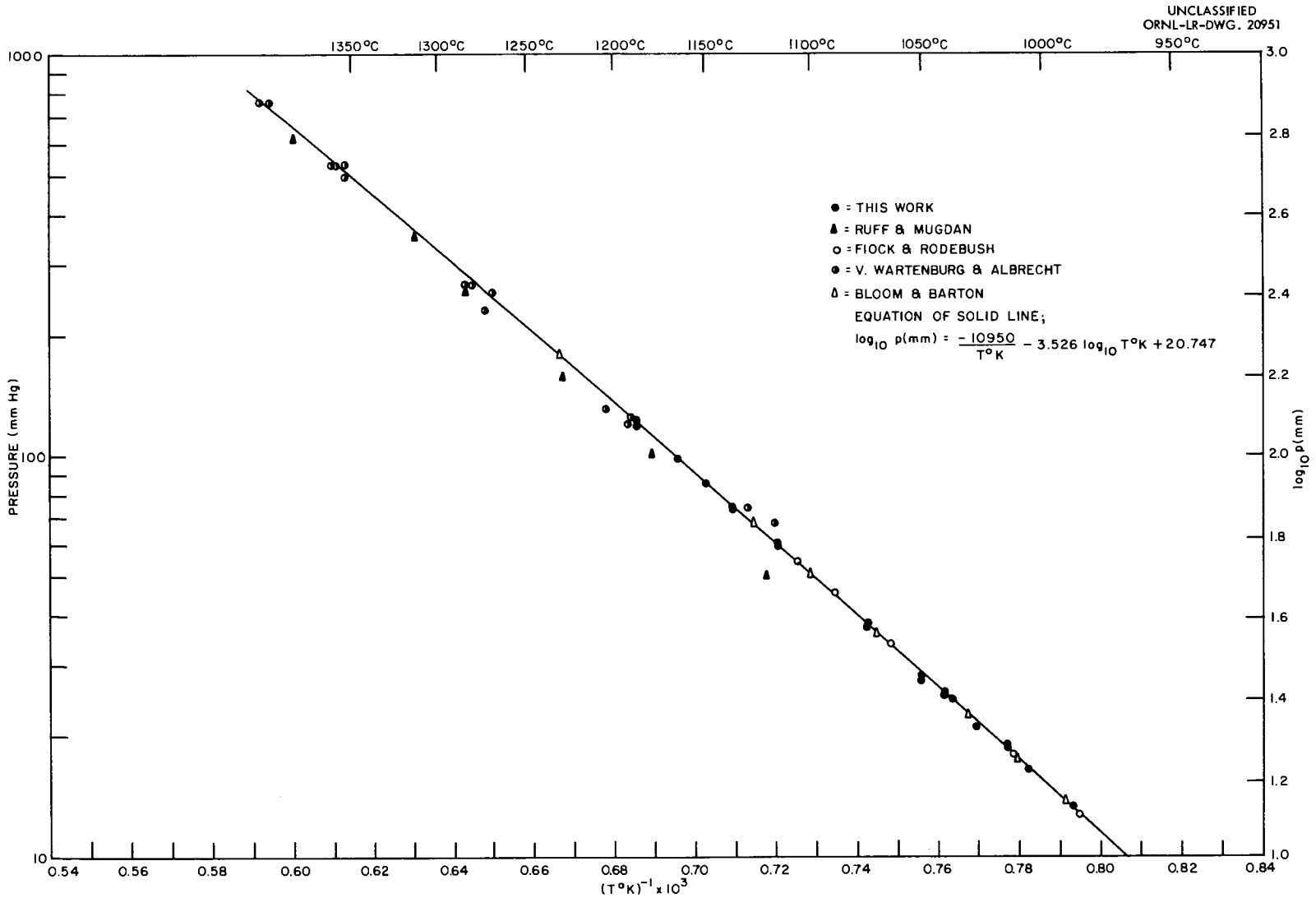

Fig. 17. Vapor Pressure of KCl as a Function of Temperature.

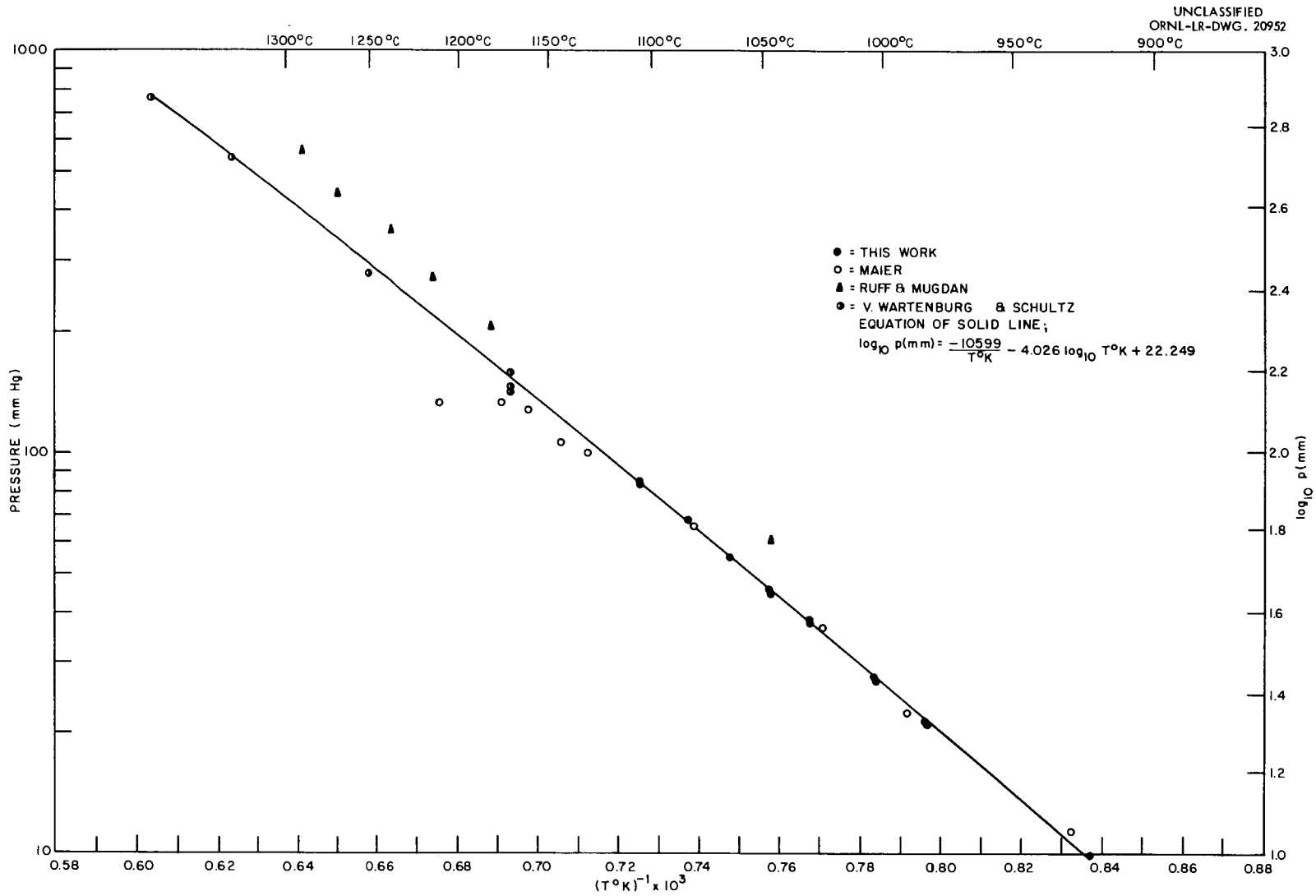

Fig. 18. Vapor Pressure of LiCl as a Function of Temperature.

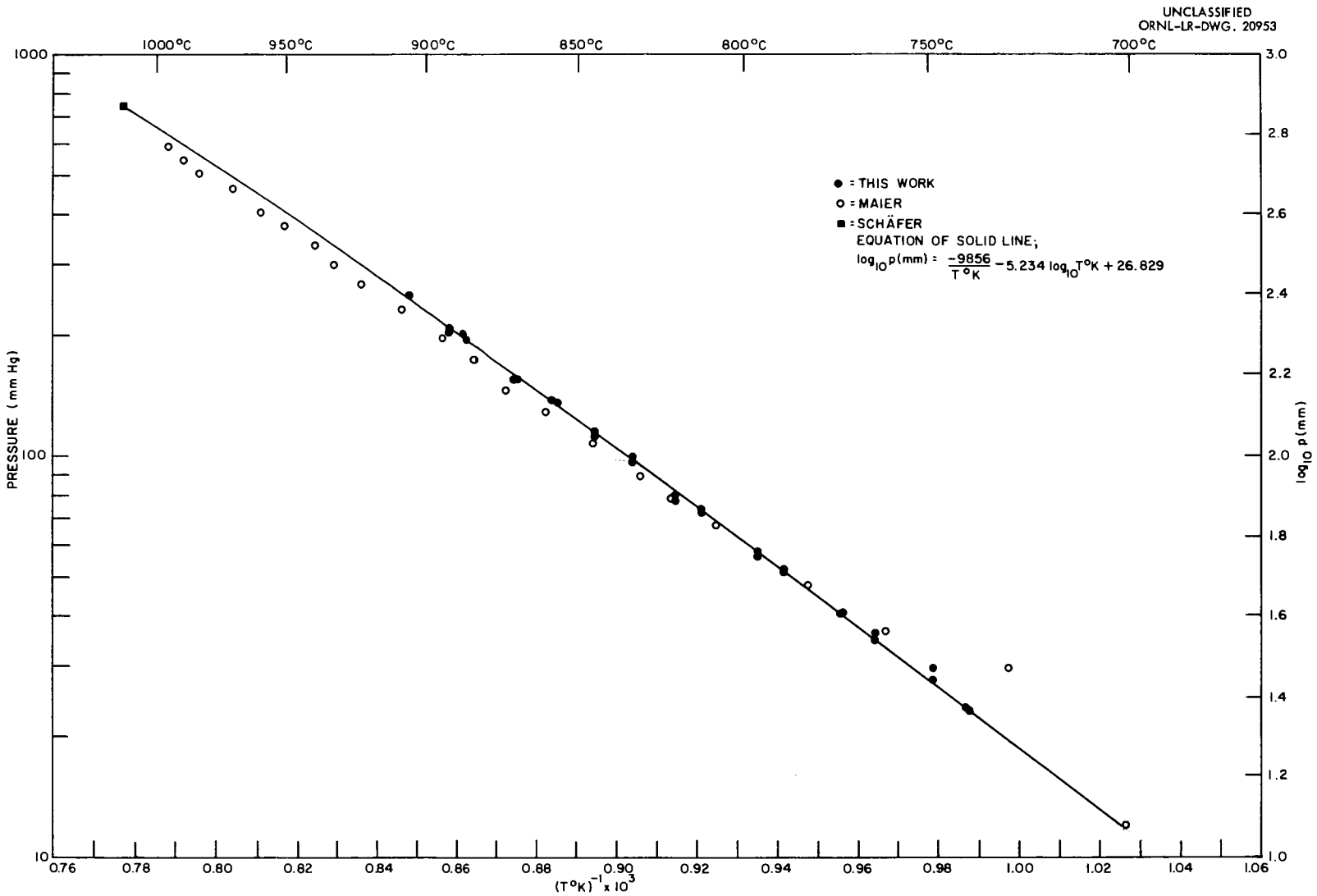

Fig. 19. Vapor Pressure of $FeCl_2$ as a Function of Temperature.

Table 5. Heat of Vaporization ΔH, kcal/Mole for Pure Salts

	This Work	Kelley[26]
KCl	$50.1 - 7.0 \times 10^{-3} T \pm 0.2$	$50.6 - 7.0 \times 10^{-3} T$
LiCl	$48.5 - 8.0 \times 10^{-3} T \pm 0.2$	$49.2 - 8.0 \times 10^{-3} T$
$FeCl_2$	$45.1 - 10.4 \times 10^{-3} T \pm 0.2$	$43.2 - 10.0 \times 10^{-3} T$

tained in this work are 5–7°K lower at a given pressure than the values of Maier, and are considerably more self-consistent. Shäfer[45] has discussed the data of Maier, pointing out possible errors in his determination. Shäfer has determined the boiling point of ferrous chloride directly, obtaining a value of 1283 ± 3°K at a pressure of 748 mm. The boiling point obtained by an extrapolation of Eq. 1 for $FeCl_2$ gives a value of 1283°K at this pressure. In view of the excellent agreement between the observed and extrapolated boiling points, and in view of the consistent results obtained for KCl and LiCl, the values for the vapor pressure of ferrous chloride by the Rodebush method are considered reliable. The heat of vaporization for $FeCl_2$ shows that the value given by Kelley (based on the data of Maier) is approximately 1 kcal too low.

DETERMINATION OF MOLECULAR WEIGHT OF INDIVIDUAL PURE SALT VAPORS

As discussed earlier in Chap. 1, a combination of static vapor pressure data with transportation data at a given temperature yields a value for the molecular weight of salt vapor under investigation. Dalton's Law of Partial Pressures applied to the transportation data can be written as Eq. 16 (Chap. 1)

$$p_{static} = \left[\frac{w/\bar{M}}{n_A + w/\bar{M}} \right] P_{total} ,$$

where

p_{static} = static vapor pressure, mm Hg,

w = weight of salt transported, mg,

$\bar{M}$ = average mol wt of salt vapor,

n_A = moles of argon transporting salt,

P_{total} = total pressure of salt vapor of argon, mm.

Solving for the vapor molecular weight gives

$$\bar{M} = \frac{w}{n_A} \left[\frac{P_T}{p_s} - 1 \right] . \tag{2}$$

Equation 2 was solved at each experimental transportation point, substituting the static pressure at the transportation temperature obtained from the Rodebush data. The weight of condensate, and the observed total pressure during the transport run (the sum of the barometric pressure and manometric pressure during the transportation determination) were known experimentally.

The number of moles of argon was calculated from the ideal gas law, using the experimental data obtained from the Mariotte flask:

$$n_A = \frac{\left[P_{Bar} - \Delta P_{H_2O} - p_{H_2O} \right] W_{H_2O}}{R(273 + T°C)\, \rho_{H_2O}} , \tag{3}$$

where

n_A = moles of argon passed through transport cell,

P_{Bar} = barometric pressure during determination, mm Hg,

ΔP_{H_2O} = difference in Mariotte flask pressure and atmosphere pressure, mm Hg,

ρ_{H_2O} = density of water at T°C, g/cc,

T°C = room temperature during determination,

W_{H_2O} = wt of water collected during determination, g,

R = gas constant cc mm/mole °C,

[45] H. Shäfer *et al.*, "Sattigungsdrucke der Chloride $MnCl_2$, $FeCl_2$, $CoCl_2$, und $NiCl_2$," *Z. anorg. u. allgem. Chem.* **278**, 300 (1955).

p_{H_2O} = partial pressure of water at T°C, mm Hg.

The substitution of n_A into Eq. 2, along with the aforementioned substitutions for w, P_T, and p_s, gives an experimental value for the molecular weight of the vapor transported. The experimental data, along with the derived average molecular weight calculated at each point for the three salts under consideration are given in Tables 6, 7, and 8. The accuracy of the average molecular weight value is ±2%, based on the following estimated accuracies n_A = ±0.5%, p_s = ±1%, P_{total} = ±0.2%, w = 1%.

Table 6. Transportation Data for Pure KCl

T, °C	962	988	1010	1030	1069	1099
Barometer pressure, mm	739.9	740.0	739.5	739.5	739.8	739.8
Manometer pressure, mm	5.3	4.3	4.2	4.2	3.6	5.4
Total pressure, mm	745.2	744.3	743.7	743.7	743.4	745.2
Flow rate, cc/min	33	27	27	27	24	31
Mariotte flask data:						
ΔP, mm	15.5	12.7	10.8	16.2	15.0	13.9
T, °C	29.9	29.6	30.8	29.8	31.0	31.1
wt H_2O, g	1060	1248	1017	698	508	493.0
cc argon	1065	1253	1022	701	511	495.5
mmoles argon (Eq. 3, chap. 4)	39.32	46.49	37.70	25.80	18.69	18.21
wt condensate, mg	44.3	76.3	85.7	75.4	88.6	123.8
p_{static}, mm (see Table 1)	9.4	13.3	17.7	22.8	36.4	51.4
Average mol wt (Eq. 2, chap. 4)	88.1	90.9	93.1	93.8	92.1	91.8

Table 7. Transportation Data for Pure LiCl

T, °C	956	977	1010	1040
Barometer pressure, mm	739.3	736.9	736.2	736.1
Manometer pressure, mm	5.5	5.5	5.4	5.2
Total pressure, mm	744.8	742.4	741.6	741.3
Flow rate, cc/min	32	30	30	27
Mariotte flask data:				
ΔP, mm	18.0	14.3	14.8	12.7
T, °C	27.3	29.3	29.2	30.0
wt H_2O, g	1954.0	1493.0	1429.0	965.0
cc argon	1960.8	1499.1	1434.9	969.2
mmoles argon	73.71	55.73	52.99	35.72
wt condensate, mg	110.7	110.0	158.4	152.9
p_{static}, mm	15.5	20.1	29.7	42.2
Average mol wt	70.9	70.9	71.6	70.6

Table 8. Transportation Data for Pure $FeCl_2$

T, °C	707	725	733	752	760	792	798	829	894
Barometer pressure, mm	732.7	734.5	731.7	734.8	730.0	729.2	734.8	734.4	734.6
Manometer pressure, mm	3.1	3.5	4.1	2.8	3.2	3.4	2.2	1.7	4.8
Total pressure, mm	735.8	738.0	735.8	737.6	733.2	732.6	737.0	736.1	739.4
Flow rate, cc/min	23	20	25	19	18	25	19	18	15
Mariotte flask data:									
ΔP, mm	13.8	14.7	12.9	13.7	11.5	16.3	12.7	11.7	9.4
T, °C	28.8	28.1	29.6	29.0	27.9	27.2	29.8	29.2	29.0
wt H_2O, g	742.0	719.5	479.0	435.0	609.5	672.5	508.0	508.0	572.5
cc argon	745.0	722.2	481.0	436.7	611.8	674.9	510.2	510.0	574.8
mmoles argon	27.39	26.71	17.62	16.09	22.60	24.83	18.77	18.77	21.35
wt condensate, mg	73.0	97.6	78.7	100.2	162.8	296.9	237.8	389.5	1371.9
p_{static}, mm	13.8	18.8	21.3	29.2	33.0	54.0	59.0	91.5	213.4
Average mol wt	139	143	150	151	153	150	146	150	159

From the average molecular weight, calculated at each experimental point, the mole fraction of monomer and dimer can be calculated for each of the pure salts, on the assumption that the vapor exists only as monomer and dimer species. The validity of this assumption will be discussed for each of the pure salts individually. In calculating the mole fraction of monomer and dimer, the following relationship is used:

$$\bar{M} = x_1 M + 2x_2 M \ , \tag{4}$$

where

$\bar{M}$ = average molecular weight,

M = molecular weight for monomer species,

x_1 = mole fraction of monomer in vapor,

x_2 = mole fraction of dimer in vapor.

With the assumption that only monomer and dimer exist in the vapor, or that $x_1 + x_2 = 1$, the mole fractions can be calculated directly from Eq. 4. From Dalton's Law of Partial Pressures, the partial pressures of monomer and dimer in the vapor must equal the static vapor pressure determined by the Rodebush method. Thus, the partial pressures of the two species can be calculated from

$$p_i = x_i p_s \ , \tag{5}$$

where

p_i = partial pressure of ith species (monomer or dimer),

x_i = mole fraction of ith species at T°C,

p_s = static vapor pressure determined by Rodebush method at T°C.

The results of the mole fraction calculations, using Eq. 4 and partial pressure calculations from Eq. 5, are summarized in Tables 9 and 10 for the three pure salts. A plot of the partial pressures as a function of temperature for the alkali halide salts is given in Fig. 20, and a similar plot for $FeCl_2$ is given in Fig. 21. The mole fractions are known to ±2%, and thus the partial pressures are known to ±3%. The lines drawn in Figs. 20 and 21 represent a least squares fit to the experimental partial pressures, except in the case of KCl, discussed below. Since the experimental temperature ranges of the partial pressure determinations are not large, the data were fitted to an equation of the form

$$\log p = \frac{A}{T} + B$$

for LiCl and $FeCl_2$. For KCl, the data were fitted with the inclusion of a heat capacity correction following the general method used for the total pressure data analysis. The heat capacity for the K_2Cl_2 molecule was estimated as 19 kcal/mole.

This heat capacity correction was needed in order to compare heats of vaporization determined at 1300°K in this work with heats of vaporization determined at 1050°K by effusion studies.

The heats of vaporization for the LiCl and $FeCl_2$ species were calculated from the constants A in the least squares equations. The heats of vaporization thus obtained are given in Table 11, along with the heats calculated for KCl, which include the heat capacity correction. The limits of error were obtained from the estimated standard deviation of the constant A in the least squares fit.

In addition to the heats of vaporization, the equilibrium constant for the dimerization reaction can be calculated from the smoothed partial pressure data:

$$(AB)_2 = 2AB$$

$$K_p = \frac{p_{AB}^2}{p_{(AB)_2}} . \tag{6}$$

The equilibrium constants calculated from these data are shown in Fig. 22 as a function of temperature for the three pure salts under consideration. These equilibrium constants are required to calculate partial pressures from transport data and total pressure data obtained for the mixtures.

Table 9. Partial Pressures of Monomer and Dimer Species Above Liquid KCl and LiCl

	T (°C)	x_{mono}	x_{dim}	p_m (mm)	p_0 (mm)	p_{static}
KCl	962	0.818	0.182	7.7	1.7	9.4
	988	0.781	0.219	10.3	2.9	13.2
	1010	0.751	0.249	13.3	4.4	17.7
	1030	0.742	0.258	16.8	5.9	22.7
	1069	0.764	0.236	27.6	8.5	36.1
	1099	0.768	0.232	38.9	11.8	50.7
LiCl	956	0.332	0.668	5.1	10.4	15.5
	977	0.332	0.689	6.7	13.4	20.1
	1010	0.311	0.668	9.2	20.5	29.7
	1040	0.332	0.668	14.0	28.2	42.2

Table 10. Partial Pressure of $FeCl_2$ and Fe_2Cl_4 Above Pure Liquid $FeCl_2$

T (°C)	x_{mono}	x_{dim}	p_m (mm)	p_0 (mm)	p_{static} (mm)
707	0.900	0.100	13.8	1.4	12.4
725	0.897	0.103	18.8	1.9	16.9
732.5	0.817	0.183	21.3	3.9	17.4
752	0.807	0.193	29.2	5.6	23.6
759.5	0.794	0.206	33.0	6.8	26.2
792	0.814	0.186	54.0	10.0	44.0
798	0.851	0.149	59.0	8.8	50.2
829	0.817	0.183	91.5	16.7	74.8
894	0.748	0.252	213.4	53.8	159.6

DISCUSSION

KCl. – The existence of measurable amounts of dimerized species in KCl beams has been conclusively shown, both in mass spectrometric studies and in magnetic resonance studies.[46] In addition, Miller and Kusch[47] have investigated the velocity distribution of a beam of KCl escaping from an isothermal oven, and find that the beam consists of about 22% dimer species at 700°C. The observed velocity distribution was explained satisfactorily without postulating the existence of a trimer. In addition, no trimer species[48] has been found in mass spectroscopy studies conducted on KCl.

[46] P. Kusch, J. Ochs, and R. Cote, "Radiofrequency Spectrum of Components of a Sodium Chloride Beam," *J. Chem. Phys.* 21, 459 (1953).

[47] R. Miller and P. Kusch, "Molecular Composition of Alkali Halide Vapors," *J. Chem. Phys.* 25, 860 (1956).

[48] H. Rosenstock *et al.*, *Mass Spectrometer Study of the Alkali Halides* (unpublished).

Table 11. Heat of Vaporizations for Monomer and Dimer Above Pure Liquid KCl, LiCl, and $FeCl_2$

	KCl	LiCl	$FeCl_2$
ΔH_{vap} (monomer), kcal/mole	$50.7 - 7.0 \times 10^{-3}\,T$	38.2 ± 1.3	31.3 ± 0.5
ΔH_{vap} (dimer), kcal/mole	$57.4 - 13.0 \times 10^{-3}\,T$	38.7 ± 0.8	41.7 ± 1.0

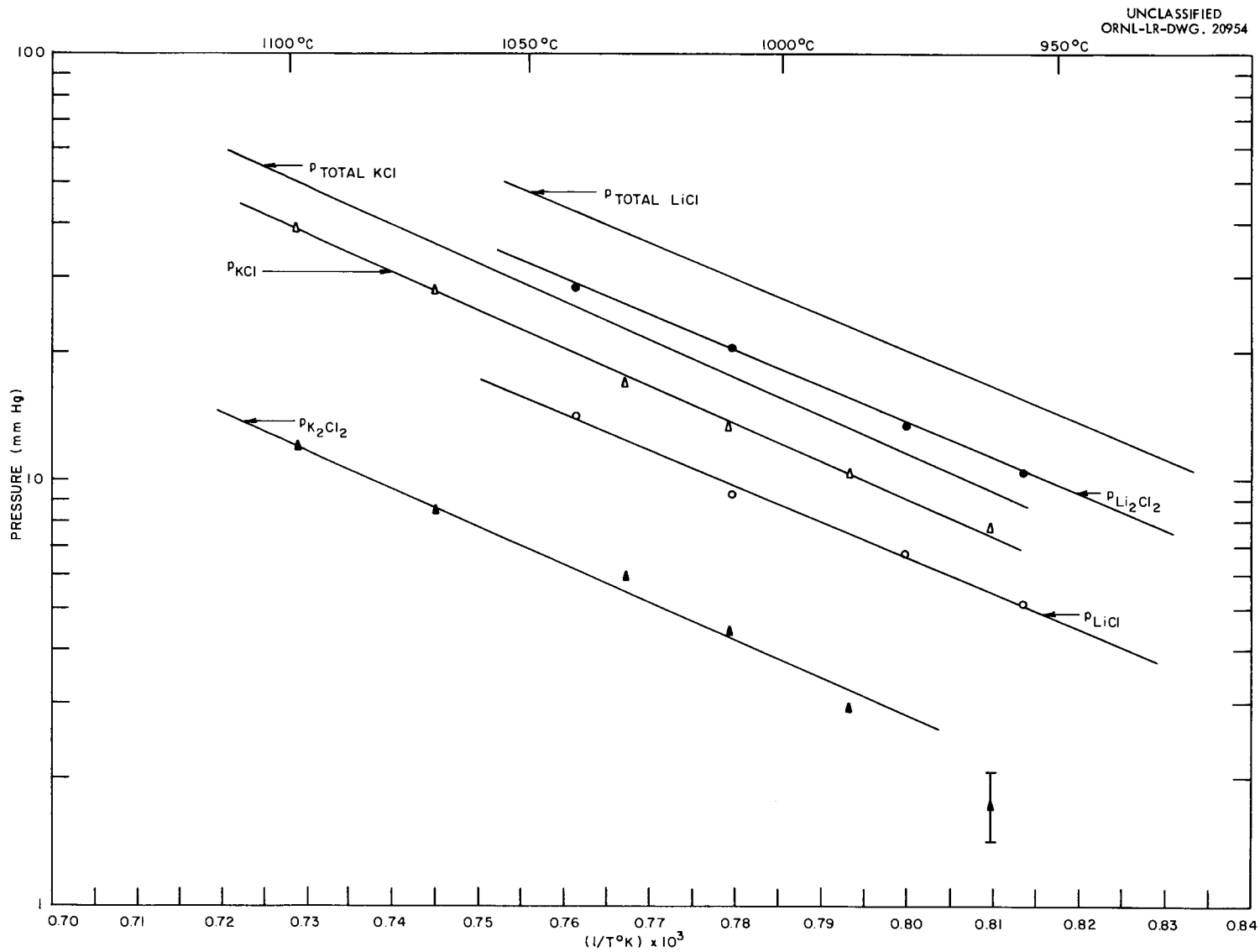

Fig. 20. Partial Pressures of Monomer and Dimer for KCl and LiCl as a Function of Temperature.

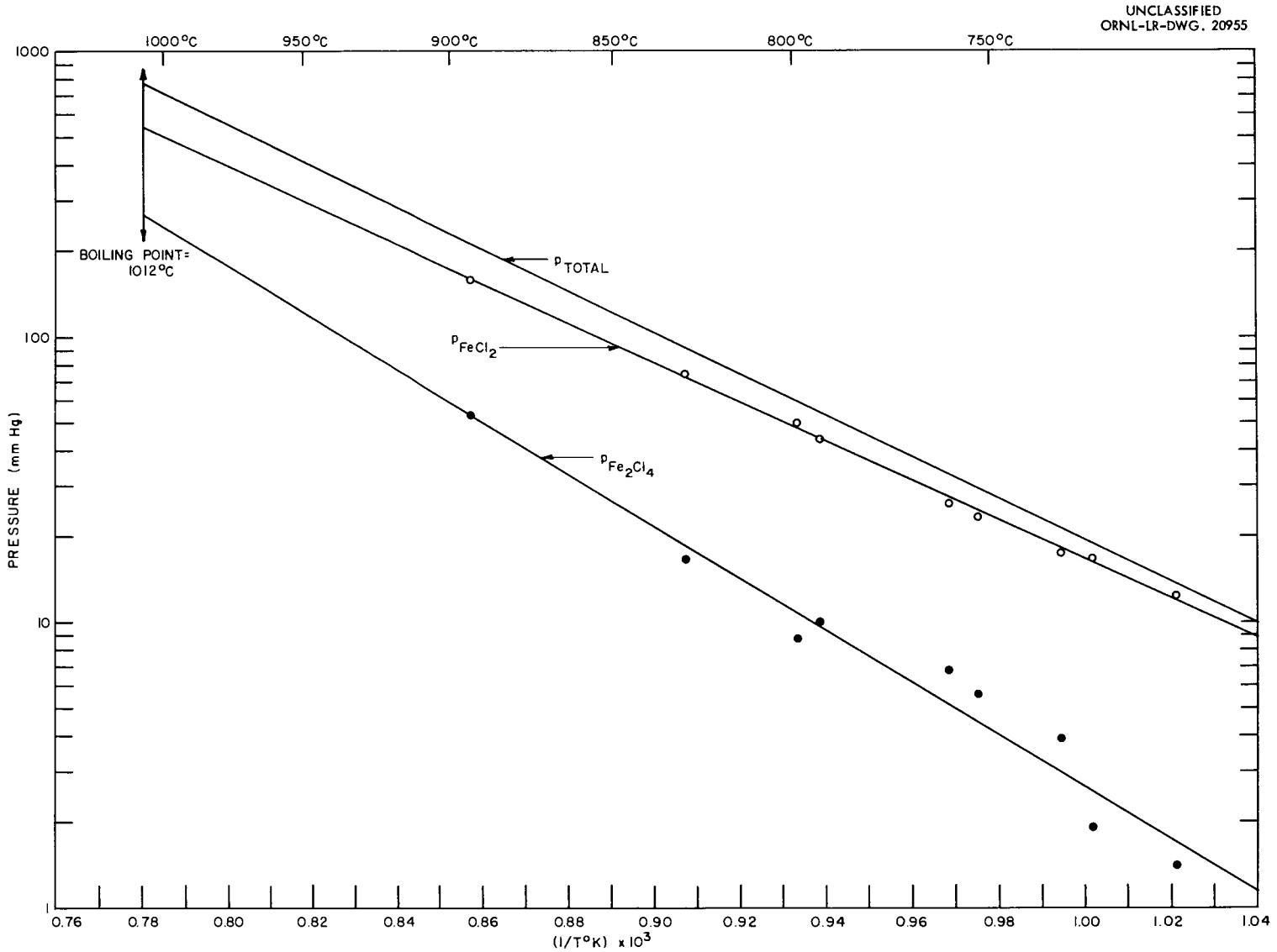

Fig. 21. Partial Pressures of Monomer and Dimer Above Liquid $FeCl_2$ Showing Relative Increase in Dimer Content with Increasing Temperature.

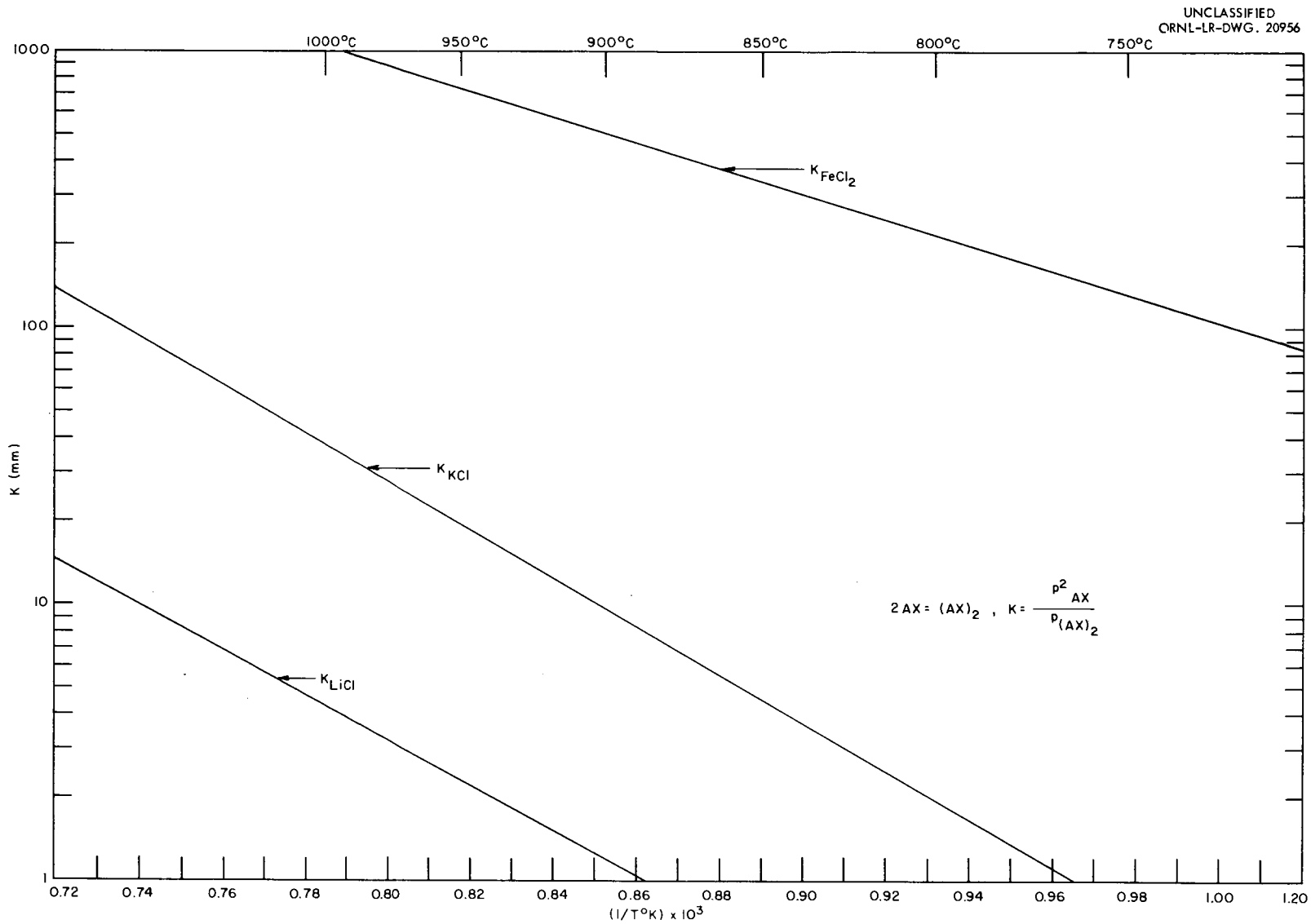

Fig. 22. Equilibrium Constants of Dimerization Reactions of Pure Salts as a Function of Temperature.

While neither of the above experiments proves conclusively that no trimer species exists in the vapor, it is certain that the amount of trimer in the equilibrium vapor mixture must be exceedingly small.

Measurements of the dipole moment of the KCl molecule showed a rather high value of 10 Debye units,[49] and early workers were quick to realize the possibilities that a double molecule could exist in the vapor phase. However, the first attempts to measure the extent of dimerization of alkali halides were generally unsuccessful.[49] The calculations of Zimm and Mayer[50] led to the conclusion that the beam cannot contain more than 2% dimer at 525°C. These calculations were based on entropy considerations which are insensitive to small amounts of dimer present in the vapor phase. Thus, the more direct methods, where the presence of the dimer molecule can be shown experimentally (e.g., mass spectroscopy, velocity distribution) generally disprove the earlier arguments for a strictly monomeric vapor phase above KCl.

The results of this work are in general agreement with those of Miller and Kusch,[47] and indicate that the equilibrium vapor phase above a KCl melt contains about 25% dimer molecules and 75% monomer molecules. Since Miller and Kusch measured the velocity distributions of vapor molecules above solid KCl, a comparison between their results and the present results must take into account the difference in the condensed phases. Miller and Kusch obtained the ratio of dimer to monomer as a direct experimental variable. In turn, this ratio fixes with some certainty the heats of vaporization of monomer and dimer. The calculation of partial pressures from their data is difficult because of the uncertainty of detector efficiency; hence the pressure values were accorded only 25% accuracy. It thus seems best to compare the results on the basis of heats of vaporization rather than absolute pressure values.

Miller and Kusch quote the following values for the heat of sublimation of monomeric and dimeric KCl, at the melting point, 1045°K:

$$\Delta H_s(\text{mono}) = 51.2 \pm 0.3 \text{ kcal/mole} ,$$

$$\Delta H_s(\text{dim}) = 54.5 \pm 0.8 \text{ kcal/mole} .$$

Converting these values into heat of vaporization values at the melting point requires subtracting the heat of fusion from the heat of monomer sublimation, while twice the heat of fusion must be subtracted from the heat of dimer sublimation (since two molecules of KCl are involved). Thus, the expected values for the heat of vaporization of the two species based on Miller and Kusch's heats of sublimation are

$$\Delta H_s(\text{mono}) - 2H_f = \Delta H_{vap}(\text{mono}) = 45.1 \text{ kcal/mole} ,$$

$$\Delta H_s(\text{dim}) - 2\Delta H_f = \Delta H_{vap}(\text{dim}) = 42.3 \text{ kcal/mole} .$$

These values may be compared with those obtained in this work. From the equations given in Table 11 for the heat of vaporization of the two species, the following values are obtained at 1045°K:

$$\Delta H_{vap}(\text{mono}) = 43.6 \text{ kcal/mole} ,$$

$$\Delta H_{vap}(\text{dim}) = 43.8 \text{ kcal/mole} .$$

A rather significant discrepancy arises upon comparison of these two sets of values. The values obtained from Miller and Kusch's data indicate that the monomer pressure should increase relative to the dimer pressure above the liquid. The present results indicate that the two pressures should remain constant relative to each other. This near constancy of the vapor composition above liquid KCl is in agreement with recent unpublished work by Bloom and Barton,[51] and also with effusion studies by Minturn and Datz.[52] It is possible that the data of Miller and Kusch were subject to error in the determination of the ΔH_s values.

The above calculation can be reversed, and heats of sublimation can be calculated from heats of vaporization obtained in the present study. The heats of sublimation are obtained quite simply:

$$\Delta H_s(\text{mono}) = 43.6 + 6.1 = 49.8 \text{ kcal/mole} ,$$

$$\Delta H_s(\text{dim}) = 43.8 + 12.2 = 56.0 \text{ kcal/mole} .$$

[49] V. Deitz, "The Vapor Pressure of Potassium Chloride and Cesium Iodide Crystals," *J. Chem. Phys.* 4, 575 (1936).

[50] B. Zimm and J. Mayer, "Vapor Pressures, Heats of Vaporization and Entropies of Some Alkali Halides," *J. Chem. Phys.* 12, 362 (1944).

[51] H. Bloom and J. L. Barton, private communication.

[52] R. Minturn and S. Datz, private communication.

The ratio of dimer heat of sublimation to that of manomer is 1.12 ± 0.4, falling between the value obtained by Miller and Kusch (1.08 ± 0.3) and that obtained by Rosenstock[48] (1.17 ± 0.5). The average heat of sublimation calculated by weighting the the individual heats of sublimation by their respective mole fractions at the melting point is 51.4 kcal/mole. This value is in good agreement with direct experimental values obtained for the average heat of sublimation, viz., 51.1 by Zimm and Mayer; 51.8 by Treadwell and Werner;[53] 50.6 by Mayer and Wintner.[54]

Except for the as yet unpublished work of Bloom and Barton,[51] there are few literature values for vapor pressures of liquid KCl based on transportation results. Such results would serve as a direct check on the values obtained in this work. Jellinek[15] and co-workers determined the vapor pressure at one temperature, basing the calculation of the vapor pressure on the assumption of pure monomer in the vapor. A recalculation of this data would indicate an average molecular weight at 1250°C of about 80. However, the temperatures varied by ±5°C during these determinations, a range which could change the average molecular weight by a factor of at least 5%. This value for the average molecular weight calculated from the one point determined by Jellinek is not in serious disagreement with those obtained in this work. Kangro and Wieking[55] have also obtained three vapor pressure points above liquid KCl by the transportation method. These values yield an extremely low figure for the heat of vaporization, and hence do not appear to be reliable. However, the pressures quoted, based on the assumption of monomeric vapor, are in general agreement with the values observed here. The transportation data of Kangro and Wieking are higher than the static pressures obtained at the same temperature, and this discrepancy can be explained by assuming an average molecular weight of 90.

[53] W. P. Treadwell and W. Werner, "Über die Bestimmung des Dampfdrucks von Festem Cäsium, Rubidium, and Kaliumchlorid nach der Mitführungsmethode," *Helv. Chim. Acta* 36, 1936 (1953).

[54] J. Mayer and I. Wintner, "Measurements of Low Vapor Pressures of Alkali Halides," *J. Chem. Phys.* 6, 301 (1938).

[55] W. Kangro and H. Wieking, "Dampfdrucke über Geschmolzenen Alkalichloriden und deren Binären Gemischen mit Natriumchlorid," Z. physik. Chem. A183, 199 (1938).

The possibility that experimental errors in the transportation data are responsible for the apparent dimerization must be considered. The maximum recognized error in temperature measurement and control is ±2°C, and in the measurement of the argon volume is 1%. Neither of these errors is large enough to have significant effect on the conclusion. The effect of flow rate on the saturation condition of the argon-vapor mixture is seen to be small, since all the experimental values were determined at different flow rates, with no observable effect on the partial pressures. If the argon passed through the transport cell and did not become saturated with vapor, the condensate would contain less potassium chloride than the amount corresponding to complete saturation of the argon. However, the observed condensates contain more KCl than can be explained on the basis of pure monomer, and a correction for "non-saturation" of the argon would increase this amount. The results obtained on the pure salts and mixtures (see later) indicate that the flow rate had no effect on the amount of condensate deposited, proving that saturation was achieved during the passage of argon. Similarly, diffusion of the vapor into the condenser was negligibly small, as shown both theoretically and experimentally. The conclusion follows that the condensed salt represented the equilibrium vapor above liquid KCl at the experimental temperatures, and that the partial pressures exhibited for the monomer and dimer species are the true partial pressures, within the experimental error.

LiCl. – According to Miller and Kusch,[47] "Lithium chloride ... vapor ... was one of the most complex studied." Velocity distribution curves obtained by Miller and Kusch above solid LiCl and liquid LiCl could only be explained by mixtures consisting of 66% dimer, 28% monomer, and 6% trimer. However, these values do not indicate the distribution of monomer, dimer and trimer that would be in equilibrium with liquid LiCl, since the velocity distribution curves were obtained from vapor samples effusing from a double oven whereby the vapor was heated about 30–60°C above the liquid LiCl saturation temperature. Extrapolation of their results would indicate a distribution of the vapor molecules above liquid LiCl at 638°C consisting of 10% trimer, about 78% dimer and about 12% monomer. The presence of a significant amount of trimer species in the LiCl vapor makes

the calculation of partial pressures of monomer, dimer and trimer impossible from a combination of total pressure and average molecular weight measurements alone. Such experiments yield only two relationships between the three unknowns and a separate unique solution for the partial pressures is clearly impossible. Miller and Kusch have calculated equilibrium constants corresponding to the dimerization and trimerization reactions, which could be used to help determine partial pressures for this work. However, Miller and Kusch point out that the detector efficiency in their apparatus was not unity for lithium chloride. This low detector efficiency would yield low values for the equilibrium constant, and since no estimate was made for the true detector efficiency, a correction factor cannot be used on the equilibrium constant values. While the data of Miller and Kusch cannot be used to help determine the partial pressures of the three species, they can be used to show the relative magnitude of the polymerization reactions.

The data shown in Fig. 20 are in substantial agreement with the results of Miller and Kusch. Using the average molecular weights shown for LiCl in Table 7, it is possible to calculate the amount of monomer and dimer species, with the assumption that these are the *only* species in the vapor. This calculation indicates that the vapor is 68% dimer above liquid LiCl in the temperature range 950°C to 1050°C. The average molecular weight calculated in this temperature range was constant, indicating that the distribution of polymerized vapor species was remaining constant. While it is impossible to calculate the amounts of polymer in the vapor, the experimental verification of a large amount of complex species is obvious.

Other values of the vapor pressure of LiCl based on transportation measurements confirm the results of the present work. Kangro and Wieking[55] measured the vapor pressure of LiCl, and obtained values which were calculated assuming only monomeric species. A recalculation of these values, in light of present knowledge, indicates an average molecular weight for LiCl of 65 in the temperature range of interest. The data of Kangro and Wieking are apparently subject to a systematic error, since the heats of vaporization obtained from their values are consistently lower than those of other reliable workers. Recalculation of their experimental data to account for the presence of dimers helps to correct these discrepancies, but the effect of dimerization is not enough to completely eliminate the systematic error. Despite this error, the values calculated from the data of Kangro and Wieking serve to substantiate those of the present work.

Experimental difficulties were encountered during the measurements of the average molecular weight of LiCl in the transportation apparatus. Severe etching of the quartz condenser and sample container were noted during all runs using LiCl. Attack of the quartz undoubtedly occurred from the action of Li_2O, produced on the surface of the quartz by the following reaction:

$$2LiCl + \tfrac{1}{2}O_2 \longrightarrow Li_2O + Cl_2$$

The standard free energy of the above reaction is +43 kcal/mole, based on Glassner's[56] tabulation of free energy values for oxides and chlorides. While the standard free energy of the reaction is unfavorable, the over-all reaction could conceivably occur, since the activity of the Li_2O would probably be reduced greatly by virtue of the reaction with the silica, with subsequent formation of a lithium silicate. Further purification of the argon stream seemed to have no effect on this corrosion reaction. It is possible that small amounts of oxygen entered the system during the exchange of condensers, or else that absorbed oxygen was responsible for this attack. In general, attack was not noted on the inside of the condenser; the corrosion was confined to the quartz surfaces first exposed to the argon flow. In view of these experimental difficulties, the transportation data on lithium chloride are subject to some question and should be regarded as tentative.

$FeCl_2$. – There is no literature evidence giving the specific distribution of polymerized species in $FeCl_2$. Attempts to measure the molecular species by techniques of mass spectroscopy are summarized in Appendix B. The type of study could not prove or disprove the existence of dimer molecules in a ferrous chloride vapor beam. The high volatility of $FeCl_2$ made impossible the investigation of vapor in equilibrium with liquid $FeCl_2$.

[56] A. Glassner, *A Survey of the Free Energies of Formation of Fluorides, Chlorides and Oxides of the Elements to 2500°K*, ANL-510.

The vapor density of $FeCl_2$ was measured by Victor Meyer,[57] giving a value for the average molecular weight of 190 ± 5 at a temperature corresponding to "yellow heat." This temperature is probably in the neighborhood of 1050–1100°C, since the Victor Meyer method for vapor densities requires that the sample evaporates entirely, i.e., the temperature of the vessel containing the vapor must be greater than the boiling point of the salt. These results are in fair agreement with the extrapolated vapor composition based on the present data, which would give an average molecular weight at the boiling point of 175. J. Dewar and A. Scott[58] also measured the vapor density of anhydrous ferrous chloride, concluding that the equilibrium mixture consisted of monomeric and dimeric species.

Shäfer[45] has recently published measurements of the vapor pressure of ferrous chloride based solely on transportation data and the observed boiling point of $FeCl_2$. As discussed previously, transportation data alone cannot give information on the molecular weight of the vapor without total pressure measurements covering a similar temperature range. The vapor pressures calculated by Shäfer with the assumption of pure monomer indicate a discrepancy of approximately 23°C between his experimental boiling point temperature and his extrapolated boiling temperature both at a pressure of 748 mm. Shäfer avoided this inconsistency by fitting the vapor pressure equation for ferrous chloride at two points: the experimental boiling point and the average value of the transportation points. This is clearly an approximation to the correct value for the vapor pressure equation, given for ferrous chloride in Table 4, since it ignores the presence of dimers at the lower temperatures, and corrects for them at the boiling point.

The experimental data obtained in this work are in excellent agreement with the transportation values obtained by Shäfer.[45] It is impossible to calculate average molecular weight values for Shäfer's data, since only the experimental pressures calculated for pure monomer are given in the literature. However, the data of this work can be calculated with the assumption that the vapor is pure monomer, putting them on an equal basis with the data of Shäfer. Fig. 23 illustrates the good agreement existing between Shäfer's values and the present values, and clearly shows the discrepancy between these assumed monomer pressures and the experimental static pressure. The experimental transport data taken on $FeCl_2$ in the present work, are a combination of measurements on two different samples of $FeCl_2$, taken over similar temperature ranges. No observable difference existed between the two series of points. One point was discarded because of parital oxidation of the ferrous chloride to ferric chloride as evidenced by a ferric chloride deposit in the condenser. In addition, a significant amount of ferric ion was found upon chemical analysis of the condensate. Apparently, some oxygen from the atmosphere entered the transport cell during the condenser exchange. In none of the other runs was the presence of ferric chloride noted in the condenser, and chemical analysis indicated that the condensate consisted solely of $FeCl_2$.

The experimental "transport" pressures calculated from this work are thus in good agreement with the "transport" pressures calculated by Shäfer ("transport" pressures are calculated on the assumption of pure monomer in the vapor). Since the total pressure values obtained for $FeCl_2$ also agreed with the boiling point determined by Shäfer, the partial pressures exhibited for $FeCl_2$ in Table 10 appear to be reliable.

[57] V. Meyer, "Vapor Density of $FeCl_2$," *Ber. deu. chem. Ges.* 12, 1193 (1879).

[58] J. Dewar and A. Scott, "On the Vapor Density of Various Salts," *B. A. Rep.* 597 (1881) (cited in ref 31).

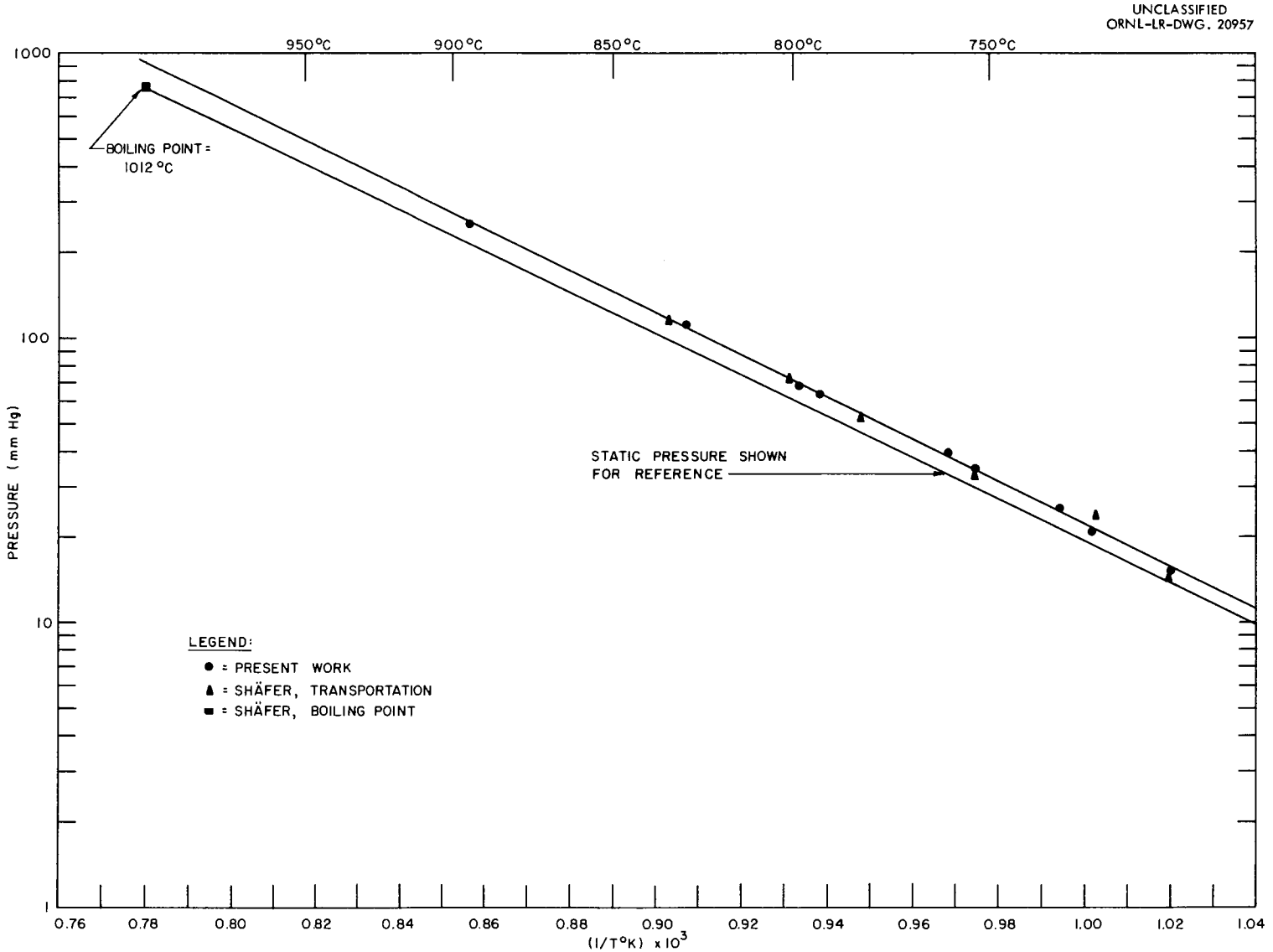

Fig. 23. Vapor Pressure of $FeCl_2$ from Transport Data, Assuming Only Monomeric Species in Vapor.

7. RESULTS OF VAPOR PRESSURE MEASUREMENTS: MIXTURES

TOTAL PRESSURES BY RODEBUSH METHOD

The Rodebush method was used to determine the total vapor pressure for the mixtures studied in this work. Compositions were synthesized at ten-mole per cent intervals in both the KCl-$FeCl_2$ system and the $LiCl$-$FeCl_2$ system. In the KCl-$FeCl_2$ system, total pressures were measured also at a number of intermediate compositions to facilitate interpolation of the total pressure-composition curves. The total vapor pressures thus obtained were treated by the method of least squares, fitting the points to a function of the type:

$$\log p = \frac{A}{T} + B \ . \tag{1}$$

The experimental data and equations derived from the least-squares analysis are given in Table 12 for the KCl-$FeCl_2$ system and in Table 13 for the $LiCl$-$FeCl_2$ system. The least-squares equations represent the experimental data to 2%. A summary of the least-squares equations pertinent to the mixtures studied is given in Tables 14 and 15 for the two systems. The least-squares Eq. 1 along with the experimental data for the mixtures are shown graphically in Figs. 24 and 25 for the KCl-$FeCl_2$ and $LiCl$-$FeCl_2$ systems, respectively.

The constants A obtained from the least-squares treatment of the experimental data represent the apparent heat of vaporization of the mixtures,

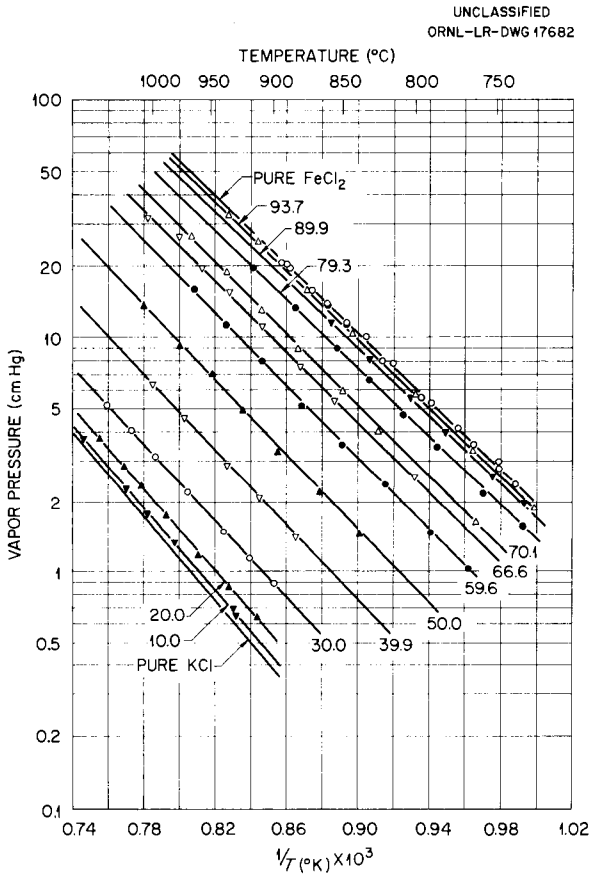

Fig. 24. Vapor Pressures vs Temperature for the $FeCl_2$-KCl System.

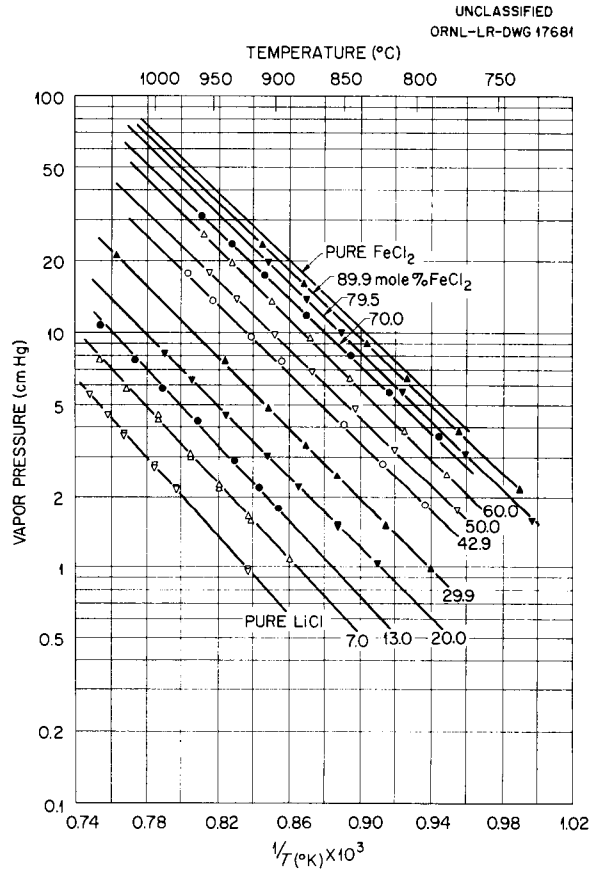

Fig. 25. Vapor Pressures vs Temperature for the $FeCl_2$-LiCl System.

Table 12. Total Pressures in $KCl-FeCl_2$ System

T (°C)	p (mm) (observed)	p (mm) (calculated)
93.7 mole % $FeCl_2$–6.3 mole % KCl		
$\log p$ (mm) = 8.6474 – 7397.4/T°K		
729	1.85	1.85
764	3.28	3.28
764	3.27	3.28
800	5.62	5.68
799.5	5.69	5.68
841.5	10.16	10.26
841.0	10.10	10.19
872	15.69	15.42
872	15.63	15.42
910	25.07	24.83
910	24.85	24.83
933.5	32.50	32.90
933	32.43	32.73
89.9 mole % $FeCl_2$–10.1 mole % KCl		
$\log p$ (mm) = 8.3717 – 7144.2/T°K		
734	1.94	1.90
753	2.52	2.57
753	2.61	2.57
781	3.90	3.93
781	3.88	3.93
804	5.50	5.49
805	5.46	5.56
830	7.96	7.87
831	7.95	7.98
857	11.35	11.23
857	11.27	11.23
85.1 mole % $FeCl_2$–14.9 mole % KCl		
$\log p$ (mm) = 8.5491 – 7373.5/T°K		
731	1.59	1.61
730.5	1.56	1.60
763	2.72	2.71
762	2.76	2.67
788.5	4.00	4.02
788.5	4.11	4.02
822.5	6.58	6.60
821	6.46	6.47
850.5	9.89	9.71
850.5	9.74	9.71
880.5	14.52	14.37
883	14.86	14.85
908	20.62	20.26
908	20.33	20.26

Table 12 (continued)

T (°C)	p (mm) (observed)	p (mm) (calculated)
79.3 mole % $FeCl_2$–20.7 mole % KCl		
$\log p$ (mm) = 8.5857 – 7476.3/T°K		
736	1.53	1.51
738	1.55	1.57
758	2.14	2.17
758	2.16	2.17
787	3.39	3.42
787	3.42	3.42
807	4.65	4.62
808	4.64	4.69
831	6.51	6.53
831	6.58	6.53
852	8.77	8.74
852	8.77	8.74
882.5	13.19	13.07
882.5	13.05	13.07
913.5	19.37	19.30
914.0	19.24	19.43
70.1 mole % $FeCl_2$–29.9 mole % KCl		
$\log p$ (mm) = 8.6371 – 7709.1/T°K		
822	4.10	3.96
822	3.94	3.96
849	5.87	5.85
849	5.73	5.85
879	8.88	8.84
877	8.23	8.61
908	12.83	12.90
908	13.15	12.90
937	18.65	18.49
937	18.62	18.49
966	26.25	26.05
967	26.16	26.38
66.6 mole % $FeCl_2$–33.4 mole % KCl		
$\log p$ (mm) = 8.6327 – 7792.5/T°K		
855.5	5.25	5.41
855.0	5.52	5.45
879.0	7.57	7.51
879	7.29	7.51
907.5	10.97	10.88
907.0	10.95	10.82
933	15.47	14.93
932.5	15.11	14.85
955	19.20	19.43
955	19.32	19.43

Table 12 (continued)

T (°C)	p (mm) (observed)	p (mm) (calculated)
973	24.49	23.90
973	24.17	23.90
59.6 mole % $FeCl_2$–40.4 mole % KCl		
log p (mm) = 8.4542 – 7749.0/T°K		
766	1.02	0.99
766	1.01	0.99
790	1.44	1.46
790	1.43	1.46
819.5	2.35	2.30
819.5	2.31	2.30
848	3.48	3.49
848	3.57	3.49
877.5	5.23	5.25
877.5	5.01	5.25
910	7.88	8.03
910	7.76	8.03
936	11.18	11.11
936	11.09	11.11
963	15.90	15.35
963	15.67	15.35
50.0 mole % $FeCl_2$–50.0 mole % KCl		
log p (mm) = 8.3563 – 7976.1/T°K		
837.5	1.44	1.50
837.5	1.52	1.50
866	2.17	2.26
867	2.36	2.30
893	3.27	3.29
893	3.36	3.29
923	4.85	4.88
923.5	5.01	4.91
948.5	6.88	6.73
949	7.04	6.77
976	9.14	9.36
976	9.18	9.36
1008.5	13.52	13.59
1008.5	13.40	13.59
39.9 mole % $FeCl_2$–60.1 mole % KCl		
log p (mm) = 8.2117 – 8297.5/T°K		
884.5	1.39	1.39
884.5	1.37	1.39
911	2.06	2.01
911	2.02	2.01

Table 12 (continued)

T (°C)	p (mm) (observed)	p (mm) (calculated)
932.5	2.82	2.85
932.5	2.83	2.85
973.5	4.52	4.46
973.5	4.37	4.46
1001.5	6.16	6.21
1001.5	6.30	6.21
30.0 mole % $FeCl_2$–70.0 mole % KCl		
log p (mm) = 8.0117 – 8297.5/T°K		
900	0.88	0.87
900	0.88	0.87
918.5	1.13	1.12
918.5	1.12	1.12
940	1.49	1.49
940	1.44	1.49
970.5	2.17	2.19
970	2.14	2.17
999	3.11	3.09
999	3.07	3.09
1020.5	4.02	3.96
1020.5	3.90	3.96
1043.5	5.21	5.14
1043.0	5.12	5.11
20.0 mole % $FeCl_2$–80.0 mole % KCl		
log p (mm) = 8.0996 – 8656.5/T°K		
913	0.64	0.63
935	0.84	0.86
934.5	0.85	0.86
960.5	1.16	1.21
960.5	1.15	1.21
988	1.74	1.72
987.5	1.66	1.71
1010	2.29	2.26
1009.5	2.27	2.24
1027	2.80	2.77
1027	2.77	2.77
1050.5	3.70	3.64
1050.5	3.66	3.64
9.8 mole % $FeCl_2$–90.2 mole % KCl		
log p (mm) = 8.0657 – 8719.6/T°K		
929	0.64	0.65
931	0.69	0.67
949	0.87	0.85

Table 12 (continued)

T (°C)	p (mm) (observed)	p (mm) (calculated)
9.8 mole % $FeCl_2$–90.2 mole % KCl		
$\log p$ (mm) = 8.0657 – 8719.6/T°K		
949	0.84	0.85
981.5	1.30	1.31
980	1.28	1.28
1005	1.75	1.76
1004.5	1.73	1.74
1025	2.24	2.23
1026.5	2.28	2.27
1067.5	3.69	3.65
1064.0	3.49	3.65

Table 13. Total Pressures in LiCl-$FeCl_2$ System

T (°C)	p (mm) (observed)	p (mm) (calculated)
89.9 mole % $FeCl_2$–10.1 mole % LiCl		
$\log p$ (mm) = 8.5344 – 7288.9/T°K		
738	2.11	2.12
738	2.10	2.12
774	3.73	3.75
774	3.74	3.75
806.5	6.17	6.07
806.5	6.15	6.07
833	8.87	8.81
833	8.86	8.81
878	15.99	15.94
878	15.91	15.94
908.5	23.09	23.26
908.5	22.91	23.26
79.5 mole % $FeCl_2$–20.5 mole % LiCl		
$\log p$ (mm) = 8.3582 – 7275.9/T°K		
769.5	3.07	3.09
769	3.03	3.07
810	5.68	5.64
809	5.57	5.56
850	10.02	9.78
849	9.80	9.65
875.5	13.51	13.63
876	13.56	13.70
907.5	19.70	20.10
905	19.79	19.61

Table 13 (continued)

T (°C)	p (mm) (observed)	p (mm) (calculated)
70.1 mole % $FeCl_2$–29.9 mole % LiCl		
$\log p$ (mm) = 8.3633 – 7228.3/T°K		
788.5	3.55	3.59
788.5	3.56	3.59
818.5	5.51	5.52
818.0	5.52	5.49
845	8.03	7.93
844	7.86	7.82
876	11.88	11.84
875.5	11.77	11.76
907	17.46	17.32
906	17.10	17.12
933.5	23.44	23.61
933	23.45	23.50
950.5	30.94	31.25
957.5	31.03	30.92
60.0 mole % $FeCl_2$–40.0 mole % LiCl		
$\log p$ (mm) = 8.4788 – 7472.0/T°K		
783	2.55	2.54
809	3.77	3.76
809	3.73	3.76
845	6.26	6.26
845	6.22	6.26
874	9.16	9.24
874	9.39	9.24
902	13.41	13.21
902	13.29	13.21
931.5	18.89	18.92
957	25.52	25.39
957.5	25.31	25.54
50.0 mole % $FeCl_2$–50.0 mole % LiCl		
$\log p$ (mm) = 8.2409 – 7335.9/T°K		
774.5	1.73	1.73
775	1.69	1.76
815.5	3.16	3.18
815.5	3.25	3.18
842	4.66	4.66
842	4.74	4.66
872	6.72	6.84
872	6.92	6.84
900	9.62	9.72
900	9.91	9.72
930	13.87	13.93

Table 13 (continued)

T (°C)	p (mm) (observed)	p (mm) (calculated)
930	13.88	13.93
952.5	17.85	18.04
952.0	17.82	17.92
42.9 mole % $FeCl_2$–57.1 mole % LiCl		
$\log p$ (mm) = 8.1428 – 7345.7/T°K		
795.5	1.81	1.86
795.5	1.84	1.86
822.5	2.76	2.74
822.5	2.75	2.74
849	3.98	3.95
849	4.05	3.95
895	7.30	7.16
895	7.27	7.16
919	9.49	9.58
919	9.51	9.58
950	13.77	13.73
949.5	13.38	13.67
974	17.63	17.91
974	18.11	17.91
29.9 mole % $FeCl_2$–70.1 mole % LiCl		
$\log p$ (mm) = 8.0476 – 7510.2/T°K		
791	0.97	0.98
791	0.98	0.98
820	1.49	1.51
820	1.52	1.51
854.5	2.40	2.44
854.5	2.52	2.44
878	3.32	3.34
877.5	3.30	3.32
906	4.79	4.77
906.5	4.89	4.80
941	7.30	7.28
939.5	6.96	7.16
1038	21.14	20.90
1038	20.84	20.90
20.0 mole % $FeCl_2$–80.0 mole % LiCl		
$\log p$ (mm) = 7.9114 – 7591.9/T°K		
826	1.03	1.01
854.5	1.51	1.51
854.5	1.49	1.51
882	2.16	2.19

Table 13 (continued)

T (°C)	p (mm) (observed)	p (mm) (calculated)
882	2.20	2.19
907	2.96	3.01
907	3.05	3.01
940	4.45	4.50
940	4.49	4.50
968	6.26	6.23
968	6.35	6.23
993	8.23	8.25
992.5	8.17	8.20
13.0 mole % $FeCl_2$–87.0 mole % LiCl		
$\log p$ (mm) = 7.9728 – 7876.0/T°K		
898	1.76	1.77
898	1.77	1.77
913.5	2.16	2.17
913.5	2.14	2.17
937	2.93	2.92
937	2.88	2.92
963.5	4.08	4.02
963.5	4.20	4.02
995	5.82	5.79
996	5.79	5.86
1020.5	7.62	7.67
1020.5	7.69	7.67
1052.5	10.62	10.76
1053	10.81	10.82
7.0 mole % $FeCl_2$–93.0 mole % LiCl		
$\log p$ (mm) = 7.9582 – 8059.9/T°K		
889	1.07	1.06
889	1.07	1.06
922	1.63	1.64
921.5	1.56	1.63
945	2.21	2.20
945.5	2.15	2.21
970	2.99	2.99
972	3.08	3.06
1000.5	4.45	4.27
1000	4.30	4.25
1028	5.69	5.81
1028	5.84	5.81
1054	7.62	7.68
1054	7.67	7.68

Table 14. Summary of Total Pressure Data: $KCl-FeCl_2$ System

$\log p$ (mm) = $A/T + B$

Composition (mole % $FeCl_2$)	Number of Points	Temperature Range (°C)	A	$\pm\sigma_A$	$-B$	$\pm\sigma_B$
100.0	30	740–900	8.5617	0.039	7274.5	42.5
93.7	13	730–935	8.6474	0.020	7397.4	22.5
89.9	11	735–860	8.3717	0.050	7144.2	53.8
85.1	14	730–910	8.5491	0.045	7373.5	49.2
79.3	16	735–915	8.5857	0.018	7476.3	19.5
70.1	12	820–970	8.6371	0.061	7709.1	71.6
66.6	12	855–975	8.5385	0.084	7677.2	100.5
59.6	16	765–965	8.4542	0.044	7749.0	49.8
50.0	14	840–1010	8.3563	0.065	7976.1	78.2
39.9	10	885–1000	8.2117	0.063	8181.6	76.4
30.0	14	900–1045	8.0117	0.040	8297.5	50.1
20.0	14	915–1050	8.0996	0.1090	8656.5	136.6
9.8	12	930–1065	8.0657	0.038	8719.6	48.4
Pure KCl	28	985–1185	8.1499	0.106	8851.5	44.9

Table 15. Summary of Total Pressure Data: $LiCl-FeCl_2$ System

$\log p$ (mm) = $A/T + B$

Composition (mole % $FeCl_2$)	Number of Points	Temperature Range (°C)	A	$\pm\sigma_A$	$-B$	$\pm\sigma_B$
100	30	750–890	8.5617	0.039	7274.5	42.5
89.9	12	740–910	8.5344	0.023	7288.9	24.2
79.5	10	770–905	8.4679	0.045	7275.6	51.0
70.1	14	790–960	8.3633	0.016	7228.3	18.5
60.0	12	785–960	8.4788	0.020	7472.0	22.7
50.0	14	775–950	8.2409	0.039	7335.9	44.4
42.9	14	795–975	8.1428	0.034	7345.7	39.6
29.9	14	790–1040	8.0476	0.029	7510.2	33.3
20.0	13	825–995	7.9114	0.032	7591.9	38.0
13.0	14	900–1055	7.9728	0.043	7876.0	53.4
7.0	14	865–1055	7.9582	0.057	8059.9	71.0
Pure LiCl	17	920–1105	8.0125	0.018	8388.1	23.2

defined by:

$$(2) \qquad \Delta H_{apparent} = \sum_{i}^{n} x_i (H_{gi} - \bar{H}_i) \ ,$$

where

$\Delta H_{apparent}$ = apparent heat of vaporization of mixture, kcal/mole,

x_i = average vapor mole fraction of ith vapor species over temperature range studied,

H_{gi} = partial molar enthalpy of ith species in vapor,

$\bar{H}_i$ = partial molar enthalpy of ith species in liquid,

n = number of species in vapor above solution.

The apparent heat of vaporization is a complicated function of partial molar enthalpies, and activities cannot be calculated solely from the apparent heat. However, the change in $\Delta H_{apparent}$ with composition does serve to indicate the general consistency of the total pressure results. From the plot of apparent heat of vaporization against composition (Figs. 26 and 27), the experimental results for each system are seen to be self-consistent.

The apparent heat of vaporization reflects the heat of solution as well as the heat of vaporization of each of the components in the solution. Thus, in the KCl-$FeCl_2$ system, the apparent heat of vaporization is seen to be changing continuously as the composition varies from pure $FeCl_2$ to pure KCl, indicating that a heat effect occurs upon mixing the two salts. However, in the LiCl-$FeCl_2$ system, the apparent heat remains equal to the heat of vaporization for $FeCl_2$ over an extended range of compositions, from pure $FeCl_2$ to 60 mole % $FeCl_2$. From the definition of the apparent heat (Eq. 2), the significance of this constancy is clear: pure $FeCl_2$ is evaporating from these mixtures (x_i = 1), and the partial molar enthalpy of the $FeCl_2$ is zero. For this range of liquid compositions, a check on the relative vapor pressures of LiCl and $FeCl_2$ indicates that the vapor is undoubtedly pure $FeCl_2$, as expected. Because of the athermal mixing of LiCl in $FeCl_2$, the activity of $FeCl_2$ would be expected to follow the ideal law (Raoult's law) provided that the entropy of mixing were also ideal.

To obtain total pressures as a function of composition and at other than the experimental temperatures, an interpolation procedure was followed. Such interpolated results were also required, since melt compositions studied by the Rodebush method did not necessarily correspond to compositions studied by the transportation method. The interpolation procedure adopted the assumption that

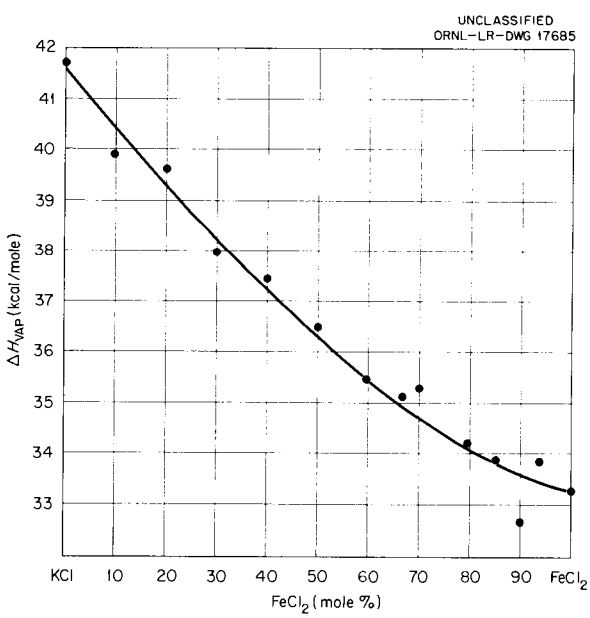

Fig. 26. Apparent Heat of Vaporization vs Composition in the $FeCl_2$-KCl System.

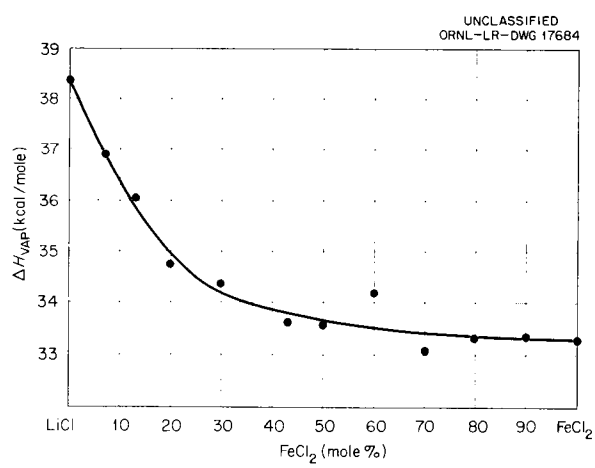

Fig. 27. Apparent Heat of Vaporization vs Composition in the $FeCl_2$-LiCl System.

the least-squares equations for the mixtures adequately represented the total pressure as a function of temperature for the mixtures studied. Using these least-squares equations, the logarithms of the total pressures were calculated at four arbitrary temperatures, viz., 850, 900, 950, and 1000°C, chosen as representative of the experimental temperature ranges covered. The logarithm of the total pressure was used rather than the total pressure, since the total pressure varies by several orders of magnitude as the composition varies from pure ferrous chloride to alkali chloride. The $\log_{10} P_T$ points thus calculated were then plotted as a function of composition at each arbitrary temperature, along with the standard deviations, which indicated the experimental error. A curve was drawn through the calculated points representing the best visual fit to the data. The $\log_{10} P_T$ composition curves obtained in this fashion are shown in Figs. 28 and 29 for the two systems. Using these curves, interpolation between experimental mixtures to any intermediate composition was possible. Finally, a plot of $\log_{10} P_T$ at the desired composition against reciprocal temperature was constructed; interpolation to any desired temperature was possible using the curve established by the four points selected.

As an example, suppose the total pressure of a 38.8 mole % $FeCl_2$ mixture was desired in the $FeCl_2$-KCl system. The smoothed $\log_{10} P_T$ curves were read at the four arbitrary temperatures from Fig. 28. These points were then plotted against the reciprocal of the four temperatures. The best straight line drawn through these four points (Fig. 30) represents the total pressure of a 38.8 mole % $FeCl_2$–61.2 mole % KCl mixture as a function of temperature. From this line, total pressure values at intermediate temperatures can be obtained for the specified mixture. Total pressure plots of this type were prepared for each mixture studied in the transportation apparatus.

An isothermal plot of total pressure against composition is given in Fig. 31 for the two systems under study. As discussed previously, this curve cannot be directly related to activity values until the isothermal partial pressure curves are obtained. However, an examination of these curves indicates a number of significant thermodynamic features about the solutions studied. Both systems show negative deviations from the ideal, or Raoult's law curve; the negative deviations in the $FeCl_2$-KCl system are much greater than those in the $FeCl_2$-LiCl system. The $FeCl_2$-LiCl system forms an ideal solution in the range 80 to 100 mole % $FeCl_2$ as was expected from the constancy of the apparent heat of vaporization over the same composition range. However, since the heat of solution was zero up to about 60 mole % $FeCl_2$, the negative deviations occurring in this concentration range must be indicative of positive excess entropy effects.

EXPERIMENTAL TRANSPORTATION DATA FOR MIXTURES

The most important application of the transportation apparatus was on mixtures high in alkali chloride content. For solutions rich in ferrous chloride, the vapor was found to be entirely $FeCl_2$, and the partial pressures of $FeCl_2$ and Fe_2Cl_4 could be calculated from a knowledge of the total pressure of the mixture and the equilibrium constant for dimerization of $FeCl_2$, given in Fig. 22. For solutions with $FeCl_2$ content lower than 60 mole %, considerable amounts of alkali halide were present in the condensate.

As in the total pressure study, mixtures were prepared at approximately ten-mole per cent intervals, ranging from pure alkali halide up to 60 mole % $FeCl_2$. Determinations were generally made at five temperatures, covering a range of 150°C. The results of these determinations are summarized in Table 16 for the $FeCl_2$-KCl system, and in Table 17 for the $FeCl_2$-LiCl system. In all cases, the number of moles of argon passed through the transport cell was calculated from Eq. 3, Chap. 6, using the Mariotte flask data. Final calculation of the partial pressures from the experimental data will be discussed later.

Two problems must be considered in evaluating the reliability of transport data:

1. The composition of the mixtures must remain essentially constant during the determination, or else a correction is needed for the change in composition caused by the removal of vapor.
2. The equilibrium or saturation condition must be established between the carrier gas and the salt vapor.

Removal of vapor from above the liquid melt occurs by convection along with the argon flowing into the condenser and by diffusion against the argon inlet stream. The amount of salt in the

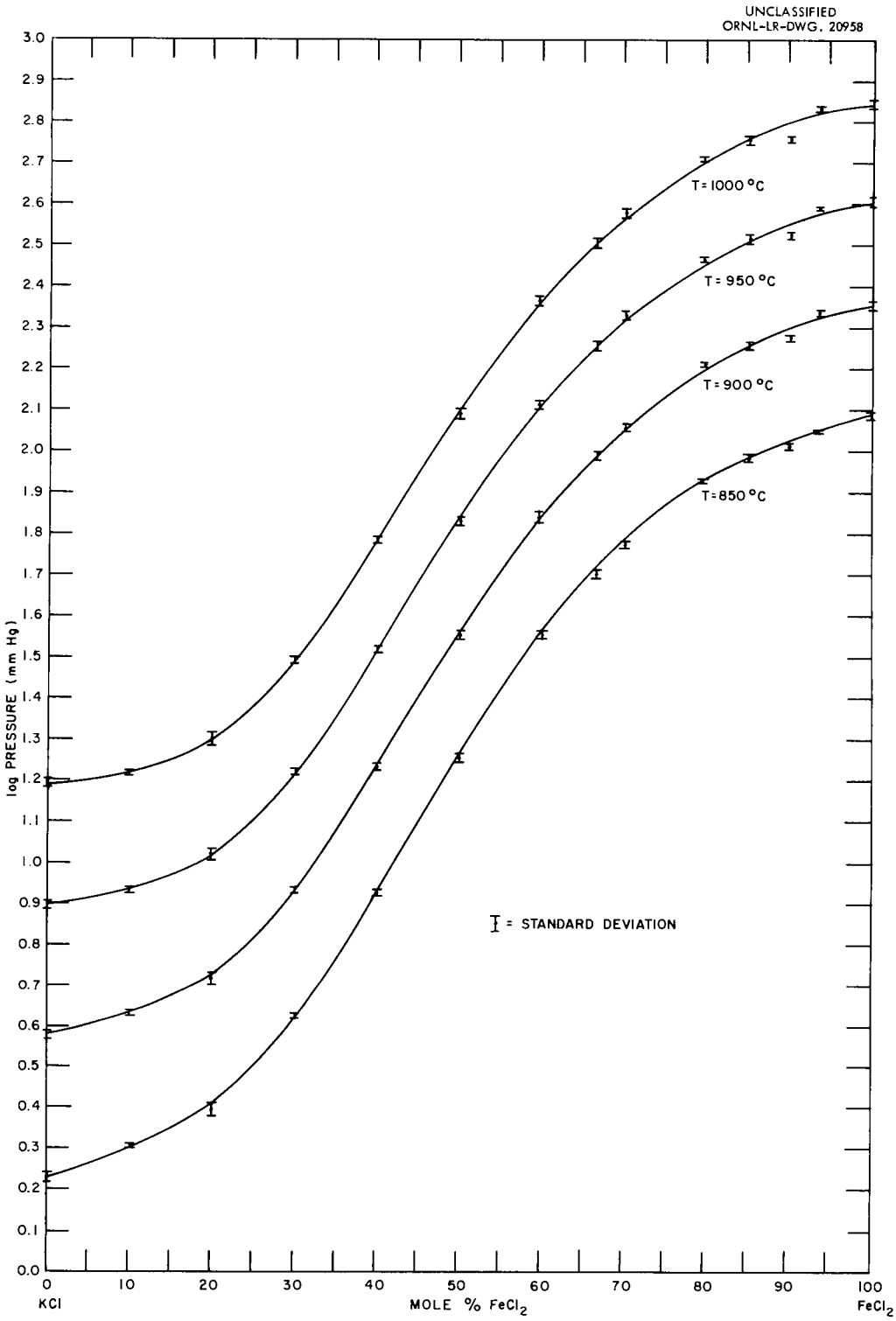

Fig. 28. Effect of Composition on the Vapor Pressure of the KCl-$FeCl_2$ System.

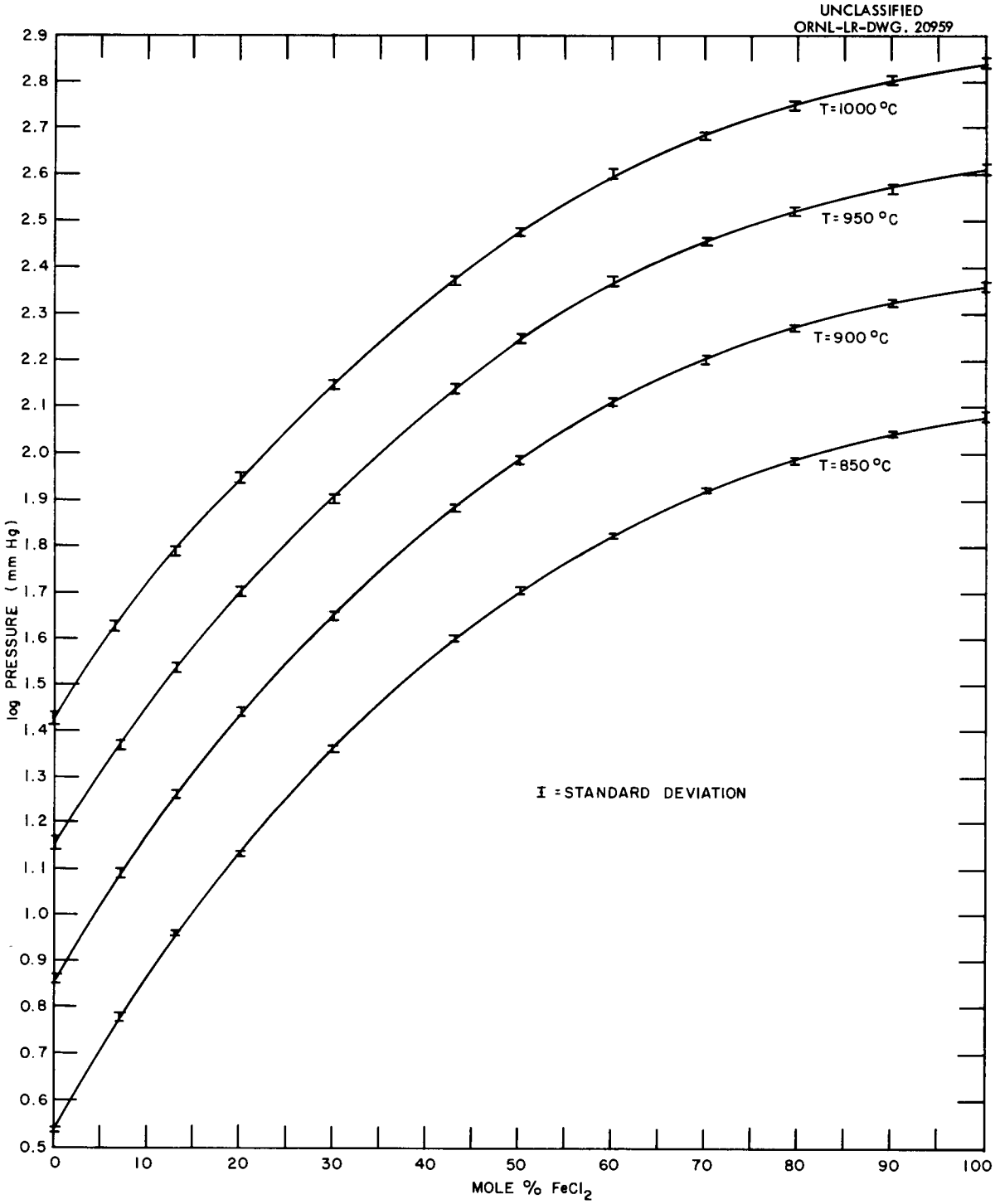

Fig. 29. Effect of Composition on the Vapor Pressure of the $LiCl-FeCl_2$ System.

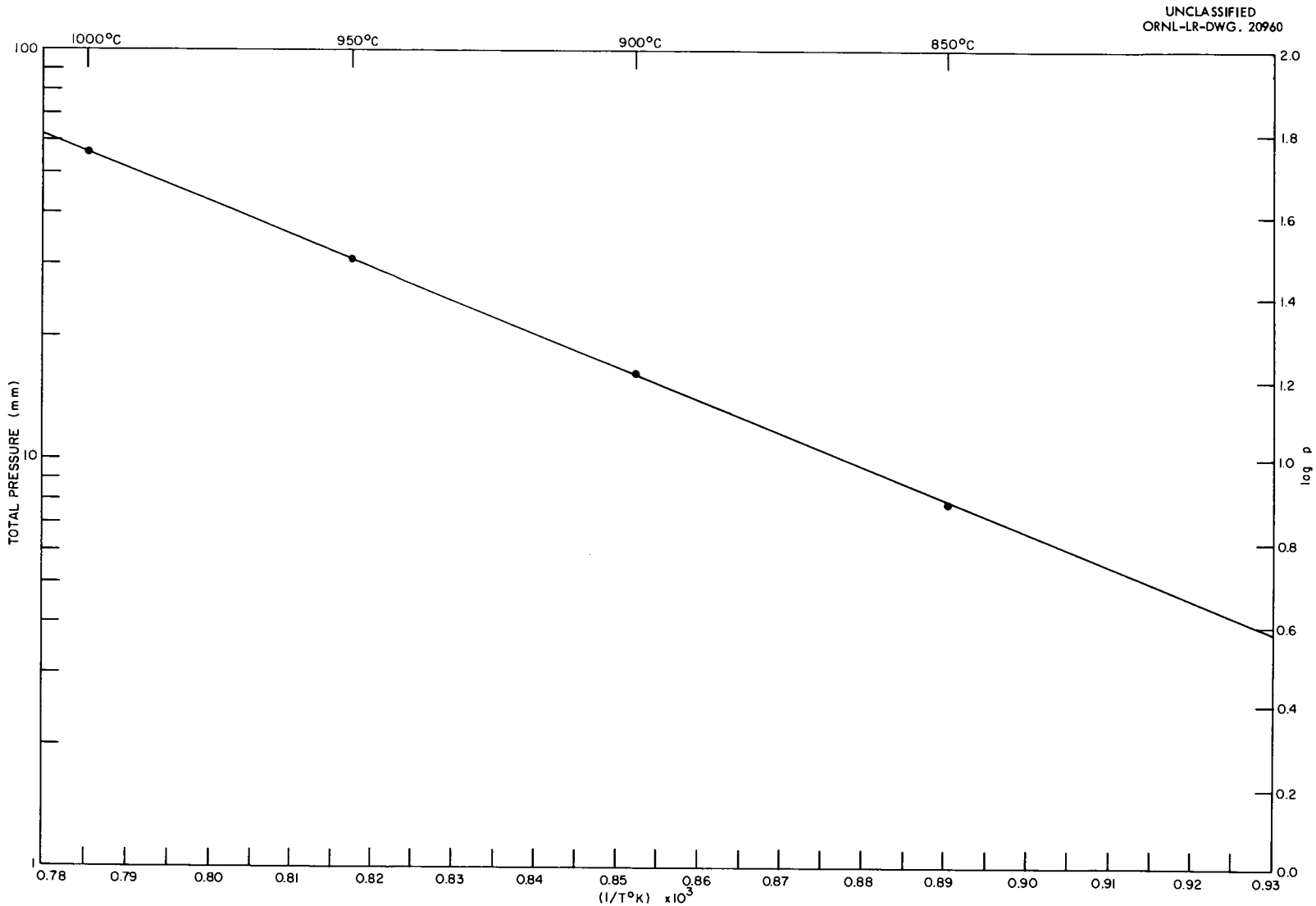

Fig. 30. Interpolated Pressures for 38.8 Mole % $FeCl_2$-KCl Mixture from *P* vs *C* Plots, Fig. 28.

Table 16. Experimental Data – Transportation Method

$FeCl_2$–KCl Mixtures

Composition (mole % $FeCl_2$)	T (°C)	$P_{barometer}$ (mm Hg)	$P_{manometer}$ (mm Hg)	P_{total} (mm Hg)	Flow Rate (cc/min)	Mariotte Flask Data				Argon Collected (mmoles)	Weight of Condensate (mg)	Condensate Analysis (mmoles)	
						$-\Delta P_A$ (mm Hg)	T_A (°C)	Weight of H_2O Collected (g)	Argon Collected (cc)			Fe^{++}	K^+
10.0	960	739.6	5.8	745.4	33	13.5	29.4	2005.5	2014	74.84	109.7	0.30	1.16
	982	744.7	4.3	749.0	33	14.1	30.6	1780	1788	66.27	130.3	0.29	1.39
	1008	739.0	5.0	744.0	25	15.2	31.1	1212.5	1219	44.63	118.2	0.27	1.28
	1037	737.7	4.1	741.8	23	16.2	30.7	825	829	30.30	127.7	0.27	1.35
	1061	737.9	6.5	744.4	35	16.7	30.0	686	689	25.36	130.1	0.27	1.50
20.0	887	743.6	6.3	749.9	39	10.9	25.0	3402	3412	131.22	104.6	0.39	0.76
	912	744.1	7.3	751.4	38	6.8	27.3	1858	1864	71.34	82.1	0.32	0.60
	940	744.1	5.2	749.3	29	19.7	27.2	1569	1575	59.49	108.3	0.40	0.78
	963	743.8	4.3	748.1	24	17.0	27.0	1003	1007	38.12	98.2	0.36	0.71
	992	743.4	5.4	748.8	20	15.1	27.0	743	745	28.29	104.5	0.35	0.78
30.0	845	741.5	5.5	747.0	44	18.0	24.7	2225	2232	85.34	66.4	0.35	0.34
	872	740.7	4.6	745.3	35	13.5	26.0	2079	2086	79.36	102.6	0.50	0.51
	899	740.8	3.6	744.4	30	6.6	28.8	1510	1516	57.13	112.7	0.59	0.57
	924	739.3	3.5	742.8	25	21.0	28.0	1204	1209	44.98	131.2	0.62	0.64
	955	738.7	2.5	741.2	20	18.8	28.4	725	728	27.01	115.6	0.59	0.59
38.8	795	742.9	4.5	747.4	39	17.0	26.0	2485	2493	94.82	73.1	0.38	0.26
	842	742.0	5.5	747.5	47	11.7	27.8	1895	1902	72.03	121.5	0.66	0.52
	892	741.2	2.8	744.0	23	7.6	29.0	1165	1170	43.96	151.6	0.85	0.61
	921	741.2	2.4	743.6	19	23.0	27.0	723	725	27.12	138.7	0.77	0.59
	961	740.9	2.8	743.7	23	21.2	28.6	467	469	17.40	153.6	0.88	0.66
49.8	833	733.0	4.8	737.8	45	13.9	30.0	981	986	36.29	109.5	0.75	0.23
	874	732.6	1.9	734.5	18	17.6	30.0	1136	1141	41.65	230.6	1.48	0.54
	912	733.0	4.7	737.7	35	19.9	29.4	804	808	29.63	277.9	1.83	0.69
	938	733.0	1.6	734.6	12	23.2	28.2	306	307	11.25	157.1	1.02	0.38
	979	733.0	2.1	735.1	18	25.1	29.4	271	272	9.89	231.9	1.50	0.56
60.0	732	737.8	4.3	742.1	35	18.2	28.1	2093	2101	78.33	85.1	0.67	0.013–0.038*
	767	737.5	3.7	741.2	29	14.9	29.1	1322	1328	49.31	100.1	0.73	0.021–0.034*
	809	736.5	4.1	740.6	24	11.8	30.4	1166	1171	43.27	176.5	1.33	0.053–0.072*
	841	735.7	3.7	739.4	28	22.6	29.0	707	710	26.11	173.8	1.24	0.074–0.090*
	880	735.7	3.9	739.6	28	20.7	30.1	488	490	17.94	216.1	1.48	0.13

* Extrapolated values.

condensate is known, since it is weighed and chemically analyzed; hence, a correction is possible for composition changes occurring as successive samples of vapor are removed. In general, argon flow rates and volumes were adjusted to deposit a 100-mg sample of salt, which was large enough to give reliable and accurate chemical analyses. Since the total weight of the mixture being studied was 50 g, these small condensate values caused essentially no change in the mixture composition, and a correction was not necessary. For the 49.8 mole % $FeCl_2$-KCl mixture, a total of 1 g of condensate was obtained from five determinations, resulting in a change of 0.4 mole % $FeCl_2$ in the liquid composition during the course of the entire determination. Consequently, a linear average of composition was used for this particular mixture.

The second possible loss of salt vapor which could change liquid composition is caused by back diffusion of the vapor against the argon stream. The vapor condenses in the cool portions of the gas inlet tube on the outside of the condenser. Since the amount of vapor diffusing in this manner is a function of the cross-sectional flow area, this area was reduced to the smallest practical

Table 17. Experimental Data – $LiCl-FeCl_2$ Mixtures

Composition (mole % $FeCl_2$)	T (°C)	$P_{barometer}$ (mm Hg)	$P_{manometer}$ (mm Hg)	P_{total} (mm Hg)	Flow Rate (cc/min)	Mariotte Flask Data				Argon Collected (mmoles)	Weight of Condensate (mg)	Condensate Analysis (mmoles)	
						$-\Delta P_A$ (mm Hg)	T_A (°C)	Weight of H_2O Collected (g)	Argon Collected (cc)			Fe^{++}	Li^+
10	883	739.8	5.2	745.0	33	13.1	29.0	2193	2202	81.99	150.8	0.85	1.48
	918	741.0	4.9	745.9	31	14.2	28.8	1531	1537	57.29	146.8	0.84	0.79
	953	740.4	3.8	744.2	32	14.8	28.9	1337	1342	49.83	187.5	1.07	1.28
	982	740.4	4.4	744.8	28	14.5	29.2	1434	1440	53.44	206.1	1.26	1.20
20	794	744.1	4.5	748.6	38	12.8	32.0	2304	2317	85.25	78.5	0.53	0.59
	840	742.4	3.5	745.9	22	14.2	32.1	1588	1597	58.36	91.5	0.63	0.41
	866	742.2	4.1	746.3	25	15.7	31.0	1056	1061	38.97		0.74	0.42
	899	741.4	4.1	745.5	26	17.1	30.0	672	675	24.88	132.4	0.73	0.96
	928	741.1	5.9	747.0	28	17.3	30.2	505	507	18.69	121.8	0.74	0.59
30*	762	739.9	5.1	745.0	34	13.2	28.0	2120	2129	79.72	86.6	0.59	1.38
	772	739.3	3.8	743.1	34	13.5	30.7	1930	1939	71.27	109.6	0.71	0.42
50*	718	741.8	5.5	747.3	35	13.1	26.7	2107	2114	80.02	122.8	0.92	0.61
	754	741.8	3.9	745.7	32	13.8	26.5	1805	1811	68.40	167.8	1.31	0.58

*Cells failed during determinations.

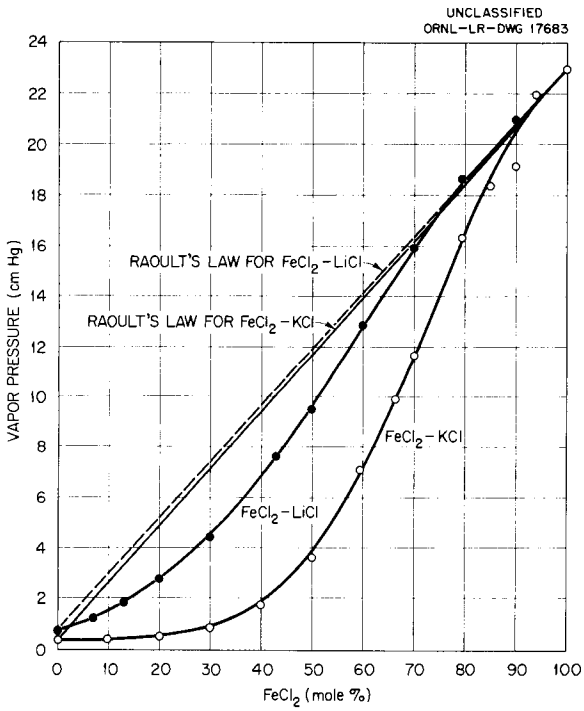

Fig. 31. Vapor Pressure at 900°C vs Composition in the $FeCl_2$-KCl and $FeCl_2$-LiCl Systems.

value so that loss by this means was minimized. As each condenser was removed from the cell, it was visually checked for salt deposits on the outer wall, and except for a few isolated cases, no deposits were observed. The inner wall of the gas inlet tube was also checked for salt deposits and no significant amounts were found. Thus, sample loss through this means was negligible, and it seems certain that the mixture compositions did not change appreciably during the course of a determination.

To observe the effect of flow rate on the amount of condensate collected, the early determinations with mixtures were run at greatly varying flow rates. While no duplicate determinations were made at a given temperature, the general consistency of the data obtained at various temperatures and flow rates indicates that the condensate weights per unit volume of carrier gas were independent of the flow rate used. Varying the flow rate from 15 ml/min to 45 ml/min had no effect on the amount of condensate (for the same total volume of gas). The flow rates were generally lower than 40 ml/min, since at higher values the salt vapor formed a "snow" or "smoke" in the argon stream and did not deposit entirely in

the condenser as desired. In recent transportation studies using similar experimental arrangements, both Sense[28] and Bloom and Barton[51] have found that saturation is achieved at flow rates even as high as 50 ml/min. This behavior is confirmed in the present work, and it seems certain that the condensate samples represent the equilibrium vapor composition above the mixtures studied.

PARTIAL PRESSURE CALCULATION FROM TRANSPORT AND TOTAL PRESSURE DATA

The effect of association was first demonstrated when attempts were made to reduce the transportation data to partial pressures. In the first approximation, the vapor species were assumed to consist solely of molecules of alkali chloride and ferrous chloride. With this assumption the partial pressures of alkali chloride and ferrous chloride, as well as the total pressure, can be obtained from the following equations:

$$(3)\quad p_{FeCl_2} = \left[\frac{n_{FeCl_2}}{n_A + n_{FeCl_2} + n_{KCl}}\right] P_{total}\ ,$$

$$(4)\quad p_{KCl} = \left[\frac{n_{KCl}}{n_A + n_{FeCl_2} + n_{KCl}}\right] P_{total}\ ,$$

$$(5)\quad p_s = p_{KCl} + p_{FeCl_2}\ ,$$

where

$p_{FeCl_2,KCl}$ = calculated partial pressures of $FeCl_2$ and KCl,

n_{FeCl_2} = moles $FeCl_2$ in condensate,

n_{KCl} = moles KCl in condensate,

n_A = moles of argon passed during transport determination,

P_{total} = total pressure of argon and salt vapor during transport determination,

p_s = total pressure of salt vapor at experimental temperature.

The partial pressures defined by Eqs. 3 and 4 were calculated for each experimental point, and plotted as a function of temperature (log p vs $1/T$). Then the values of the partial pressures were read at 900°C and cross-plotted as a function of composition. If the assumption of purely monomeric vapor species were correct, the total pressure calculated from Eq. 5 should equal the experimental total pressure obtained directly at 900°C. Figures 32 and 33 illustrate the results of this calculation for the two systems, and clearly show that the calculated total pressure greatly exceeds the observed total pressure. A more significant feature of this plot is the apparent *increase* in the partial pressure of alkali chloride with the addition of $FeCl_2$. The activity of alkali chloride would increase with dilution, reaching a maximum value of 3 for certain mixtures in the KCl-$FeCl_2$ case.

The explanation for this discrepancy lies in the assumption of purely monomeric vapor species. Clearly, the alkali chloride present in the condensate from mixtures in the 20–50 mole % $FeCl_2$ range cannot exist in the vapor as alkali chloride molecules, but must be in the form of double molecules with the ferrous chloride. The problem then arises to determine what vapor compound is formed between the alkali chloride molecules and ferrous chloride molecules. Since there is strong experimental evidence for significant amounts of dimer molecules in the pure salt vapors studied, a reasonable assumption for a vapor compound would be that the salts can readily form a "mixed dimer." If the dimer bond in the pure salts is based on dipole interactions, the formation of a "mixed dimer" having a 1:1 ratio of alkali chloride to ferrous chloride seems plausible. To verify these assumptions the vapor from a mixture composed of 50 mole % $FeCl_2$–50 mole % KCl was analyzed with a mass spectrometer. Conclusive evidence for a $KFeCl_2^+$ species was found from examination of the spectral peaks (see Appendix B), indicating that the proposed 1:1 vapor compound must exist in the vapor.

Vapor compounds of this type have been proposed in the literature to explain anomalous transport vapor pressure data, e.g., $NaZrF_5$,[28] $NaAlF_4$,[59] $NaAlCl_4$,[20,60] $KCdCl_3$.[51] With the assumption of these compounds, reasonable values can be calculated for the partial pressures of the various components from transport data. However, the present work is the first instance where the actual

[59] E. H. Howard, "Vapor Pressures on the NaF-AlF_3 System," *J. Am. Chem. Soc.* 76, 2941 (1954).

[60] I. Naryshkin, "Studies in the NaCl-$AlCl_3$ System," *J. Phys. Chem. (U.S.S.R.)* 13, 690 (1939).

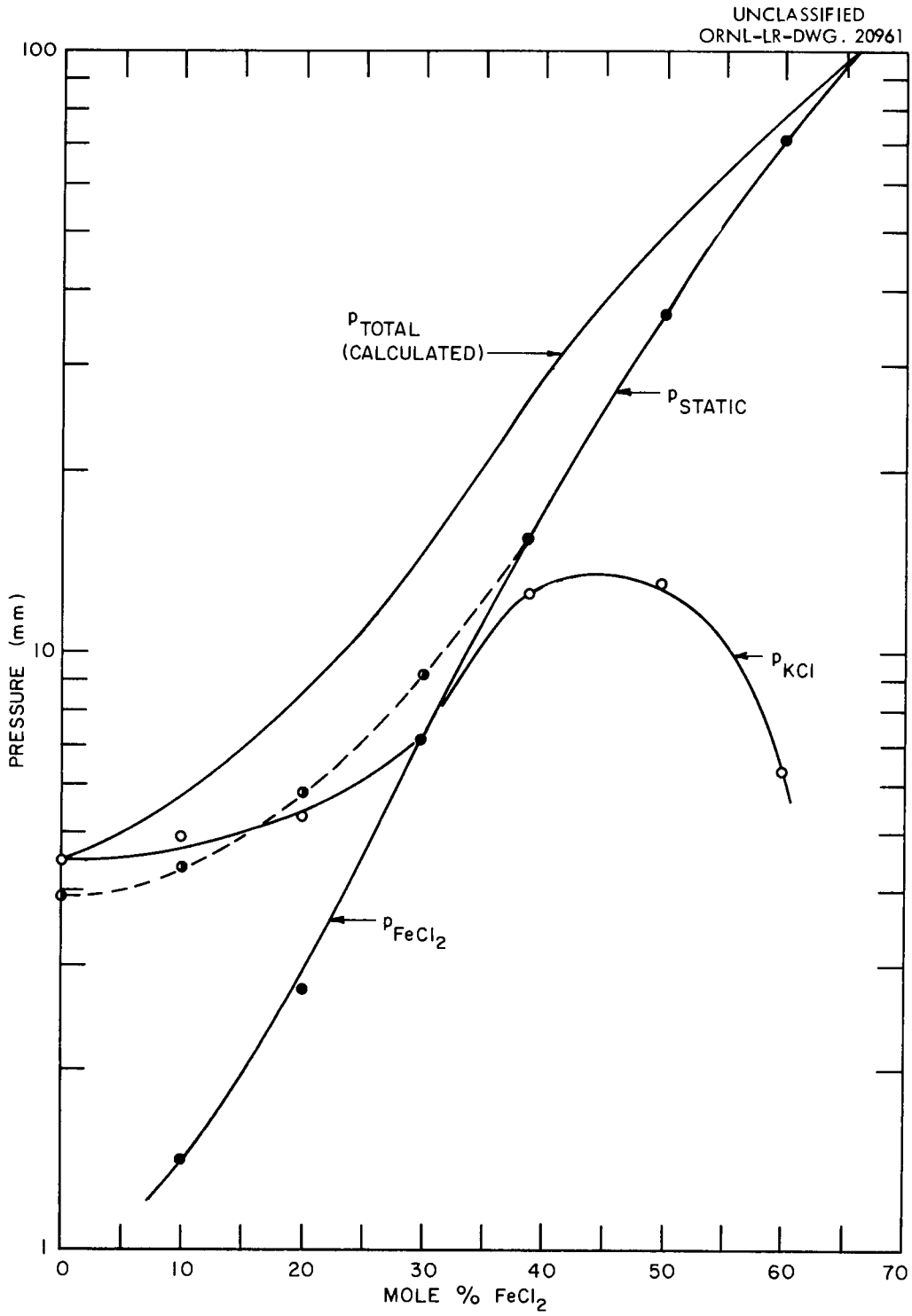

Fig. 32. Partial Pressures in KCl-$FeCl_2$ System, Assuming Only Monomers in Vapor at 900°C.

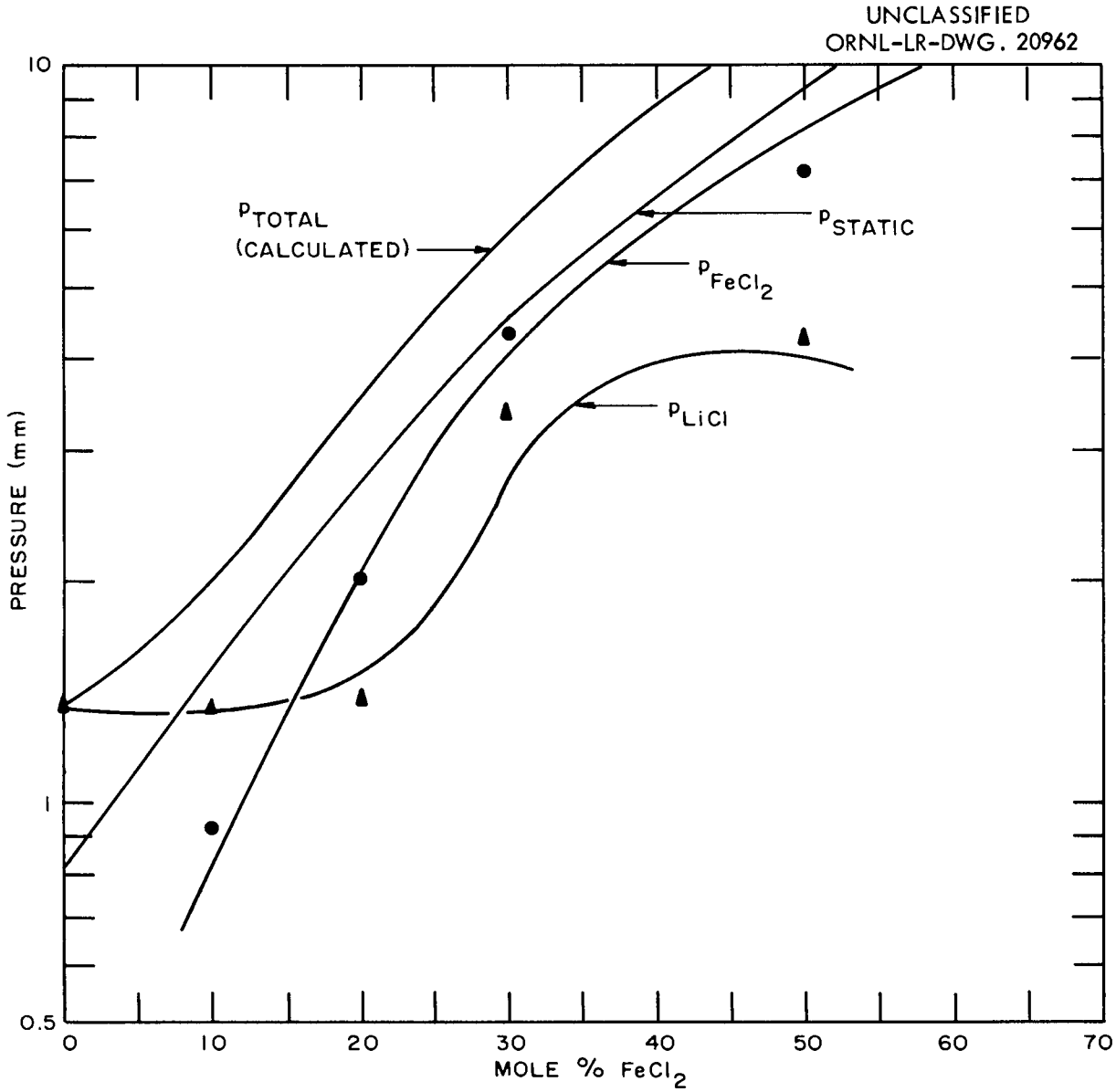

Fig. 33. Partial Pressure in LiCl-$FeCl_2$ System, Assuming Only Monomers in Vapor at 900°C.

existence of the vapor compounds has been demonstrated by independent experimental means. It is highly probable that more vapor compounds of this type will be found, since the vapor polymerization of salt molecules is just beginning to be fully appreciated.

The existence of a vapor compound complicates the calculation of partial pressures. In order to fully analyze the data, the following unknowns must be evaluated:

n_1 = moles of $FeCl_2$ in the vapor sample,

n_2 = moles of Fe_2Cl_4 in the vapor sample,

n_3 = moles of vapor compound $KFeCl_3$ in the vapor sample,

n_4 = moles of KCl in the vapor sample,

n_5 = moles of K_2Cl_2 in the vapor sample.

These variables can be related by a combination of total pressure data with transport data, forming a set of equations which are readily solved. The following relations apply:

First, the total moles of vapor n_v must equal the sum of the moles of the individual vapor species:

$$n_v = \sum_{i=1}^{5} n_i \ . \tag{6}$$

The number of moles of vapor transported can be obtained from Dalton's Law:

$$\frac{n_v}{n_A + n_v} = \frac{p_s}{P_T} \ , \tag{7}$$

or

$$n_v = n_A \left[\frac{p_s}{P_T - p_s} \right] \ .$$

Second, the moles of iron present in the vapor must equal the moles of iron found on chemical analysis of the condensate:

$$N_{Fe} = n_1 + 2n_2 + n_3 \ , \tag{8}$$

where

N_{Fe} = moles of iron analyzed in the condensate.

A similar equation holds true for the potassium content:

$$N_K = n_3 + n_4 + 2n_5 \ , \tag{9}$$

where

N_K = moles of potassium analyzed in the condensate.

Finally, the equilibrium condition between monomer and dimer species of the pure salts must be maintained:

$$K_{FeCl_2} = \frac{\left(p_{FeCl_2}\right)^2}{p_{Fe_2Cl_4}} = \frac{\left(\frac{n_1}{n_v} p_s\right)^2}{\left(\frac{n_2}{n_v} p_s\right)} = \frac{n_1^2}{n_2} \cdot \frac{p_s}{n_v} \ . \tag{10}$$

Similarly,

$$K_{KCl} = \frac{n_4^2}{n_5} \cdot \frac{p_s}{n_v} \ . \tag{11}$$

The net result of these relations is the following series of equations, which can be explicitly solved for the five variables at each experimental temperature and for each experimental mixture studied:

$$n_v = n_1 + n_2 + n_3 + n_4 + n_5 \ ,$$

$$N_{Fe} = n_1 + 2n_2 + n_3 \ ,$$

$$N_K = n_3 + n_4 + 2n_5 \ ,$$

$$\left(K_{FeCl_2}\right) \frac{n_v}{p_s} = \frac{n_1^2}{n_2} \ ,$$

$$\left(K_{KCl}\right) \frac{n_v}{p_s} = \frac{n_4^2}{n_5} \ ,$$

$$n_v = n_A \left[\frac{p_s}{P_T - p_s} \right] \ .$$

By algebraic manipulation, these will reduce to a quadratic equation in n_4, in terms of known experimental constants:

$$n_4^2 \left(\frac{A}{B} - 1 \right) + n_4 (A + 2C) + AN_{Fe} - An_A \left(\frac{p_s}{P_T - p_s} \right) - C^2 = 0 \ , \tag{12}$$

where

$$A = K_{FeCl_2} \left(\frac{n_A}{P_T - p_s} \right) \ ,$$

$$B = K_{KCl} \left(\frac{n_A}{P_T - p_s} \right) \ ,$$

$$C = 2n_A \left(\frac{p_s}{P_T - p_s} \right) - N_{Fe} - N_K \ .$$

After solving Eq. 12 for n_4, calculation of the other values of n_i follows by simple arithmetic.

This group of equations was solved for each experimental point obtained in the transportation

determinations, by using an IBM 650 digital computer. While the numerical process is rather simple, the large number of calculations needed made the use of the computer invaluable. In some instances, where one of the variables was extremely small, the machine data resulted in negative answers. For these cases, hand calculations were used, and provision was made for the experimental limits of the constants. The final solutions fit the experimental data to better than 2%; in most cases, the machine calculation was used, and the solutions represent an exact fit to the experimental data.

Having the number of moles of each species at each experimental temperature, the partial pressures were obtained directly from Dalton's Law:

$$p_i = \left(\frac{n_i}{n_v}\right) p_s \ ,$$

where

p_i = partial pressure of ith species in vapor.

The partial pressures calculated in this manner are summarized in Table 18 for the $FeCl_2$-KCl system. As a check the calculation can be reversed to generate N_K, N_{Fe}, and p_s, based on the calculated partial pressures. The relative agreement between these calculated constants and the experimental constants is seen to be quite good.

The partial pressures for the monomer species (KCl and $FeCl_2$) and the vapor compound are given in Figs. 34, 35, and 36, along with the best visual straight line drawn through the data. As a further check on the calculation process, the equilibrium constant for the compound reaction was calculated from the partial pressures at each experimental point:

$$FeCl_2 + KCl = KFeCl_3$$

$$K_c = \frac{p_{KFeCl_3}}{p_{KCl} \cdot p_{FeCl_2}} \ .$$

This equilibrium constant is plotted in Fig. 37, and the calculated constant shows a good approximation to the expected functional dependence:

$$\log K_c = \frac{A}{T} + B \ .$$

The transport data for the $FeCl_2$-LiCl system could not be analyzed by the preceding calculation scheme, because of the presence of a trimer species in pure LiCl vapor. In addition, the chemical analysis on the $FeCl_2$-LiCl system showed a great deal of scatter in the values for the lithium ion. This was partly due to purely analytical difficulties, and primarily due to experimental difficulties centering around attack of the quartz inlet tube by LiCl vapor (discussed earlier). Consequently, it was not feasible to generate partial pressure curves from the data for the $FeCl_2$-LiCl system.

In order to use the partial pressure obtained in the $FeCl_2$-KCl system to calculate activities of the two components, isotherms must be cross-plotted; this was done at the four temperatures used in the total pressure interpolation. The results are shown in Figs. 38 to 41, giving the various partial pressures as a function of composition for 850, 900, 950, and 1000°C. The calculation of the activity is based on these curves, and is discussed in detail in the following section.

Table 18. Partial Pressures of Vapor Species in $KCl-FeCl_2$ System

T (°C)	p_{FeCl_2} (mm)	$p_{Fe_2Cl_4}$ (mm)	p_{KFeCl_3} (mm)	p_{KCl} (mm)	$p_{K_2Cl_2}$ (mm)	P_{total} Calculated (mm)	P_{total} Observed (mm)	n_{vapor} Observed	Cation in Vapor (mmoles) n_{Fe} Calculated	n_{Fe} Observed	n_K Calculated	n_K Observed	$K = \frac{p_{KFeCl_3}}{p_{KCl} \cdot p_{FeCl_2}}$
10.0 mole % $FeCl_2$–90.0 mole % KCl													
960	0.36	0	2.3	6.1	1.7	10.5	10.2	1.04	0.27	0.30	1.20	1.16	1.1
982	0.42	0	2.7	8.2	2.3	13.6	13.5	1.22	0.28	0.29	1.40	1.39	0.8
1008	0.62	0	4.0	11.1	3.0	18.7	18.7	1.15	0.28	0.27	1.30	1.28	0.6
1037	0.81	0	5.0	16.6	4.8	27.2	26.8	1.13	0.25	0.27	1.32	1.35	0.4
1061	1.0	0	6.5	21.7	6.3	35.5	35.1	1.25	0.27	0.27	1.45	1.50	0.3
20.0 mole % $FeCl_2$–80.0 mole % KCl													
887	0.45	0	1.9	1.7	0.35	4.4	4.5	0.79	0.40	0.39	0.75	0.76	2.5
912	0.60	0	2.75	2.55	0.55	6.5	6.4	0.61	0.32	0.32	0.61	0.60	1.8
940	0.75	0	4.20	3.75	0.80	9.5	9.3	0.75	0.39	0.40	0.77	0.78	1.5
963	0.85	0	6.00	4.95	1.05	12.8	12.5	0.65	0.36	0.36	0.68	0.71	1.4
992	0.95	0	8.30	7.10	1.50	17.8	17.8	0.70	0.37	0.35	0.77	0.78	1.2
30.0 mole % $FeCl_2$–70.0 mole % KCl													
845	0.93	0	2.15	0.68	0.10	3.9	3.9	0.44	0.35	0.35	0.35	0.34	3.4
872	1.28	0	3.45	0.95	0.14	5.8	5.8	0.62	0.50	0.50	0.50	0.51	2.8
899	1.65	0	5.55	1.35	0.17	8.7	8.5	0.67	0.57	0.59	0.57	0.57	2.5
824	1.95	0	8.20	1.75	0.22	12.0	11.9	0.73	0.62	0.62	0.64	0.64	2.4
955	2.80	0	12.7	2.3	0.25	18.0	17.9	0.67	0.58	0.59	0.58	0.59	2.0
38.8 mole % $FeCl_2$–61.2 mole % KCl													
795	1.25	0.010	1.80	0.22	0.02	3.31	3.34	0.42	0.38	0.38	0.27	0.26	5.8
842	2.15	0.012	4.45	0.43	0.05	7.1	7.0	0.68	0.65	0.66	0.49	0.52	4.6
892	4.5	0.041	9.5	0.70	0.07	14.7	14.4	0.86	0.84	0.85	0.61	0.61	3.1
921	5.8	0.05	14.8	1.0	0.08	21.7	21.3	0.80	0.77	0.77	0.60	0.59	2.4
961	9.0	0.1	25.4	1.5	0.11	36.1	35.6	0.87	0.86	0.88	0.66	0.66	2.0
49.8 mole % $FeCl_2$–50.2 mole % KCl													
833	8.9	0.27	4.8	0.10	0	14.0	13.9	0.20	0.72	0.75	0.25	0.23	4.9
874	15.5	0.5	9.1	0.15	0	25.2	25.2	1.48	1.49	1.48	0.54	0.54	4.0
912	25.1	1.1	15.5	0.25	0	42.9	42.5	1.81	1.83	1.83	0.69	0.69	2.5
938	35.3	1.85	22.5	0.35	0	59.9	59.7	1.00	1.03	1.02	0.39	0.38	1.8
979	57.7	3.7	35.5	0.60	0	97.5	98.8	1.54	1.56	1.50	0.56	0.56	1.1
60.0 mole % $FeCl_2$–40.0 mole % KCl													
732	5.1	0.25	0.22	0	0	5.7	5.5	0.58	0.63	0.67	0.023	0.013–0.038*	
767	9.1	0.5	0.5	0	0	10.1	10.2	0.69	0.72	0.73	0.034	0.021–0.034*	
809	17.6	1.4	1.2	0	0	20.2	19.9	1.19	1.29	1.33	0.072	0.053–0.072*	
841	26.9	2.3	2.2	0.02	0	31.4	32.0	1.18	1.25	1.24	0.081	0.074–0.090*	
880	44.6	4.7	4.95	0.05	0	54.3	55.5	1.46	1.50	1.48	0.13	0.13	

* Extrapolated range.

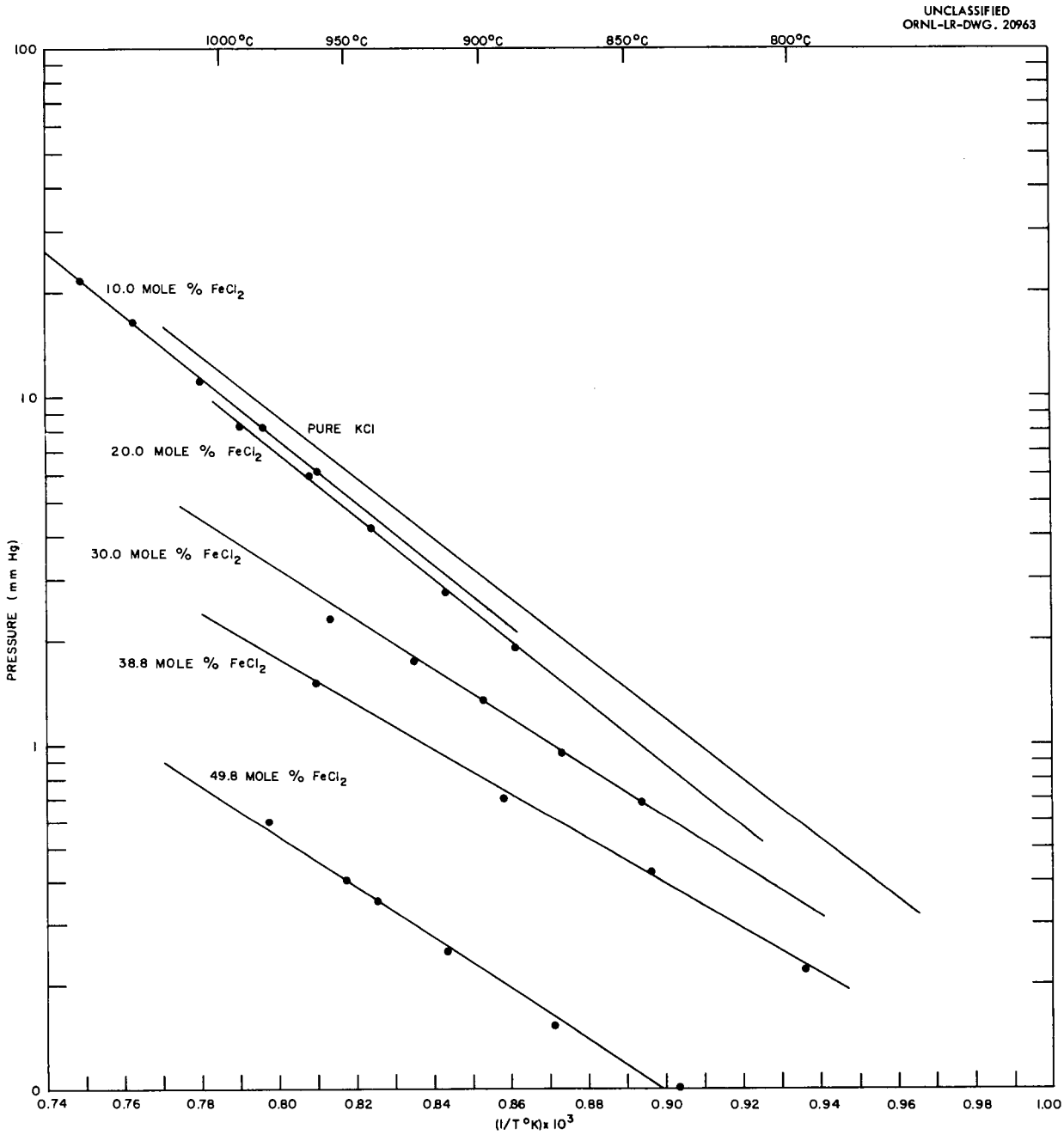

Fig. 34. Partial Pressure of KCl in the KCl-$FeCl_2$ System as a Function of Temperature at Various Compositions.

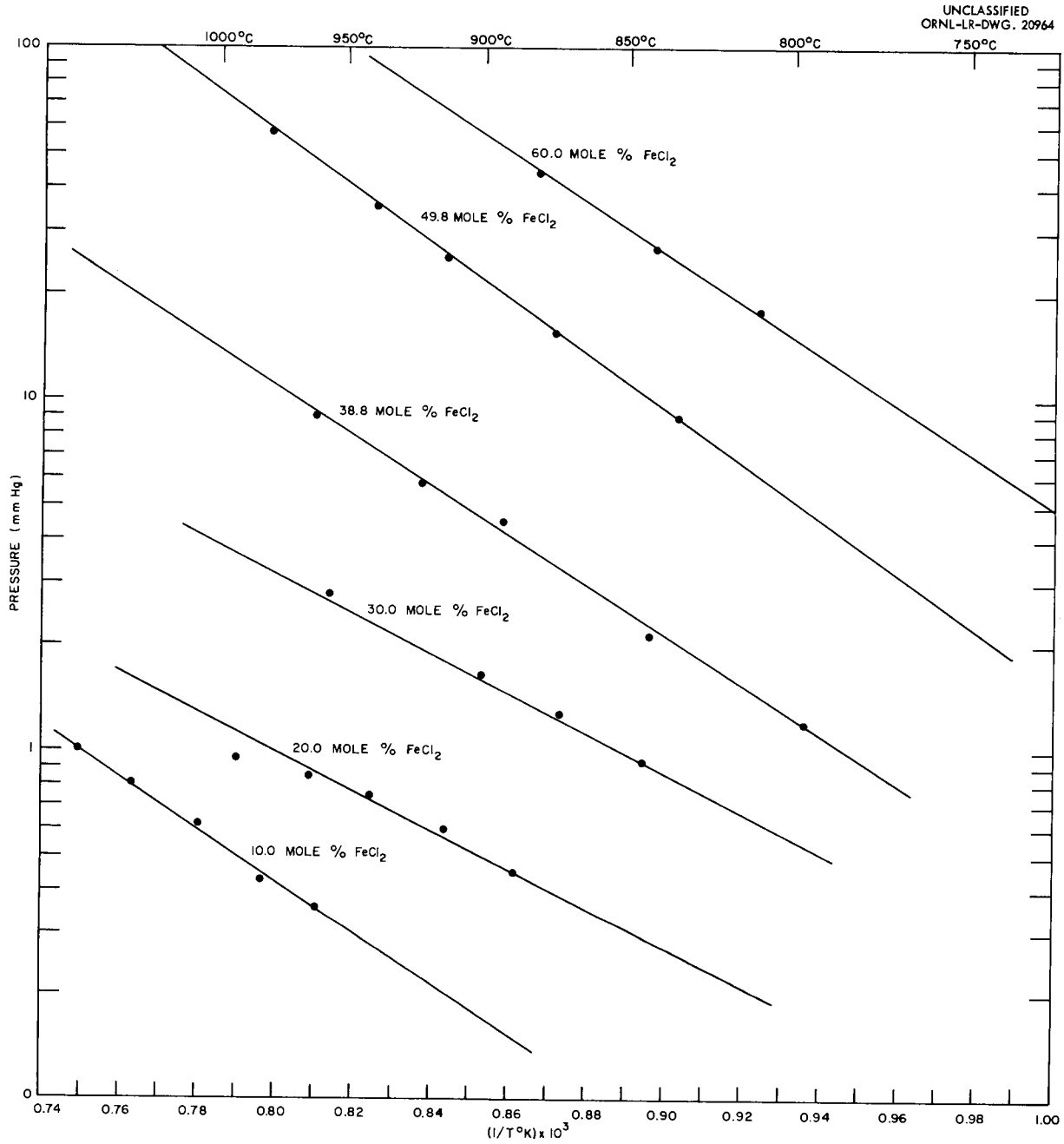

Fig. 35. Partial Pressure of $FeCl_2$ in the KCl-$FeCl_2$ System as a Function of Temperature at Various Compositions.

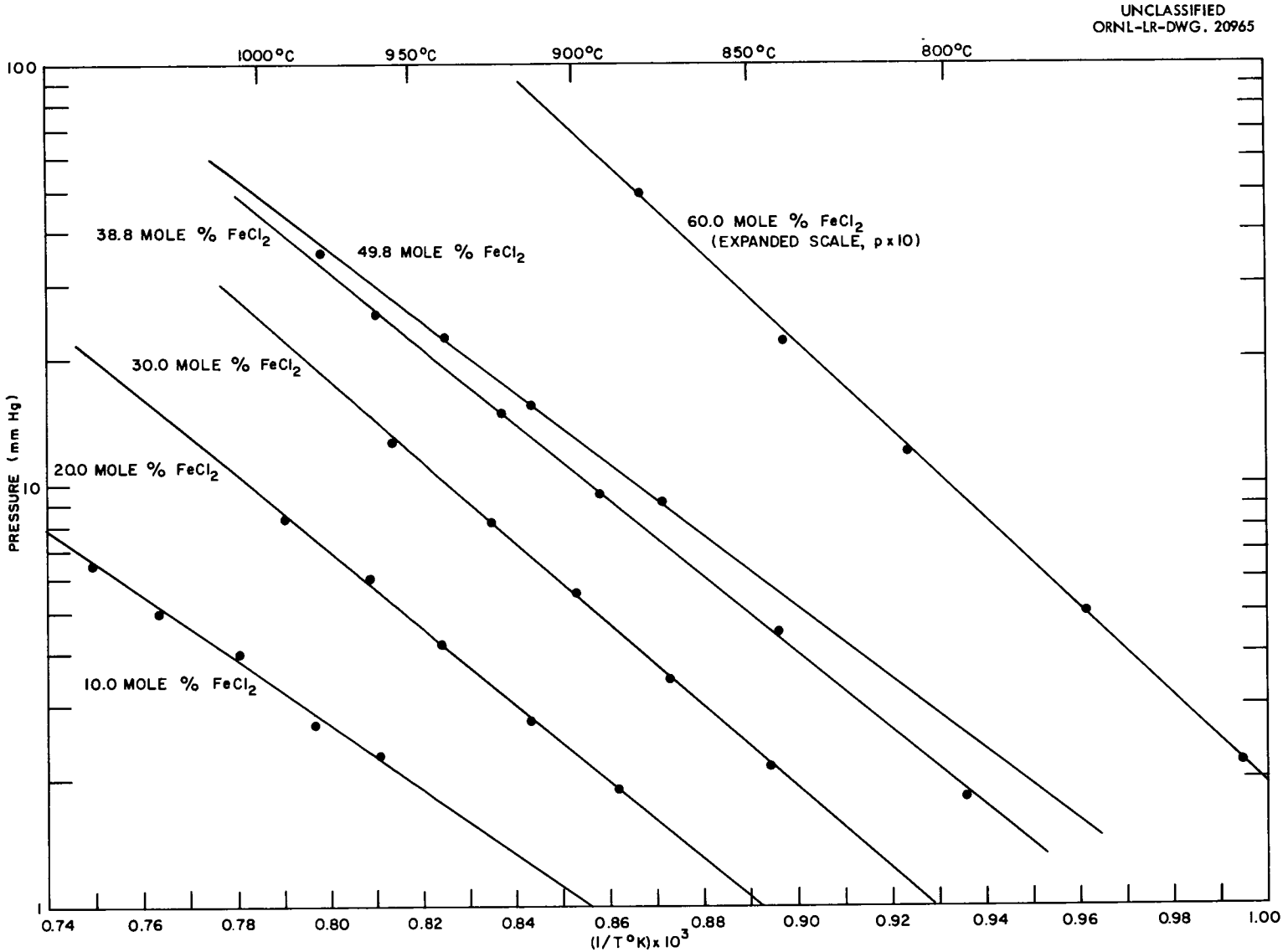

Fig. 36. Partial Pressure of $KFeCl_3$ in the KCl-$FeCl_2$ System as a Function of Temperature at Various Compositions.

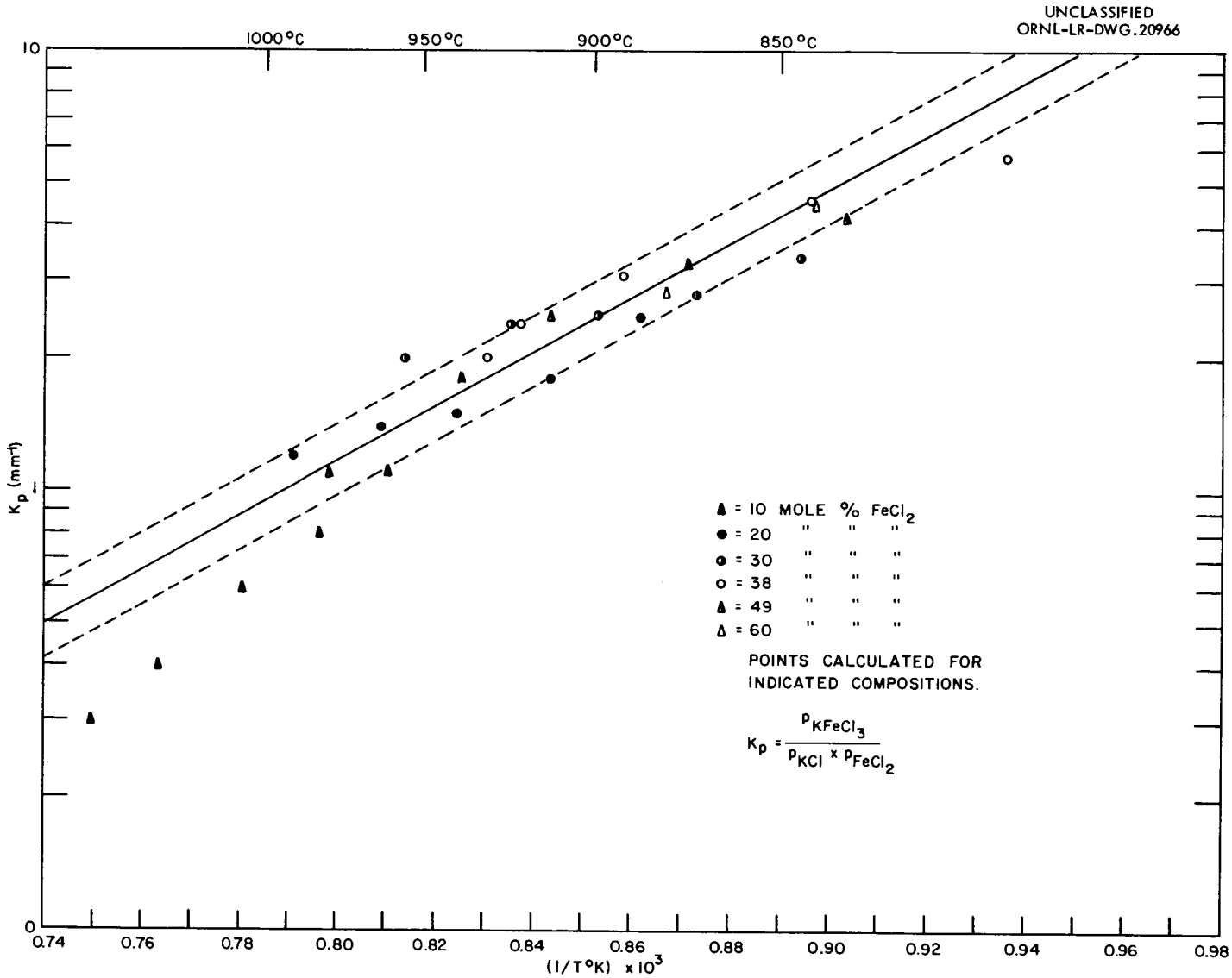

Fig. 37. Equilibrium Constant for Compound Formation in the Vapor as a Function of Temperature.

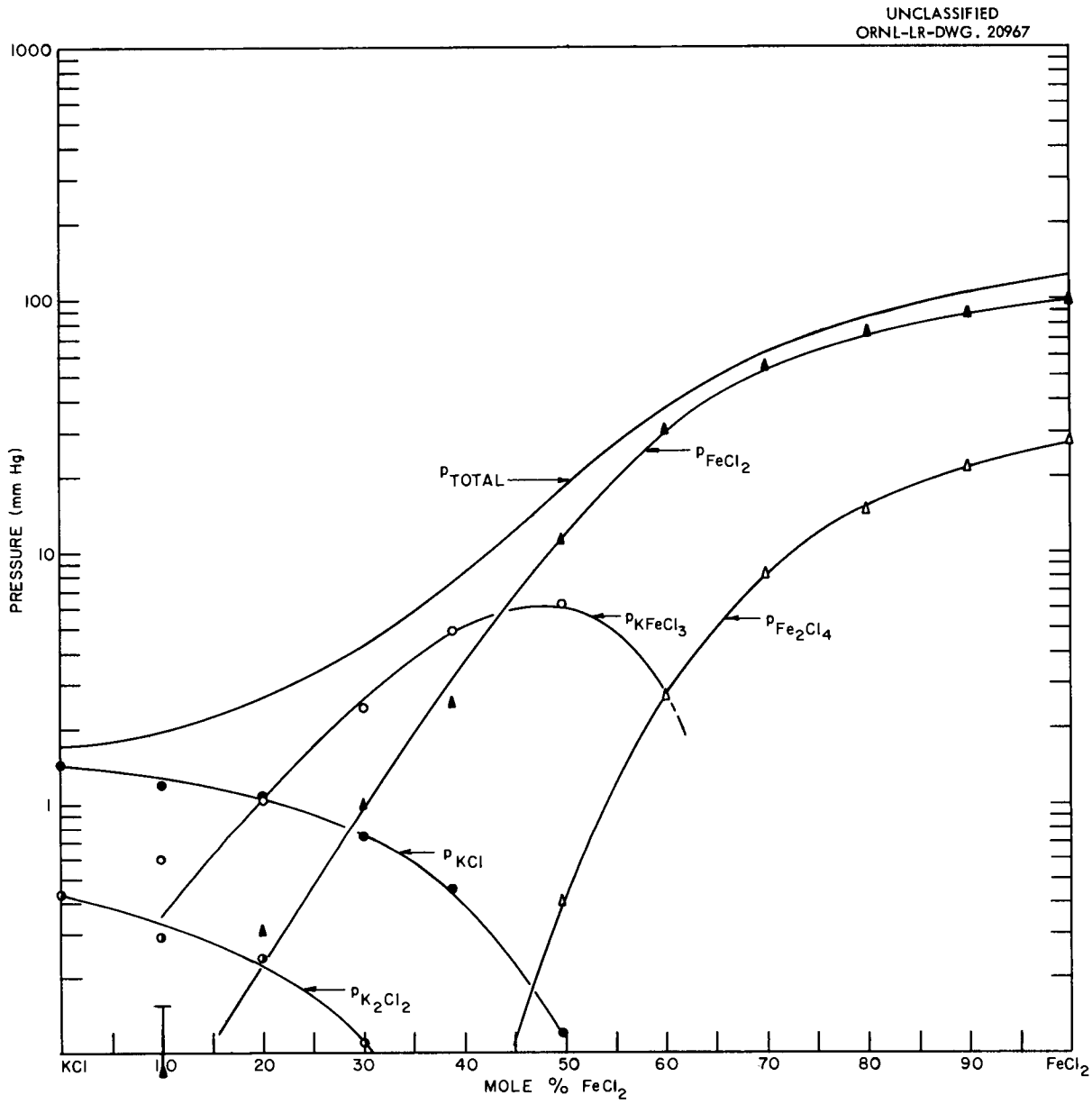

Fig. 38. Partial Pressures of Vapor Species in the KCl-$FeCl_2$ System at 850°C.

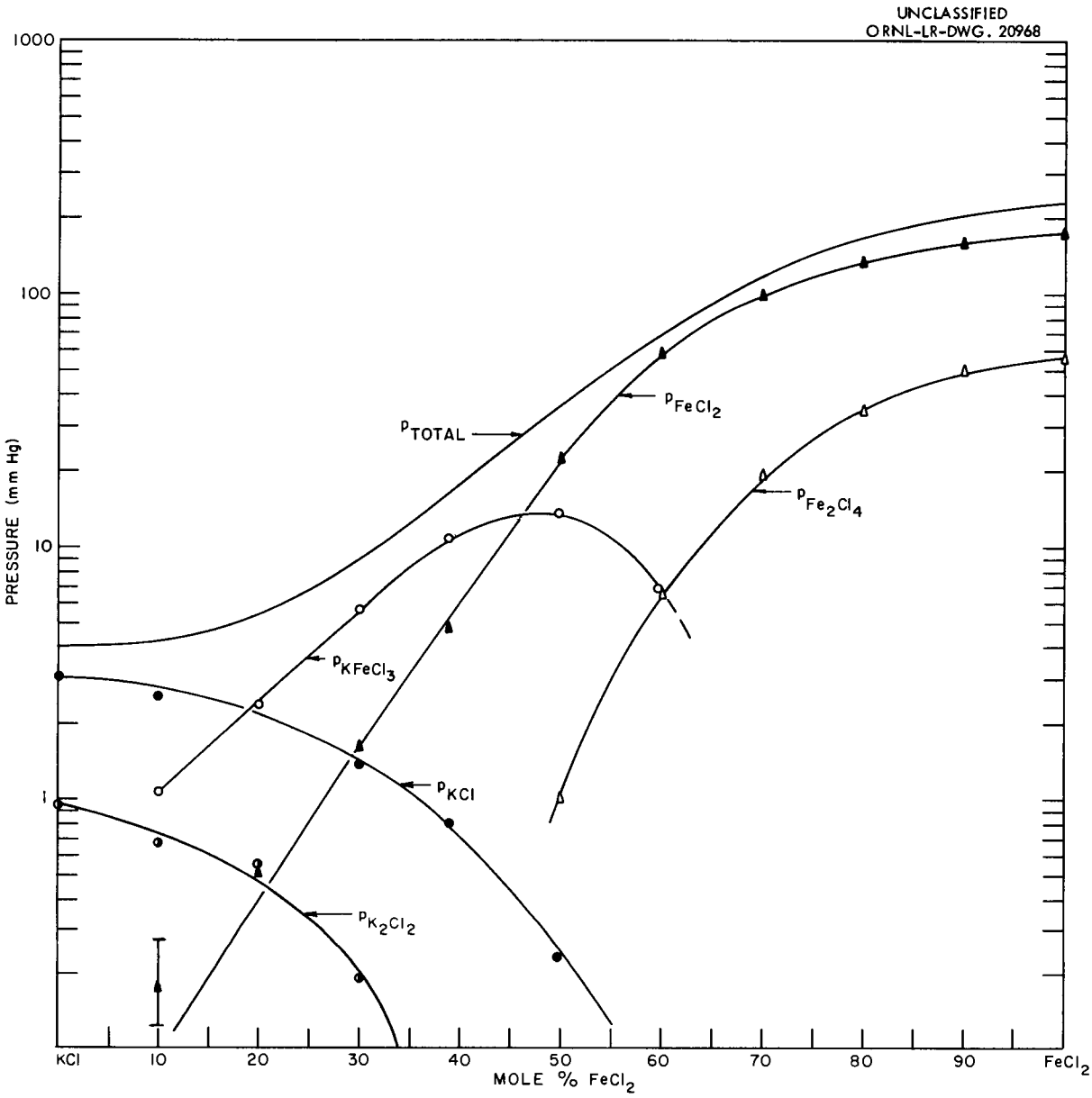

Fig. 39. Partial Pressures of Vapor Species in the KCl-$FeCl_2$ System at 900°C.

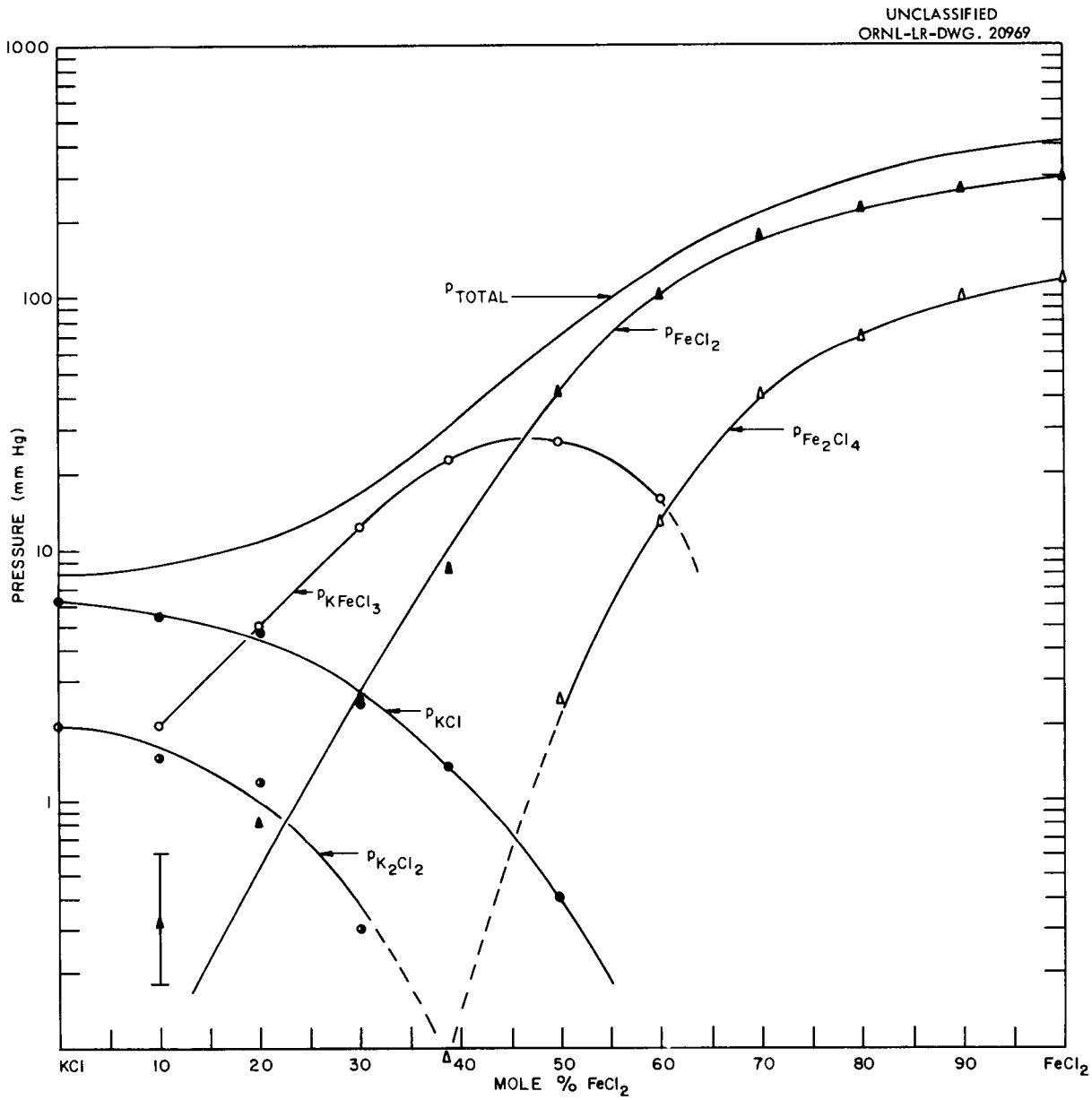

Fig. 40. Partial Pressures of Vapor Species in the KCl-$FeCl_2$ System at 950°C.

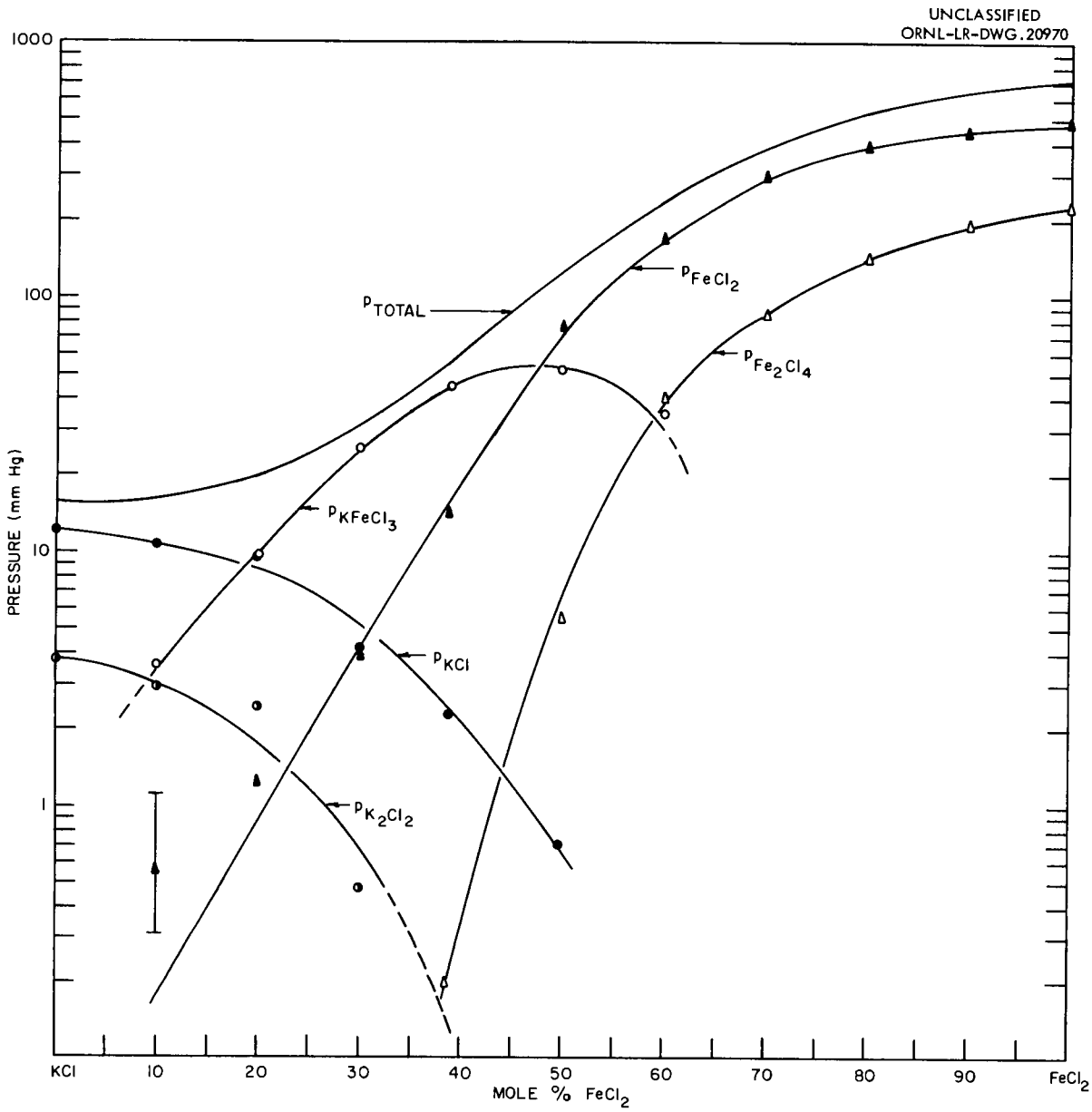

Fig. 41. Partial Pressures of Vapor Species in the KCl-$FeCl_2$ System at 1000°C.

8. THERMODYNAMIC CALCULATIONS

RELATING ACTIVITY TO PARTIAL PRESSURE OF MONOMER SPECIES

The partial molar free energy of a volatile component in a liquid mixture can be shown to equal the partial molar free energy of the corresponding monomer species in the equilibrium vapor above the liquid mixture. Consider a mixture of $FeCl_2$ and KCl, with enough evaporation of $FeCl_2$ to produce a mole of gas mixture containing the equilibrium amounts of monomer and dimer:

$$y\ FeCl_2 = x_m\ FeCl_2 + x_d\ Fe_2Cl_4\ ,$$

where

y = number of formula weights of $FeCl_2$ evaporating to produce one mole of gas,
x_m = mole fraction of monomer in vapor,
x_d = mole fraction of dimer in vapor.

By considering the reaction indicated, y is seen to equal

$$y = x_m + 2x_d\ .$$

Thus, the reaction may be written:

$$FeCl_2(liq) = \frac{x_m}{x_m + 2x_d}\ FeCl_2 + \frac{x_d}{x_m + 2x_d}\ Fe_2Cl_4\ .$$

At constant temperature, when the equilibrium partial pressures of monomer and dimer have been established above the liquid mixture, the partial molar free energy of ferrous chloride must be equal in the vapor and in the liquid:

$$(1)\quad \bar{F}_{FeCl_2(liq)} = \frac{x_m}{x_m + 2x_d}\bar{F}_m + \frac{x_d}{x_m + 2x_d}\bar{F}_d\ ,$$

where

$\bar{F}_{FeCl_2(liq)}$ = partial molar free energy of $FeCl_2$ in liquid mixture, kcal/mole,
$\bar{F}_m$ = partial molar free energy of monomer species ($FeCl_2$) in vapor, kcal/mole,
$\bar{F}_d$ = partial molar free energy of dimer species (Fe_2Cl_4) in vapor, kcal/mole.

The additional equilibrium exists between the monomer and dimer in the vapor phase, corresponding to the dimerization reaction:

$$2FeCl_2 = Fe_2Cl_4$$

Since a true equilibrium exists between these two species, the partial molar free energies are related as:

$$(2)\qquad 2\bar{F}_m = \bar{F}_d\ .$$

Substitution of Eq. 2 into Eq. 1, recognizing that $x_m + x_d = 1$, gives

$$(3)\qquad \bar{F}_{FeCl_2(liq)} = \bar{F}_m\ .$$

Thus, the partial molar free energy of ferrous chloride in the solution equals the partial molar free energy of the monomer species in the vapor. A comparable relation could be developed for the partial molar free energy of the dimer; the monomer was more convenient, since the partial pressure of monomer species was known with greater accuracy from the experimental data.

The partial molar free energy of the monomer species in the gaseous mixture is known to be:

$$(4)\qquad \bar{F}_m = F_m^0 + RT\ \ln\ p_m\ ,$$

where

F_m^0 = a constant of integration, depending on the temperature of the mixture and the nature of the gas,
p_m = partial pressure of monomer species at temperature T.

Equation 4 is derived with the assumption that the monomer and dimer form an ideal mixture of gases.

Equation 4 is now substituted into Eq. 3, yielding

$$(5)\qquad \bar{F}_{FeCl_2(liq)} = F_m^0 + RT\ \ln\ p_m\ .$$

Recalling the definition of activity, given in Eq. 1, Chap. 1:

$$\bar{F}_{FeCl_2(liq)} = F^0_{FeCl_2(liq)} + RT\ \ln\ a_{FeCl_2}\ .$$

Substitution of Eq. 1, Chap. 1, into Eq. 5 yields

$$(6)\quad F^0_{FeCl_2(liq)} + RT\ \ln\ a_{FeCl_2} = F_m^0 + RT\ \ln\ p_m\ .$$

The arbitrary constant $F^0_{FeCl_2(liq)}$ can now be determined, based on the chosen standard state of pure liquid at temperature T. When pure liquid $FeCl_2$ evaporates at temperature T, there exists an equilibrium vapor pressure of monomer, p^0_m. Since the activity of $FeCl_2$ equals unity under standard state conditions, Eq. 6 becomes:

$$(7) \qquad F^0_{FeCl_2(liq)} = F^0_m + RT \ln p^0_m \ .$$

Equation 7 defines the arbitrary constant $F^0_{FeCl_2(liq)}$ based on the pure liquid $FeCl_2$ as the standard state. Substitution of Eq. 7 into Eq. 6, with subsequent rearrangement gives

$$RT \ln a_{FeCl_2} = RT \ln (p_m/p^0_m) \ .$$

Thus:

$$(8) \qquad a_{FeCl_2(liq)} = p_m/p^0_m \ .$$

In simple terms, Eq. 8 states: the activity of a component, e.g., $FeCl_2$, in a mixture equals the ratio of the partial pressures of the monomeric vapor species above the mixture and above the pure liquid component at the same temperature. While the derivation of Eq. 8 was based on simple monomer and dimer formation, there are no restrictions on gas phase reactions implied. Thus, the activity follows Eq. 8 even where higher polymers exist, or where vapor compounds exist between components.

CALCULATION OF ACTIVITIES

Activities in the KCl-$FeCl_2$ system were calculated according to Eq. 8 at four temperatures: 850°, 900°, 950° and 1000°C. The pressure vs composition plots, shown in Figs. 37 and 38, were used to read the monomer pressure at a given composition. The activity data are shown in Fig. 42, at 850° and 1000°C, the intermediate temperatures being omitted for clarity. Since monomer pressures were not obtained for the LiCl-$FeCl_2$ system, activities could not be calculated from the partial pressure data.

The activities calculated for $FeCl_2$ extend from pure $FeCl_2$ down to 20 mole % $FeCl_2$, while the KCl activities only extend from pure KCl to 50 mole % KCl. Partial pressures of monomeric KCl could not be measured at compositions richer in $FeCl_2$. In order to extend the activity curve for KCl, a graphical Gibbs-Duhem calculation was made for the ferrous chloride activity, using the equation

$$(9) \quad \log \frac{a_{KCl}}{x_{KCl}} = -\int_{0.20}^{x_{FeCl_2}} \frac{x_{FeCl_2}}{x_{KCl}} \, d\left(\log \frac{a_{FeCl_2}}{x_{FeCl_2}}\right) + \log \frac{a_{KCl}}{0.80} \ .$$

Since the activity of ferrous chloride was not known between 0 and 20 mole % $FeCl_2$, the graphical integration was carried out over the limits 20–100 mole % $FeCl_2$, with the assumption that the experimental activity for KCl was correct at 20 mole % $FeCl_2$. The calculated activity for KCl is shown as a dotted line in Fig. 42 for the two temperatures. In the region 20–50 mole % $FeCl_2$, the calculated and experimental activities overlap, and the relative agreement between the two values shows that the data are consistent. A similar graphical integration was performed, extending the ferrous chloride activity across the entire diagram.

Strong negative deviations from ideality exist for both components, which can be interpreted in a number of ways. Negative deviations of this type are often explained on the basis of "association" in the liquid: that is, the two components A and B form a tightly bound "compound" AB in the liquid. No direct experimental evidence can be presented for a complex of the form $KFeCl_3$ or K_2FeCl_4, existing in the liquid. However, the existence in the solid state of both compounds, coupled with the existence in the vapor of the $KFeCl_3$ compound, makes the existence of one or both of these forms in the liquid more plausible. The $FeCl_3^-$ ion is difficult to believe, because of the tendency for the ferrous ion to form four-coordinated complexes of the type $FeCl_4^{--}$, as discussed in Chap. 3. Flood and Urnes[37] suggest that the following equilibrium may occur when an equimolar liquid mixture freezes to form $KFeCl_3$:

$$FeCl_4^{--} + 2K^+ \rightleftharpoons KFeCl_3 \downarrow + K^+ + Cl^-$$

On the basis of this equilibrium, the liquid complex could reasonably be $FeCl_4^{--}$. Such a complex could account for negative deviations of the type shown in Fig. 42.

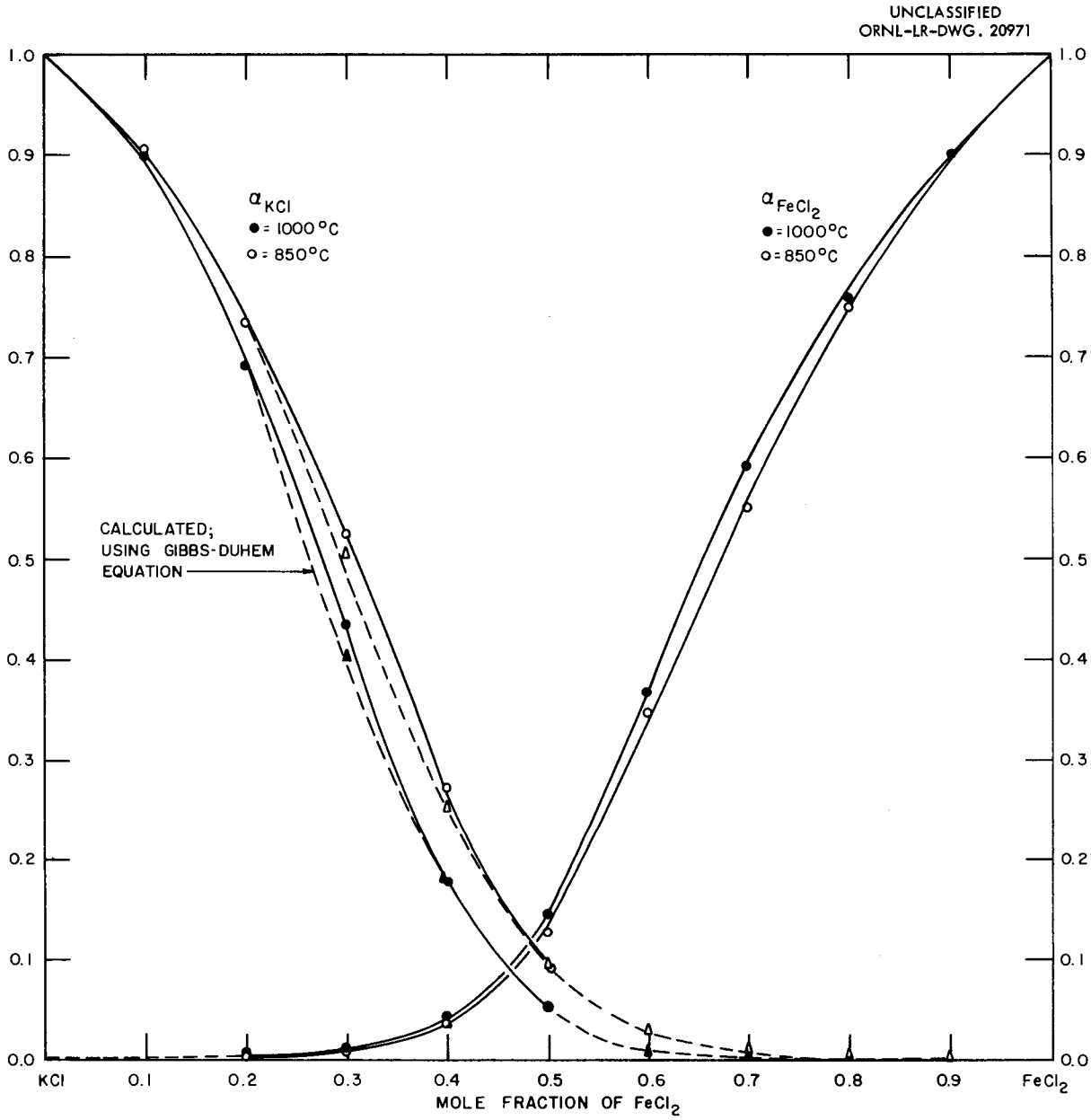

Fig. 42. Activities in the KCl-$FeCl_2$ System as a Function of Composition at 850 and 1000°C.

CALCULATION OF PARTIAL MOLAR ENTROPIES AND ENTHALPIES OF SOLUTION

The assumption of complexation in the liquid causing negative deviations from ideality assumes that these deviations can be explained on a purely entropic basis, and neglects enthalpic effects which occur upon mixing. Using equations developed in Chap. 1, the partial molar enthalpy of solution and the partial molar entropy of solution for the two components can be calculated from the activity curves given in Fig. 42. The equations relating the activity to the partial functions are given below for reference:

$$(10)\quad \bar{S}_i - S_i^0 = -4.576 \left(T \frac{d \log a_i}{dT} + \log a \right),$$

$$(11)\quad \bar{H}_i - H_i^0 = -4.576\, T^2 \frac{d \log a_i}{dT}.$$

Integration of these two equations yields a form suitable for numerical calculation:

$$(12)\quad \bar{S}_i - S_i^0 = -4.576 \left(\frac{T_1 + T_2}{2} \frac{\log a_2 - \log a_1}{T_2 - T_1} + \frac{\log a_2 + \log a_1}{2} \right),$$

$$(13)\quad \bar{H}_i - H_i^0 = -4.576 \left(T_1 T_2 \frac{\log a_2 - \log a_1}{T_2 - T_1} \right).$$

The partial molar entropies and enthalpies were calculated by Eqs. 12 and 13 at 900°C, and are shown in Figs. 43 and 44 as functions of the composition. Table 19 summarizes the values obtained in this manner, along with the partial molar free energy, calculated from Eq. 1, Chap. 1.

Figures 43 and 44 clearly indicate that the deviations from ideality arise from enthalpic as well as entropic effects. It is therefore incorrect to attribute the negative deviations in this system solely to the formation of complex species in the liquid; enthalpic factors cannot be ignored. Activities as a function of temperature for selected compositions are shown in Figs. 45 and 46.

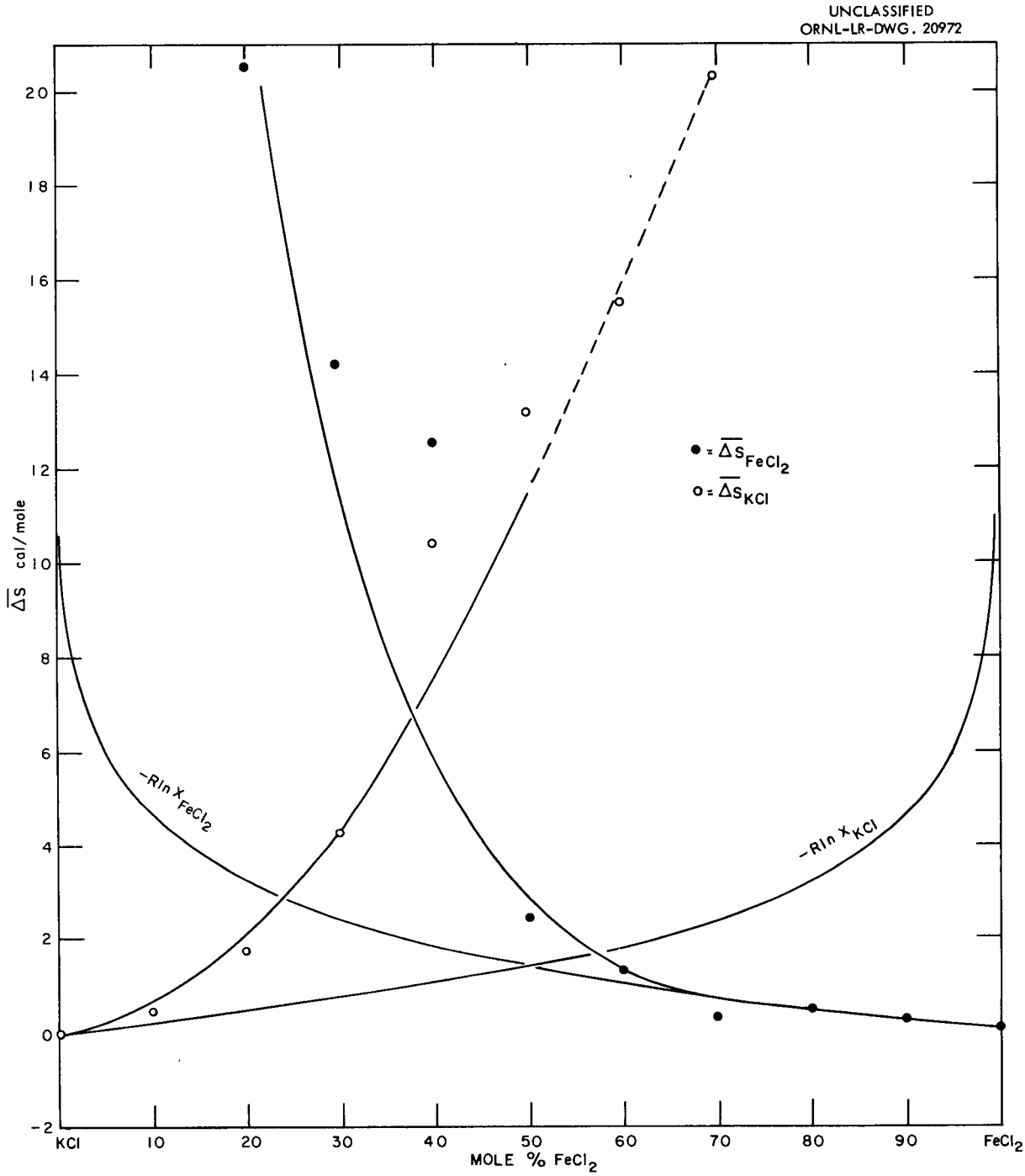

Fig. 43. Partial Molar Entropy of Solution as a Function of Composition in the KCl-$FeCl_2$ System at 900°C.

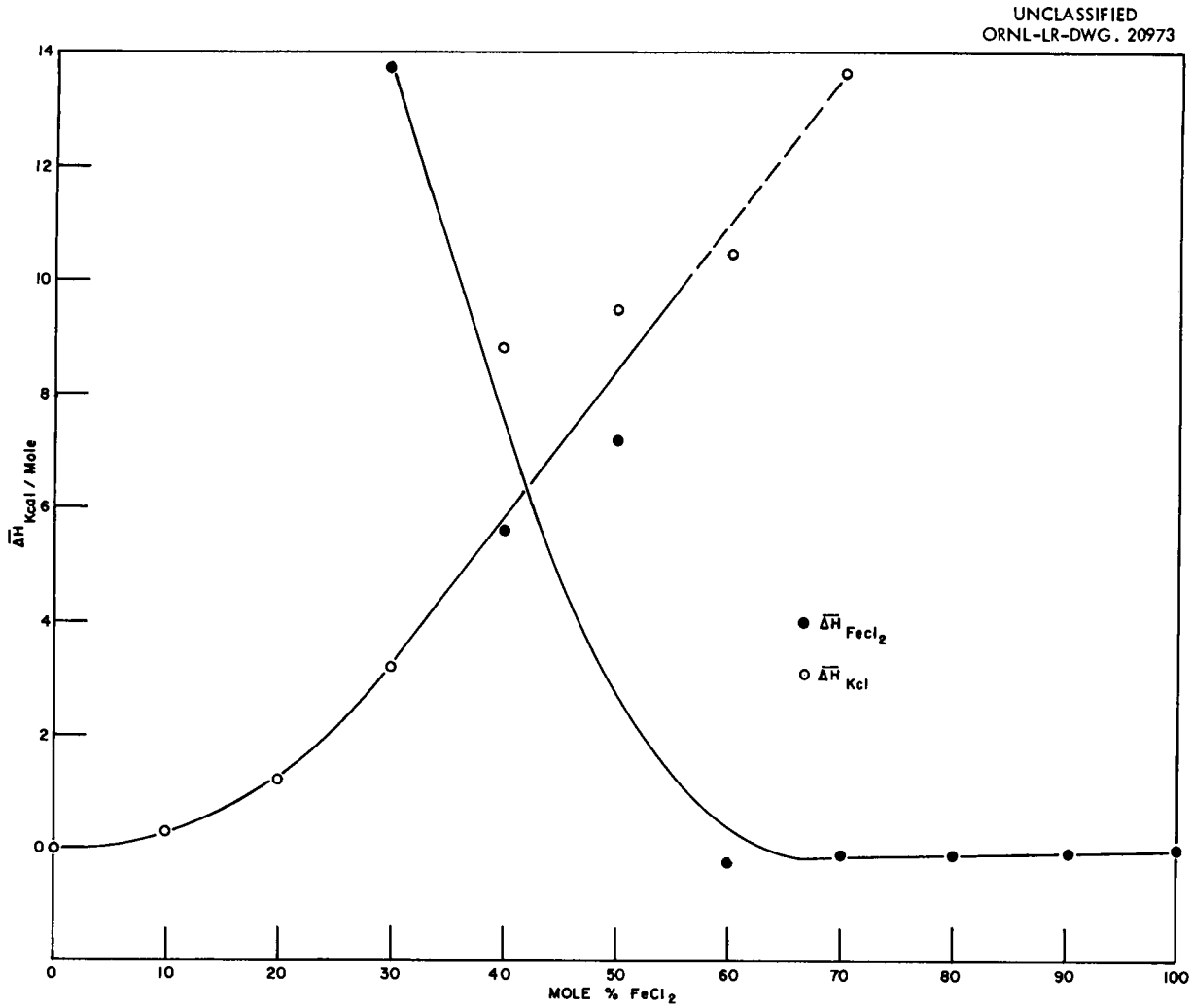

Fig. 44. Partial Molar Heat of Solution as a Function of Composition in the KCl-$FeCl_2$ System at 900°C.

Table 19. Partial Thermodynamic Functions at 900°C in $KCl-FeCl_2$ System

$FeCl_2$ (mole %)	a_{FeCl_2}	a_{KCl}	$(\bar{F}_{FeCl_2} - F^0)_{FeCl_2}$ (kcal/mole)	$(\bar{F} - F^0)_{KCl}$ (kcal/mole)	$(\bar{S} - S^0)_{FeCl_2}$ (cal/deg·mole)	$(\bar{S} - S^0)_{KCl}$ (cal/deg·mole)	$(\bar{H} - H^0)_{FeCl_2}$ (kcal/mole)	$(\bar{H} - H^0)_{KCl}$ (kcal/mole)
100	1.00		0		0	∞	0	
90	0.896		0.22		0.20		0.02	
80	0.737		0.61		0.42		0.1	
70	0.555	0.009*	1.16		0.24	20.3*	0.04	14.5*
60	0.341	0.028*	2.14		1.27	15.5*	0.2	10.5
50	0.127	0.081	4.10	4.99	2.40	13.2	7.2	9.45
40	0.034	0.231	6.72	2.91	12.6	10.4	5.7	8.81
30	0.009	0.465	9.31	1.52	14.2	4.23	15.7	3.21
20	0.003	0.715	11.59	0.67	20.5	1.73		1.26
10	0.001*	0.910	13.72	0.19		0.42		0.2
0	0	1.00		0	∞	0		

*Extrapolated values.

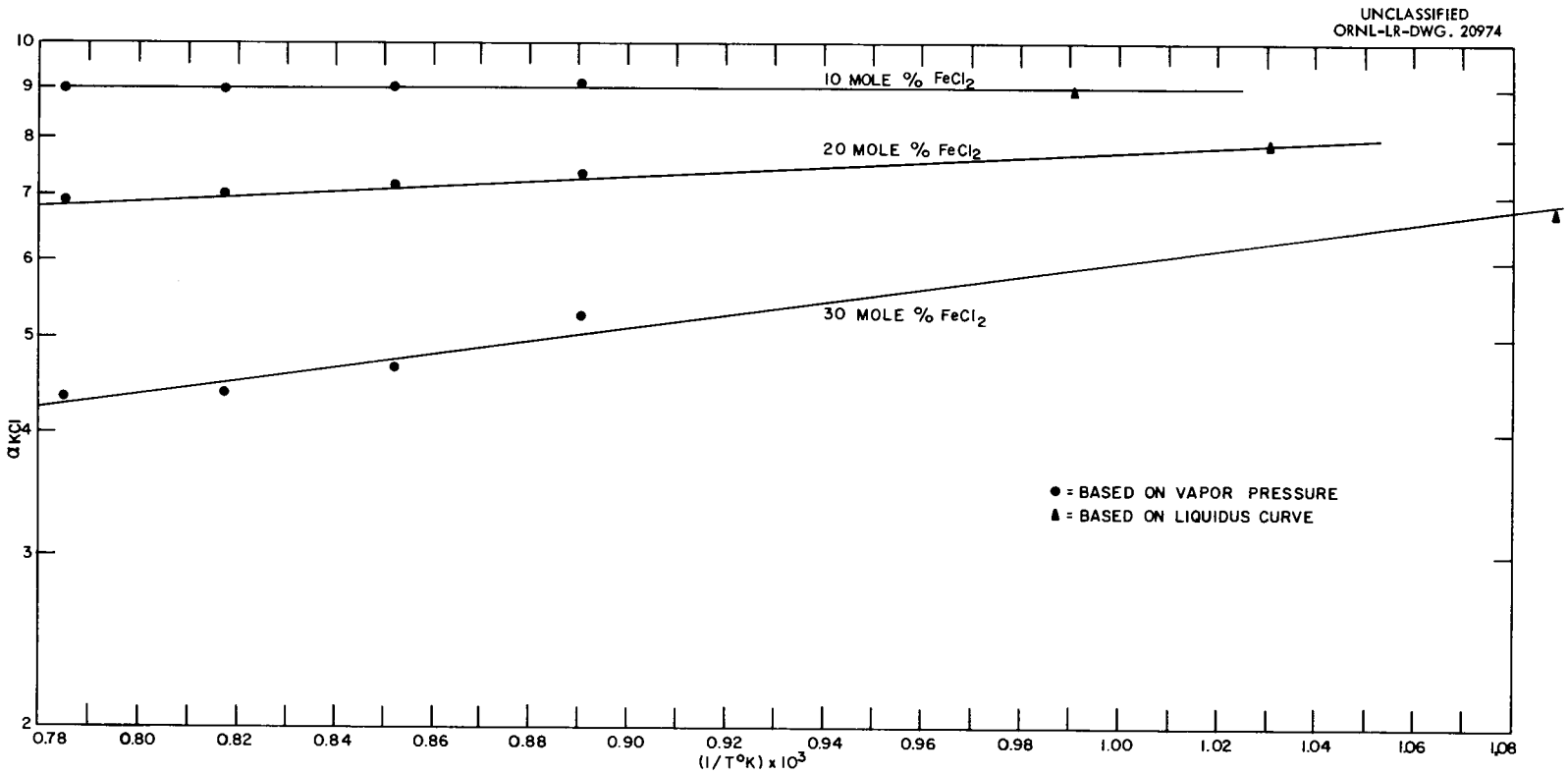

Fig. 45. Activity of KCl as a Function of Temperature for Various Compositions.

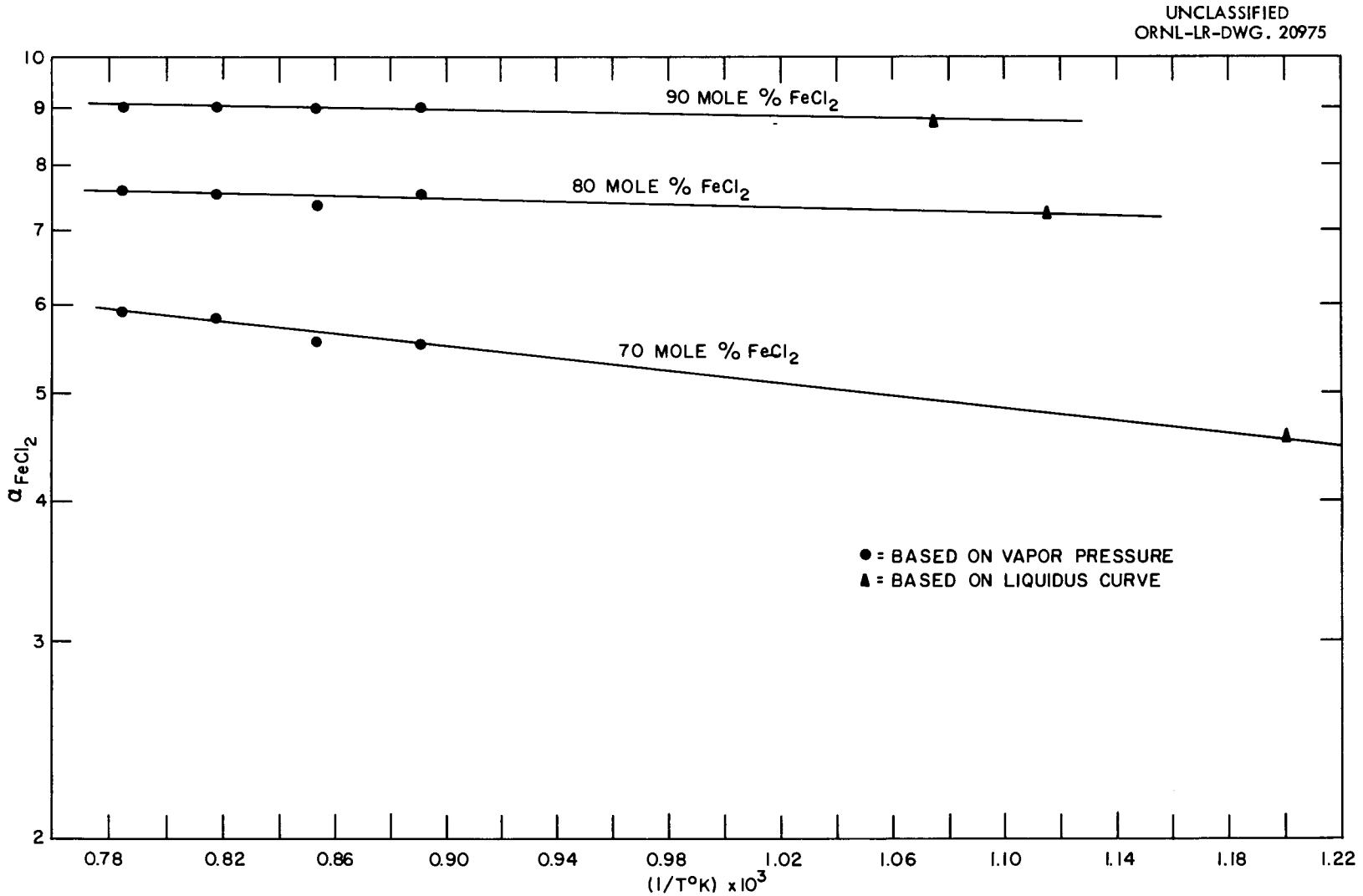

Fig. 46. Activity of $FeCl_2$ as a Function of Temperature for Various Compositions.

9. SUMMARY

Phase equilibria in the $FeCl_2$-KCl and the $FeCl_2$-LiCl systems were studied by means of thermal analysis and vapor pressure measurements. The solid-liquid equilibria were studied by simultaneous conventional cooling curves and differential cooling curves. Petrographic and X-ray analysis helped identify two compounds in the $FeCl_2$-KCl system: K_2FeCl_4 and $KFeCl_3$. The $FeCl_2$-LiCl system showed no compounds, and consisted of continuous solid solution formation.

By combining total vapor pressure measurements with transportation measurements, average molecular weight values were calculated for the pure salt vapors studied, as well as for vapors from binary mixtures. From these data, vapor phase association was found to exist not only in pure salt vapor, but also in the vapor mixtures studied, with the formation of "mixed dimer" vapor species. As direct confirmation, mass spectrographic evidence was obtained for a $KFeCl_2^+$ species in the vapor above an equimolar $FeCl_2$-KCl sample, proving the existence of the $KFeCl_3$ compound or "mixed dimer" in the vapor phase.

Thermodynamic activities and associated thermodynamic functions were calculated from the monomer pressures obtained in the $FeCl_2$-KCl system. Various structural interpretations can be given to the observed partial molar entropy and enthalpy data.

10. BIBLIOGRAPHY

1. G. N. Lewis, "Outline of a New System of Thermodynamics," *Z. Physik. Chem.* **61**, 129 (1908).

2. C. Wagner, *Thermodynamics of Alloys*, Addison-Wesley, Cambridge, 1952.

3. O. Kubachewski and E. L. Evans, *Metallurgical Thermochemistry*, 2d ed., Wiley, New York, 1956.

4. P. Herasymenko, "Electrochemical Theory of Slag-Metal Equilibria," *Trans. Faraday Soc.* **34**, 1295 (1938).

5. M. Temkin, "Mixtures of Fused Salts as Ionic Solutions," *Acta. Physicochim. (U.R.S.S.)* **20**, 411 (1945).

6. H. Flood, T. Forland, and K. G. Rjotheim, "Über den Zusammenhang Zwischen Konzentrationen und Aktivitäten in Geschmolzenen Salzmischungen," *Z. anorg. u. allgem. Chem.* **276**, 289 (1954).

7. B. F. Markov *et al.*, "Thermodynamic Properties of Magnesium Chloride in Alloys of $MgCl_2$-LiCl; $MgCl_2$-NaCl; $MgCl_2$-KCl; $MgCl_2$-RbCl," *J. Phys. Chem. (U.S.S.R.)* **29**, 51 (1955).

8. B. F. Markov, "Calculation of Thermodynamic Constants of Unsaturated Halides from EMF's and $\Delta T/\Delta E$ of Chemical and Daniel-Jacobi Cells," *J. Phys. Chem. (U.S.S.R.)* **30**, 1537 (1956).

9. S. I. Rempel and I. N. Ozeryanaya, "The Series of Tensions for Heavy Non-Ferrous Metals and Their Sulfides in Molten Chlorides of Alkaline Metals," *J. Phys. Chem. (U.S.S.R.)* **25**, 1181 (1951).

10. H. Schutza, "Halogen Exchange Equilibrium in the $CdBr_2$-$CdCl_2$ System," *Z. anorg. u. allgem. Chem.* **239**, 245 (1938).

11. E. J. Salstrom and J. H. Hildebrand, "The Thermodynamic Properties of Molten Solutions of Lead Chloride in Lead Bromide," *J. Am. Chem. Soc.* **52**, 4641 (1930).

12. E. Rinck, "Equilibria Between Na-K Alloys and Molten Salts," *Ann. Chim. Justus Liebigs* **18**, 395 (1932).

13. H. F. Johnstone *et al.*, "The System Ferric Chloride–Sodium Chloride," *J. Am. Chem. Soc.* **64**, 241 (1942).

14. K. Jellinek and A. Golubowski, "Über die Dampfspannungen Geschmolzener Mischungen von $PbBr_2$ und $PbCl_2$ bei Höheren Temperaturen," *Z. Physik. Chem.* **A47**, 464 (1930).

15. K. Jellinek and B. Greiner, "Über die Dämpfe des Reziproken Salzpaares NaCl, KI, und der Binären Gemische $PbCl_2$, $PbBr_2$, $PbCl_2$, PbI_2," *Z. Physik. Chem.* **A165**, 97 (1933).

16. K. Jellinek and H. Hintz, "Über die Verdampfungsgleichgewichte der Binären Salzmischung $HgCl_2$-$HgBr_2$, sowie des Reziproken Salzpaares (Na,K) (Cl,Br)," *Z. Elektrochem.* **42**, 187 (1936).

17. H. Rosenstock *et al.*, *Mass Spectra Studies of Silver Halides and Alkali Halides*, Paper No. 34, ASTM Committee E-14 on Mass Spectrometry, 4th Ann. Meeting, Pittsburgh, 1956.

18. L. Friedman, "Mass Spectrum of Lil Vapor," *J. Chem. Phys.* **23**, 477 (1955).

19. R. Miller and P. Kusch, "Molecular Composition of Alkali Halide Vapors," *J. Chem. Phys.* **25**, 860 (1956).

20. E. Dewing, "Vapor Pressures of the System Sodium Chloride-Aluminum Chloride," *J. Am. Chem. Soc.* **77**, 2639 (1955).

21. J. Osugi, "A Sensitive Diaphragm Method for Static Pressures," *Rev. Phys. Chem. Japan* **21**, 86 (1951).

22. H. von Wartenburg and P. Albrecht, "Die Dampfdrucke Einiger Salze," *Z. anorg. u. allgem. Chem.* **27**, 162 (1921).

23. J. L. Barton and H. Bloom, "A Boiling Point Method for Determination of Vapor Pressures of Molten Salts," *J. Phys. Chem.* **60**, 1413 (1956).

24. W. H. Rodebush and A. L. Dixon, "The Vapor Pressures of Metals: A New Experimental Method," *Phys. Rev.* **26**, 851 (1925).

25. W. H. Rodebush and E. Fiock, "The Vapor Pressures and Thermal Properties of Potassium and Some Alkali Halides," *J. Am. Chem. Soc.* **48**, 2522 (1926).

26. K. K. Kelley, "Free Energy of Vaporization and Vapor Pressures of Inorganic Substances," *Bull. 383, U.S. Bureau of Mines*, 1935.

27. S. S. Yosim and T. A. Milne, *Vapor Pressure of ThF_4 and Some Other Properties*, NAA-SR-1603.

28. K. A. Sense *et al.*, *Vapor Pressures and Derived Information of the Sodium Fluoride–Zirconium Fluoride System*," BMI-1064.

29. W. Fischer and R. Gewehr, "Eine Neve Anordung zur Dampfdruckmessung bei der Mitführungsmethode," *Z. anorg. u. allgem. Chem.* **209**, 17 (1932).

30. C. Wagner and V. Stein, "Die Flüchtigkeit von Chromhalogeniden und über Gleichgewichte bei der Chromierung von Eisen," *Z. Physik. Chem.* **192A**, 324 (1943).

31. J. W. Mellor, *Inorganic and Theoretical Chemistry*, Vol. XIV, Sect. 36, p 9–40, Longmans, New York, 1935.

32. G. H. Gloss, "A Gravimetric Determination of Potassium Ion," *Chemist Analyst* **42**, 50 (1953).

33. E. R. Caley and H. D. Axelrod, "Anhydrous 2-Ethyl Hexanol as a Specific Extractant for Alkali Chlorides," *Ind. Eng. Chem., Anal. Ed.* **14**, 242 (1942).

34. G. Goldberg and J. C. White, "Application of the Volhard Method Titration to the Determination of LiCl Using 2-Ethyl Hexanol," *Anal. Chem.* **27**, 1188 (1955).

35. W. Hückel, "Structural Chemistry of Inorganic Compounds," p 731, Elsevier, New York, 1951.

36. K. K. Kelley, "Evaluation of the Heats of Fusion of Metals and Metal Compounds from Data on Freezing Point Lowering," *Bull. No. 393, U.S. Bureau of Mines* (1936).

37. H. Flood and E. Ürnes, "Calculation of the Activities in Magnesium Chloride–Alkali Chloride Melts from Structure Models," *Z. Elektrochem.* **59(a)**, 834 (1955).

38. W. Gäede, "Die Molekularluft Pumpe," *Ann. Physik* **46**, 357 (1915).

39. S. Dushman, "Vacuum Technique," Wiley, New York, 1954.

40. American Society for Metals: *Metals Handbook*, 1948 ed., p 1045.

41. G. E. Moore, "Heat Contents at High Temperatures of the Anhydrous Chlorides of Ca, Fe, Mg, Ni, and K," *J. Am. Chem. Soc.* **65**, 1700 (1943).

42. O. Ruff and S. Mugdan, "Messung die Dampfdruck bei Hohen Temperaturen der Alaklihalogenide," *Z. anorg. u. allgem. Chem.* **117**, 147 (1921).

43. C. G. Maier, "Vapor Pressures of the Common Metallic Chlorides and a Static Method for High Temperatures," *Tech. Paper 360, Bureau of Mines*, 1929.

44. H. von Wartenburg and H. Schulze, "Der Dampfdruck Einiger Salze," *Z. Elektrochem.* **27**, 568 (1921).

45. H. Shäfer *et al.*, "Sattigungsdrucke der Chloride $MnCl_2$, $FeCl_2$, $CoCl_2$, und $NiCl_2$," *Z. anorg. u. allgem, Chem.* **278**, 300 (1955).

46. P. Kusch, J. Ochs, and R. Cote, "Radiofrequency Spectrum of Components of a Sodium Chloride Beam," *J. Chem. Phys.* **21**, 459 (1953).

47. R. Miller and P. Kusch, "Molecular Composition of Alkali Halide Vapors," *J. Chem. Phys.* **25**, 860 (1956).

48. H. Rosenstock *et al.*, *Mass Spectrometer Study of the Alkali Halides* (unpublished).

49. V. Deitz, "The Vapor Pressure of Potassium Chloride and Cesium Iodide Crystals," *J. Chem. Phys.* **4**, 575, (1936).

50. B. Zimm and J. Mayer, "Vapor Pressures, Heats of Vaporization and Entropies of Some Alkali Halides," *J. Chem. Phys.* **12**, 362 (1944).

51. H. Bloom and J. L. Barton, private communication.

52. R. Minturn and S. Datz, private communication.

53. W. P. Treadwell and W. Werner, "Über die Bestimmung des Dampfdrucks von Festem Cäsium, Rubidium, and Kaliumchlorid nach der Mitführungsmethode," *Helv. Chim. Acta* **36**, 1936 (1953).

54. J. Mayer and I. Wintner, "Measurements of Low Vapor Pressures of Alkali Halides," *J. Chem. Phys.* **6**, 301 (1938).

55. W. Kangro and H. Wieking, "Dampfdrucke über Geschmolzenen Alkalichloriden und deren Binären Gemischen mit Natriumchlorid," *Z. Physik. Chem.* **A183**, 199 (1938).

56. A. Glassner, *A Survey of the Free Energies of Formation of Fluorides, Chlorides and Oxides of the Elements to 2500°K*, ANL-510.

57. V. Meyer, "Vapor Density of $FeCl_2$," *Ber. deu. Chem. Ges.* **12**, 1193 (1879).

58. J. Dewar and A. Scott, "On the Vapor Density of Various Salts," *B.A. Rep.* 597 (1881) (cited in ref 31).

59. E. H. Howard, "Vapor Pressures on the NaF-AlF_3 System," *J. Am. Chem. Soc.* **76**, 2941 (1954).

60. I. Naryshkin, "Studies in the $NaCl$-$AlCl_3$ System," *J. Phys. Chem.* (*U.S.S.R.*) **13**, 690 (1939).

61. A. F. Wells, "Structural Inorganic Chemistry," 2d ed., Oxford Press, London, 1952.

APPENDIX A

CHEMICAL MICROSCOPY AND X-RAY DIFFRACTION SUMMARY

The petrographic microscope was the primary tool for identification of phases in samples. The identification was based on optical properties (see Table 20) determined from well-crystallized samples of compounds synthesized in the course of this study. Differences in the indices of refraction served to show the presence of trace amounts of one crystalline material in another; a number of other properties could also be used to recognize the crystals. Considerable skill and experience were required for the successful use of petrographic examinations in this manner. All the petrographic examinations were made by Dr. T. N. McVay, of

Table 20. Optical Properties and X-Ray Diffraction Patterns*

K_2FeCl_4

Optical Data:
Uniaxial (+)
$\omega = 1.600$
$\epsilon = 1.636$

X-ray Data:

d (Å)	I/I_1
6.02	100
5.69	15
4.06	25
3.47	75
3.10	15
2.86	30
2.675	100
2.615	50
2.590	100
2.518	25
2.489	15
2.467	50
2.203	15
2.108	15
2.022	15
1.994	25
1.884	30
1.749	25

Table 20 (continued)

$KFeCl_3$

Optical Data:
Biaxial (+)
$\alpha = 1.700$
$\gamma = 1.740$
$2V \cong 20°$

X-ray Data:

d (Å)	I/I_1
7.5	30
7.2	30
4.17	30
3.43	30
3.11	25
2.89	20
2.83	100
2.75	30
2.695	35
2.660	100
2.495	15
2.276	30
2.243	15
2.124	15
1.980	15
1.957	10
1.940	35
1.924	50
1.899	10
1.851	10
1.832	25
1.789	15

*The symbol d (Å) denotes the distance between reflecting planes measured in angstroms. The term I/I_1 refers to the relative intensity as compared with an arbitrary value of 100 for the strongest line. Under optical properties, α and γ refer to the lowest and highest indices of refraction, respectively, for biaxial crystals, and $2V$ refers to the acute angle between the optic axes in biaxial crystals; ω and ϵ refer to the ordinary and extraordinary indices of refraction of uniaxial crystals.

the Oak Ridge National Laboratory; sincere thanks are expressed for his valuable contribution to this work.

Supplementary phase identification and semi-quantitative analyses were made by X-ray diffraction of powdered samples obtained from phase diagram melts. The X-ray patterns were made with a General Electric XRD-4 power unit and a Norelco-Phillips diffraction unit equipped with a Geiger counter detector. Cobalt K-α radiation was used. This technique was quite useful for the determination of microcrystalline materials and it also permitted determination of relative amounts of crystalline phases present as well as the extent of solid solution formation. As in the case of optical identification, it was necessary to provide pure compounds in order to obtain standard diffraction patterns for compounds not reported in the literature. The purity of the compounds prepared as standard samples was established by chemical microscopy. X-ray patterns were determined routinely on all phase diagram melts. The melts were ground and homogenized, and mounted in a Plexiglas holder, covered by a 0.0005-in. polystyrene film to prevent hydration of the samples. The X-ray data (see Table 20) were obtained by R. E. Thoma of the Oak Ridge National Laboratory; a great deal of credit for the phase diagrams exhibited is due to his efforts.

APPENDIX B

MASS SPECTROMETERIC STUDY OF SALT VAPORS IN THE KCl-$FeCl_2$ SYSTEM

Mass spectra of the vapor state of $FeCl_2$ and $KFeCl_3$ were investigated in an effort to clearly identify the vapor species present. The mass spectra were obtained on an all metal 8-in. radius 60-deg sector mass spectrometer using magnetic scanning. The ions formed under 75 v electron bombardment were accelerated through a potential of 2000 v, and the ion current was measured by a vibrating reed electrometer, connected to a Speedomax recorder. The samples were placed on tantalum filament strips and were heated by a well-regulated a-c source until a sufficiently rapid vaporization was attained; sample temperatures were estimated to be in the range of 400–500°C.

Two determinations were attempted with pure $FeCl_2$. In the first, the sample had completely vaporized before satisfactory scans of the mass peaks could be obtained. In the second, two complete scanning attempts failed to show any significant mass peaks other than those expected for pure monomeric $FeCl_2$, e.g., $FeCl_2^+$, $FeCl^+$, Fe^{++}. This evidence does not conflict with the dimer evidence obtained from vapor pressure determinations, since:

1. mass spectra determinations were made above solid $FeCl_2$, at temperatures where little dimer would be expected from extrapolation of the vapor pressure results,
2. dimer species may decompose under the highly energetic electron bombardment needed to create ions.

Two determinations were completed with equimolar mixtures of KCl and $FeCl_2$. This composition corresponds to the compound, $KFeCl_3$, found in the phase diagram study. Strong mass peaks were found in the mass-number range 165–169; the peak intensities were in the ratio expected for an ion of the type $KFeCl_2^+$. A weaker array of peaks was observed in the 200–204 mass number region, with intensities that could be explained by the presence of a $KFeCl_3^+$ peak. Additional peaks were observed corresponding to the vapor molecules KCl, K_2Cl_2, and $FeCl_2$. The presence of the $KFeCl_2^+$ peak is strong evidence for the existence of a $KFeCl_3$ molecule in the vapor above the liquid mixture cited.

The mass spectrometric work reported here was done under the supervision of J. R. Sites, of the Oak Ridge National Laboratory; sincere thanks are expressed for his contribution to this work.

ACKNOWLEDGMENTS

This report is based upon a thesis submitted to the University of Cincinnati in partial fulfillment of the requirements for the doctoral degree. The report describes research carried out in the Chemistry Division at the Oak Ridge National Laboratory.

The research was supported by the Oak Ridge Graduate Fellowship Program of the Oak Ridge Institute of Nuclear Studies and was directed by a committee appointed by Dean H. S. Green of the University of Cincinnati Graduate School which was composed of Dr. J. W. Sausville and Dr. T. B. Cameron of the Department of Chemistry at the University of Cincinnati and Dr. F. F. Blankenship and Dr. R. F. Newton of the Chemistry Division of the Oak Ridge National Laboratory.

The writer wishes to sincerely thank all the members of the Chemistry Division of the Oak Ridge National Laboratory for their consideration and assistance in this work. In particular, the discussions with Dr. M. Blander, Dr. S. Cantor, Dr. M. Panish, and Dr. S. Datz were most helpful and constructive.